Finite Set Model Predictive Control of the PMSM with Sine-Wave Filter

Von der Naturwissenschaftlich-Technischen Fakultät

der Universität Siegen

zur Erlangung des akademischen Grades

Doktor der Ingenieurwissenschaften

(Dr.-Ing.)

genehmigte Dissertation

von

M.Sc.E.E. Paúl Marcelo Pozo Palma

aus Quito, Ecuador

1. Gutachter: Prof. Dr.-Ing. Mario Pacas
2. Gutachter: Prof. Dr.-Ing. Ralph Kennel

Tag der mündlichen Prüfung: 13.03.2015

ACKNOWLEDGEMENT

This work was carried out thanks to the financial support of the “Secretaría Nacional de Educación Superior, Ciencia, Tecnología e Innovación del Ecuador (SENESCYT)” under the scholarship program “Academia 2010”.

I would like to express the deepest appreciation to my supervisor and head of the institute, Prof. Dr.-Ing. Mario Pacas, who has been an excellent mentor for me. I would like to thank him for the continuous support of my work and the related research, for his patience, motivation, and immense knowledge and for allowing me to be part of his working group. His guidance helped me during the research and while writing my thesis.

In addition to my advisor, I would like to thank Prof. Dr.-Ing. Ralph Kennel and Prof. Dr.-Ing. Dietmar Ehrhardt for their work as co-examiners. I am also very grateful with Prof. Dr. rer. nat. Rainer Brück for his support pertaining to the doctoral procedure.

I would like to thank the staff of the chair of Power Electronics and Electrical Drives for the friendly and cooperative atmosphere. Especially Dipl.-Ing. E. Oerter, Dipl.-Ing. Bruch and Mrs. S. Leukel for supplying technical and administrative assistance as well as my colleagues and friends at the Institute: Dipl.-Ing. M. Steinbring, Dipl.-Ing. H. Zoubek, Dipl.-Ing. S. Feuersänger, M.Sc.E.E. M. Perdomo, M.Sc.E.E. F. Ramirez, M.Sc.E.E. S. Dufoo, M.Sc.E.E. The Minh Phan, M.Sc.E.E. Van Trang Phung , M.Sc.E.E. Othman Abdulhadi and M.Sc.E.E. Harith Ahmed M. Al-Badrani for their support and for their invaluable help during my stay in Germany.

A very special thanks is owed to Simon Feuersänger´s family (Anne, Marina Gracia and Lilia Gloria) and Rosemarie Weiske for their exceptional friendship, they will always be in our hearts.

Special thanks to my parents for supporting me spiritually throughout this work and in my life in general and for giving me a valuable legacy: my education.

Last but not the least, I would like to thank my wife for her unconditional support, never-ending patience, constant encouragement, sensitive understanding and for always reminding me that behind of science the other side of life is the love.

Finally, I thank God for the wisdom and perseverance that he has been bestowed upon me during this work, and indeed, throughout my life.

Marcelo Pozo Palma

INDEX OF CONTENTS

ACKNOWLEDGEMENT i

INDEX OF CONTENTS ii

NOMENCLATURE 1

1. INTRODUCTION 5

2. THEORETICAL FUNDAMENTALS 9

2.1. The Space Phasor 9

2.2. Coordinate Transformations 13

2.3. Synchronous Machine 16

2.3.1. Introduction 16

2.3.2. Magnets for Permanent-Magnet-Synchronous-Machine 16

2.3.3. Type of Construction of the Rotor of Permanent Magnet Synchronous Machines 18

2.3.4. Model of the Synchronous Machine 19

2.3.5. Model of the Synchronous Machine in the Stator-Fixed Coordinate System 26

2.4. Control Schemes for the PMSM 29

2.4.1. Direct Torque Control Principle 29

2.4.2. Field Oriented Control Principle 31

2.5. Voltage Source Inverter 33

2.5.1. Two-Level VSI 33

2.5.2. Multi-Level VSI 35

2.6. Space Phasor Modulation 39

2.7. Sinusoidal Pulse Width Modulation 42

2.8. Summary of the Chapter 44

3. PREDICTIVE CONTROL FOR THE SYSTEM LC FILTER- PMSM 45

3.1. Predictive Control Principle 45

3.1.1. Principle 45

3.1.2. Cost Function 48
3.1.3. Optimization 50
3.1.4. Constraints 50
3.1.5. Relationship with other Controllers 51
3.1.6. Properties, Advantages and Disadvantages of the Predictive Control 51
3.1.7. Predictive Control Applied to Power Electronics and Control Drive Systems 52
3.1.8. Selection of the Cost Functions in Power Electronics and Drive Systems 55
3.1.9. Constraints in Cost Functions Applied in Power Electronics and Drives 56
3.2. The System LC Filter – PMSM 57
3.2.1. State-Space Model of the System LC Filter - PMSM 58
3.2.2. Observer Model 60
3.3. Numerical Integration 61
3.4. Control Strategy of the Predictive Control for the System PMSM-LC Filter 63
3.4.1. Principle of Operation 63
3.4.2. Ideal Voltage Space Phasor Reference 66
3.4.3. Cost function and optimization 66
3.4.4. Virtual Multilevel Inverter and Mesh with Voltage Space Phasors as Finite Set 67
3.4.5. Inverter Voltage Limit 70
3.4.6. Enhanced Cost Function 73
3.5. Summary of the Chapter 77
4. SENSORLESS CONTROL, ON-LINE PARAMETER IDENTIFICATION AND ADAPTIVE TUNING 78
4.1. Sensorless Control 78
4.1.1. Introduction 78
4.1.2. Observer Based Methods 79
4.1.3. Voltage Model Method 80

4.2. On-Line PMSM Parameter Identification and Adaptive Tuning 83
4.2.1. Enhanced On-line PMSM Adaptive Parameter Tuning 84
4.3. Summary of the Chapter 90
5. LABORATORY SET-UP AND EXPERIMENTAL RESULTS 91
5.1. Experimental Set-up 91
5.2. Experimental Results for the Predictive Control of the System PMSM-LC Filter with Observer 93
5.2.1. Predictive Control 93
5.2.2. The Predictive Control at the Voltage Limit of the Inverter 100
5.2.3. Predictive Control with Enhanced Cost Functions 103
5.3. Sensorless Control with On-line Adaptive Parameter Tuning 106
5.3.1. Sensorless Control 106
5.3.2. On-line Adaptive Parameter Tuning 107
5.4. Summary of the Chapter 110
6. CONCLUSIONS 111
7. ABSTRACT 112
8. ZUSAMMENFASSUNG 113
9. APPENDICES 114
Parameters of the utilized PMSM 114
Sine-Wave Filter Parameters 114
Load Machine Parameters 114
Load Driver Parameters 115
10. REFERENCES 116

NOMENCLATURE

Symbols

$\lvert x \rvert$	absolute value
$\lvert \underline{x} \rvert$	magnitude of a space phasor
$\arg\{\underline{x}\}$	phase of the space phasor in polar-coordinate
$\lfloor \ \rfloor$	operator "greatest integer smaller value than or equal to"
C	capacitor, cartesian coordinates
D	diode, damper-winding D
d,q	reference frame, aligned with the estimated but erroneous angle γ
d,q	rotor flux oriented coordinate system, arbitrary reference frame
e	error
f	frequency
f_m	maximum frequency
f_r	resonance frequency
f_{sw}	switching frequency
g	cost function
i, I	current
Im	imaginary part
J	moment of inertia, cost function
j	imaginary unit
K_I	integral gain
K_P	proportional gain
k	discrete time point
L	inductance, phase of the main supply
M	torque
N	horizon (of prediction or of control)
p	pair of poles
P	polar coordinates
Q	damper-winding Q
R	resistance
Re	real part
S	switch power semiconductor
slp	slope
t	time
Ts	sample time, modulation period
Tz	cycle time
u, U	voltage, phase U
U_{DC}	DC link voltage

UVW	three-phase AC system UVW
V	phase V
W	phase W
w	weight factor
α, β	stator-fixed coordinate system
α', β'	stator-fixed coordinate system transformed by the matrix [T]
γ	angle between the real axis of the fixed system and the real axis of a new system of coordinates
Δ	difference operator
δ	difference operator, weight factor
λ	weight factor
μ_r	relative permeability
ϑ	angle between the stator- and of rotor-fluxes space phasors, temperature
ψ	flux-linkage
φ	angle between the α -axis and the stator flux $\underline{\psi}_1$
ω	angular velocity
Ω	mechanical velocity

Matrices

$[A]$	state matrix
$[B]$	input matrix
$[C]$	output matrix
$[L]$	observer gain matrix
$[T]$	transformation matrix
$[u]$	control vector
$[x]$	state vector
$[y]$	output vector
$[w]$	reference vector (set-point or reference trajectory)

Superscripts

$[x]^{-1}$	inverse matrix
$[x]^{T}$	transposed matrix
x'	variable in the α'β' coordinate system
x^{*}	reference, conjugate complex
$\dot{x}$	time derivative

$\hat{x}$	estimated, maximum value
$\tilde{x}$	error
x^N	base value
x^p	predicted value
x^{Param}	parameter

Subscripts

x_1	stator quantity, phase 1 of the main supply, first slope
x_2	rotor quantity, phase 2 of the main supply, second slope
x_3	phase 3 of the main supply, third slope
x_4	fourth slope
x_-	phase is connected to the negative potential
x_+	phase is connected to the positive potential
$\underline{x}$	space phasor, vector
x_d	real part of a space phasor in an arbitrary reference frame dq
x_d	real part of a space phasor in an arbitrary reference frame dq
x_e	field winding, electromagnetic
x_f	filter
x_H	high value of the prediction horizon
x_i	elements of a vector
x_{inv}	inverter quantity
x_k	discrete time point
x_L	load, low value of the horizon (prediction or control)
x_{Lim}	limit
$x_{\max}$	maximum value
x_m, x_{mech}	mechanical
x_p	permanent
x_q	imaginary part of a space phasor in an arbitrary reference frame dq
x_q	imaginary part of a space phasor in an arbitrary reference frame dq
x_U	phase U
x_u	high value of the control horizon
x_{uL}	low value of the control horizon
x_V	phase V
x_W	phase W
L_x	self-inductance
L_{xy}	mutual-inductance
x_α	real part of a space phasor in a coordinate frame fixed to the stator
x_β	imaginary part of a space phasor in a coordinate frame fixed to the

	stator
x_Σ	integration weight

Acronyms

AC	Alternating Current
ADC	Analog to Digital Converter
AlNiCo	Iron with Aluminum, Nickel, and Cobalt magnet
AP	Active voltage space Phasor
DAC	Digital to Analog Converter
DC	Direct Current
DTC	Direct Torque Control
DSP	Digital Signal Processor
EMI	Electromagnetic Interference
FOC	Field Oriented Control
FPGA	Field Programmable Gate Array
IGBT	Insulated Gate Bipolar Transistor
MIMO	Multiple Input Multiple Output
NdFeB	Neodymium-Iron-Boron magnet
PI	Proportional Integral (controller)
PID	Proportional Integral Derivative (controller)
PLC	Programmable Logic Control
PMSM	Permanent Magnet Synchronous Machine
PWM	Pulse Width Modulation
RHC	Receding-Horizon-Control
SISO	Single Input Single Output
$SmCo_5$	Samarium-Cobalt magnet
SPM	Space Phasor Modulation
VSI	Voltage Source Inverter
ZP	Zero voltage space phasor

1. INTRODUCTION

Electrical drives are key components in automated processes in all industries. For this reason in the past decades, many research efforts were dedicated towards their development or their control schemes covering a broad spectrum of different types of electrical machines and inverters.

Modern electrical drives feature a range of motion control functions and PLC functions that ease the realization of complex production machines. Besides, they are equipped with interfaces that allow the communication in networks of the factory automation and so their utilization as slaves in the sensor actuator level is possible, with all the advantages that are derived from this feature. Electrical drives not only allow the reduction of production time and effort but they also lead, if properly designed, to an increased efficiency of processes. The typical energy consumption of electrical machines in an industrialized country represent between 50% and 70% of the total electrical energy consumption. Therefore, the goal to save energy, by its rational utilization and by applying an adequate control strategy of the electrical machines in order to optimize the efficiency of the processes, is a very important task.

The research in electrical drives in the past years was aimed at the enhancement of the control characteristics and at making the system more user friendly. In the course of time the focus has changed from fundamental questions [1] [2] to more sophisticated methods especially those that can be realized without a mechanical sensor for the position of the shaft [3].

The present work is intended as a contribution in the area of predictive control of electrical drives, yet the control of electrical drives is a very mature area of electrical engineering and therefore totally new developments are rare in this field. Nevertheless, this work is motivated by the application of the predictive control theory to a given drive topology with the aim of elucidating the advantages or disadvantages of such a control strategy by examining the system under different aspects like reduction of the number of sensors, reduction of the computational effort and parameter adaption among others.

The predictive theory has existed for many decades [4] [5] but only in the last twenty years it has been widely developed and applied with good results e.g. in the chemical industry [6] [7].

Today in power electronics and drives, the predictive control has become an interesting topic of research. Detailed explanations about predictive control applied in electrical drives can be found in the fundamental literature [8] [9].

The predictive control theory can be applied in the field of electrical drives, for example for a permanent magnet synchronous machine (PMSM) with a filter as shown in this work. Within this control scheme a cost function is defined. This function can be minimized according to given criteria in order to determine the voltage of the utilized inverter. In this way a modulator might not be necessary for the control of the inverter [10] [11], and depending on the realization not even a conventional control is used. Yet the mathematical task of minimization of the cost function can be cumbersome and time consuming.

The voltage source inverter (VSI) commonly used for feeding the electrical machine in electrical drives, generates steep voltage pulses, which can produce undesired or even hazardous effects like voltage stress in the machine insulations, excessive electromagnetic interference (EMI), bearing currents and torque pulsation, reducing thus the service life of the drive.

Thus, to avoid or to reduce these problems caused by these steep voltage pulses and to improve the service life of the electrical machine a low pass filter (LC-filter), also known as sine-wave filter, is used between the frequency converter and the machine. However, the disadvantages of the additional component are the extra cost, the increment of the installation space and the filter losses. Because of the use of the LC-filter, the order of the whole system is increased and more signals have to be known for the control. Due to cost, size and reliability issues, additional sensors are avoided but a Luenberger observer is used to obtain the signals that are not measured. Yet the observer demands the knowledge of all the system parameters.

The main objective of the present work is the examination of a simple approach that combines the advantages of the predictive control theory, the use of a LC-filter, the utilization of a conventional Pulse Width Modulation (PWM) and the use of the Runge-Kutta method for the digital implementation. The main idea is the definition of a virtual multilevel inverter, which discretizes the entire voltage plane in a finite number of points given by the number of levels of the virtual inverter. This procedure allows a very easy minimization of the cost

function by keeping an adjustable resolution of the output voltage but dramatically reduces the computational effort.

To complement and to improve the proposed predictive control strategy, a sensorless operation, as well as a parameter identification and adaptive parameter tuning procedures are included. Both, sensorless operation and parameter identification procedure are based on the voltage model of the machine. In this way, the reliability of the system is improved and the control robustness is enhanced.

The specific state of the art is discussed at the beginning of each chapter of the work. Regarding fundamental works, Steinke in [12] and Salomäki in [13] describe in detail the different possibilities of topologies for 3-phase sine-wave filters (LC-filters) and also a conventional field oriented control for the whole system "LC-Filter-Electrical Machine". Another application for the same system is analyzed by Szczupak, et al. in [14] but in this case he investigated the parameter identification in the frequency domain. As the LC-filter also introduces delays to the system, Mastellone, et al. in [15] propose an indirect predictive control by means of the so called virtual inverter-torque and –flux. Rodriguez, et al. in [8] propose a predictive control with a finite control set without modulator, i.e. under the direct torque control scheme. In contrast, other authors like Morari [16] [17], et al. propose a predictive control with a continuous control set with modulator, i.e. under the field oriented control scheme. Departing from this well-known state of the art, the present work analyzes the system inverter-LC-filter-PMSM and tries to enhance the control by reducing the computational effort in case of a predictive control with an infinite control set. In addition the predictive control structure is combined with a sensorless control scheme and an on-line adaption of the system parameters as a contribution to the state of the art.

The structure of this works is as follows: in the chapter 1, the motivation of the work and the aim of the work are described. In chapter 2, the theoretical fundamentals about the space phasor theory, coordinate transformation, synchronous machine and permanent magnet synchronous machine, control schemes for the PMSM, voltage source inverter, space phasor modulation and the pulse width modulation are summarized. In chapter 3, the predictive control principle, the application of the predictive control to power converter and control drives, the system PMSM-LC filter, the Runge-Kutta numerical integration, the control strategy of the predictive control for the system PMSM-LC filter are presented. For the minimization of the cost function for the proposed predictive control strategy, the virtual

multilevel inverter and the mesh with voltage space phasor close to the ideal are described. The inverter voltage constrains and enhanced cost functions are presented as well. In chapter 4, the sensorless operation as well as the parameter identification and adaptive parameter tuning procedures are proposed. Chapter 5 contains exemplary some of the experimental results that were obtained to validate the proposed predictive control strategy as well as the sensorless operation and the parameter identification and adaptive parameter tuning.

2. THEORETICAL FUNDAMENTALS

2.1. The Space Phasor

The formal space phasor theory was firstly introduced by K. P. Kovács [18] in the fifties of the last century. After that it was further developed by Stepina [19] and Serrano-Iribarnegaray [20], and considered as a standard theory in the German literature in the seventies and eighties of the last century. The space phasor theory is a useful and powerful tool for the description of the dynamic behavior of three-phase AC machines [21].

The space phasor is a complex function that summarizes the instantaneous value of three-phase quantities. The great advantage of working with instantaneous values is that the analysis of the machine is not only restricted to steady-state but also it is valid for the transient-states and non-sinusoidal analysis and therefore it is suitable for the modelling of the AC-machines and inverters [22].

The space phasor theory is based on the idea that the revolving field generated by currents in a symmetrical spatially distribute winding can be represented by a space phasor pointing to the maximum of the wave of the magnetic flux density. Similar to a vector, the space phasor takes into account both the temporal and the spatial location of a physical quantity, in this specific case of a magnetic quantity. The space phasor theory can be extended to other electrical and magnetic quantities in the AC-machine i.e. fluxes, currents and voltages [21].

In general, the instantaneous values $r_U(t)$, $r_V(t)$ and $r_W(t)$ of a three-phase quantity r can be summarized in the space phasor $\underline{r}(t)$ as follow:

$$\underline{r}(t) = \frac{2}{3}\left(\underline{a}^0 \cdot r_U(t) + \underline{a}^1 \cdot r_V(t) + \underline{a}^2 \cdot r_W(t)\right) \cdot e^{j\gamma_i} \tag{2.1}$$

where

$$\underline{a} = e^{j\frac{2\pi}{3}} = -\frac{1}{2} + j\frac{\sqrt{3}}{2} \tag{2.2}.$$

For stator quantities the angle is $\gamma_i = \gamma_1$ and for rotor quantities $\gamma_i = \gamma_2$. So, the stator current space phasor can be defined as:

$$\underline{i}_1 = \frac{2}{3}\left(i_{1U}(t) + \underline{a}\cdot i_{1V}(t) + \underline{a}^2\cdot i_{1W}(t)\right)\cdot e^{j\gamma_1} \tag{2.3}$$

In this space phasor it is necessary to include the definition of the angle γ_1, which is the position of the axis of the stator winding U with regard to a given reference frame. Often, $\gamma_1 = 0$ is selected, then (2.3) can be rewritten as:

$$\underline{i}_1 = \frac{2}{3}\left(i_{1U} + \underline{a}\cdot i_{1V} + \underline{a}^2\cdot i_{1W}\right) \tag{2.4}$$

The coefficient $2/3$ is introduced to scale the length of the space phasor to the correspondent amplitude $\hat{}$ of the phase current in a symmetric sinusoidal system.

In general, the winding of a conventional three-phase AC machine is either delta-connected or star-connected but with isolated neutral point. Thus, it is assumed that the zero sequence disappears:

$$i_{1U} + i_{1V} + i_{1W} = 0 \tag{2.5}$$

The instantaneous values in each phase can be obtained by mean of the projection of the space phasor to the corresponding axis:

$$\begin{aligned} i_{1U} &= \mathrm{Re}\left\{\underline{i}_1\right\} \\ i_{1V} &= \mathrm{Re}\left\{\underline{i}_1\cdot\underline{a}^{-1}\right\} \\ i_{1W} &= \mathrm{Re}\left\{\underline{i}_1\cdot\underline{a}^{-2}\right\} \end{aligned} \tag{2.6}$$

Fig. 2.1 shows a representation of the stator current space phasor for a symmetric sinusoidal system ($i_U = \hat{}$ $\hat{}$ $\hat{}$. The space phasor is a complex function with time dependent real and imaginary parts and it is referred to a given complex plane, whose orientation in the space has to be defined. One common frame of coordinates is defined by orienting the real axis in the direction of the axis of first-winding (U-winding in the case of the UVW three-phase AC system) of the stator. This reference frame is known as stator-fixed coordinate system and the real and the imaginary axis are designed as alpha and beta axis respectively.

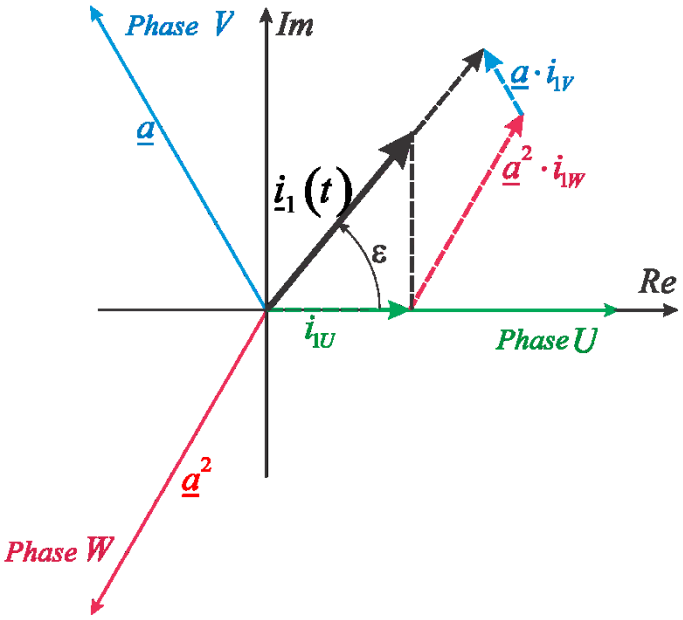

Fig. 2.1. Graphic representation of the stator current space phasor for $\omega t = \varepsilon = 50°$

So, for the current space phasor in this frame of coordinates can be written:

$$\underline{i}_1 = \frac{2}{3}\left(i_{1U} + \underline{a}\cdot i_{1V} + \underline{a}^2\cdot i_{1W}\right) = i_{1\alpha} + j\cdot i_{1\beta} \tag{2.7}$$

with:

$$\begin{aligned}
i_{1\alpha} &= \mathrm{Re}\{\underline{i}_1\} \\
i_{1\alpha} &= \mathrm{Re}\left\{\frac{2}{3}\left(i_{1U} + \underline{a}\cdot i_{1V} + \underline{a}^2\cdot i_{1W}\right)\right\} \\
i_{1\alpha} &= \mathrm{Re}\left\{\frac{2}{3}\left(i_{1U} + \left(-\frac{1}{2} + j\frac{\sqrt{3}}{2}\right)\cdot i_{1V} + \left(-\frac{1}{2} - j\frac{\sqrt{3}}{2}\right)\cdot i_{1W}\right)\right\} \\
i_{1\alpha} &= \frac{2}{3}\left(i_{1U} - \frac{1}{2}\left(i_{1V} + i_{1W}\right)\right) \\
i_{1\alpha} &= i_{1U}
\end{aligned} \tag{2.8}$$

and

$$
\begin{aligned}
i_{1\beta} &= \mathrm{Im}\left\{\underline{i}_1\right\} \\
i_{1\beta} &= \mathrm{Im}\left\{\frac{2}{3}\left(i_{1U} + \underline{a}\cdot i_{1V} + \underline{a}^2\cdot i_{1W}\right)\right\} \\
i_{1\beta} &= \mathrm{Im}\left\{\frac{2}{3}\left(i_{1U} + \left(-\frac{1}{2} + j\frac{\sqrt{3}}{2}\right)\cdot i_{1V} + \left(-\frac{1}{2} - j\frac{\sqrt{3}}{2}\right)\cdot i_{1W}\right)\right\} \\
i_{1\beta} &= \frac{2}{3}\left(\frac{\sqrt{3}}{2}i_{1V} - \frac{\sqrt{3}}{2}i_{1W}\right) \\
i_{1\beta} &= \frac{1}{\sqrt{3}}\left(i_{1V} - i_{1W}\right)
\end{aligned}
\tag{2.9}
$$

(2.8) and (2.9) are valid under the assumption of (2.5), i.e. a system without zero sequence. Thus $i_{1\alpha}$ and $i_{1\beta}$ can always be reduced to a function of just two phase currents of the three-phase system.

$i_{1\alpha}$ and $i_{1\beta}$ can be understood as the instantaneous currents in an equivalent two orthogonal phase winding that establish the same mmf-wave as the three-phase windings. From this point of view, (2.8) and (2.9) implies a three-phase to a two-phase transformation of variables with the α-phase of the equivalent two-phase machine coincident with the *U*-phase of the three-phase machine.

Conversely, the instantaneous values of the phase quantities associated with the stator current space phasor obtained by the projection of $\underline{i}_1$ on the three-phase axes described by (2.6), this can also be expressed as function of the current components $i_{1\alpha}$ and $i_{1\beta}$:

$$
\begin{aligned}
i_{1U} &= \mathrm{Re}\left\{\underline{i}_1\right\} = i_{1\alpha} \\
i_{1V} &= \mathrm{Re}\left\{\underline{i}_1\cdot\underline{a}^{-1}\right\} = -\frac{1}{2}\cdot i_{1\alpha} + \frac{\sqrt{3}}{2}\cdot i_{1\beta} \\
i_{1W} &= \mathrm{Re}\left\{\underline{i}_1\cdot\underline{a}^{-2}\right\} = -\frac{1}{2}\cdot i_{1\alpha} - \frac{\sqrt{3}}{2}\cdot i_{1\beta}
\end{aligned}
\tag{2.10}
$$

The equations from (2.8) until (2.10) are valid also for other electrical or magnetic quantities like for example voltage $\underline{u}$, flux linkages $\underline{\psi}$, magnetic flux density $\underline{B}$, mmf $\underline{\theta}$, etc.

An alternative description of the same phenomena using waves or vectors is actually possible yet it yields to more complex and less understandable equations.

2.2. Coordinate Transformations

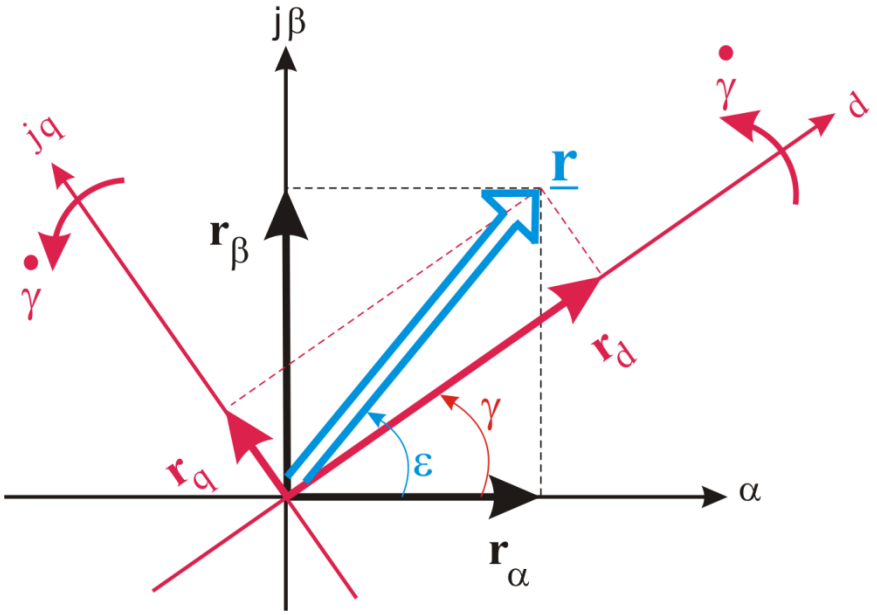

Fig. 2.2. Transformation of the space phasor $\underline{r}$ from fixed $\alpha,\beta-$ to $d,q-$reference frame

The space phasors can be also represented in an arbitrary frame of coordinates. For a general space phasor $\underline{r}$ referred to a stator-fixed system of coordinates α,β, can be transformed into a new arbitrary reference frame d,q, where γ is the angle between the real axis α of the fixed system and the real axis of the new system of coordinates and can vary with the time $\gamma(t)$ (see Fig. 2.2).

In such a case, and by taking into account the rotation of the system, the following relations hold: $r_\alpha + j\cdot r_\beta = \underline{r}\cdot e^{j\varepsilon}$ and $r_d + j\cdot r_d = \underline{r}\cdot e^{j(\varepsilon-\gamma)}$ so that, the transformation from the two-phase α,β reference frame to the two-phase dq reference frame is as follows:

$$\begin{aligned}\left(r_\alpha + j\cdot r_\beta\right) &= \left(r_d + j\cdot r_q\right)\cdot e^{j\gamma}\\ \left(r_\alpha + j\cdot r_\beta\right) &= \left(r_d + j\cdot r_q\right)\cdot\left(\cos(\gamma) + j\cdot\sin(\gamma)\right)\\ \left(r_\alpha + j\cdot r_\beta\right) &= \left(r_d\cdot\cos(\gamma) - r_q\cdot\sin(\gamma)\right) + j\cdot\left(r_d\cdot\sin(\gamma) + r_q\cdot\cos(\gamma)\right)\end{aligned} \quad (2.11).$$

And inversely
$$\left(r_d + j\cdot r_q\right) = \left(r_\alpha + j\cdot r_\beta\right)\cdot e^{-j\gamma} \quad (2.12).$$

Comparing real and imaginary terms in (2.11), the matrix notation can be expressed as:

$$[r]_{\alpha\beta} = [T][r]_{dq} \quad (2.13)$$

where

$$[r]_{\alpha\beta} = \begin{bmatrix} r_\alpha \\ r_\beta \end{bmatrix} \quad (2.14)$$

$$[r]_{dq} = \begin{bmatrix} r_d \\ r_q \end{bmatrix} \quad (2.15)$$

and
$$[T] = \begin{bmatrix} \cos(\gamma) & -\sin(\gamma) \\ \sin(\gamma) & \cos(\gamma) \end{bmatrix} \quad (2.16).$$

The inverse transformation of (2.13) is calculated as:

$$[r]_{dq} = [T]^{-1}\cdot[r]_{\alpha\beta} \quad (2.17).$$

The operation of coordinate transformation is also known as vector-rotation and is represented often by the symbols shown in Fig. 2.3.

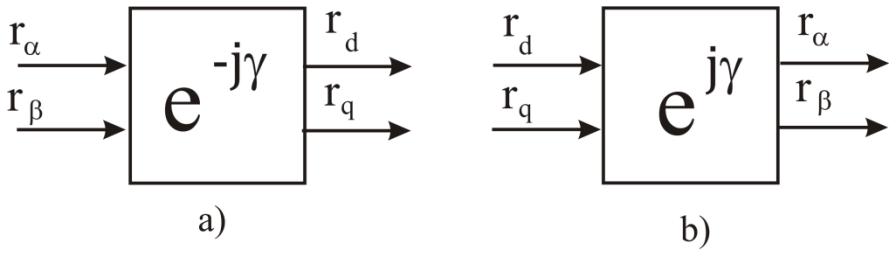

Fig. 2.3. Symbols for the transfer element “vector-rotation”

The transformation of a three-phase system to an orthogonal two-phase $\alpha,\beta-$coordinate system can be described by the following expression (symbol is shown in Fig. 2.4):

$$\begin{bmatrix} r_\alpha \\ r_\beta \end{bmatrix} = \frac{2}{3}\begin{bmatrix} 1 & -\frac{1}{2} & -\frac{1}{2} \\ 0 & \frac{\sqrt{3}}{2} & -\frac{\sqrt{3}}{2} \end{bmatrix} \cdot \begin{bmatrix} r_U \\ r_V \\ r_W \end{bmatrix} = \begin{bmatrix} 1 & 0 & 0 \\ 0 & \frac{\sqrt{3}}{3} & -\frac{\sqrt{3}}{3} \end{bmatrix} \cdot \begin{bmatrix} r_U \\ r_V \\ r_W \end{bmatrix} \tag{2.18}$$

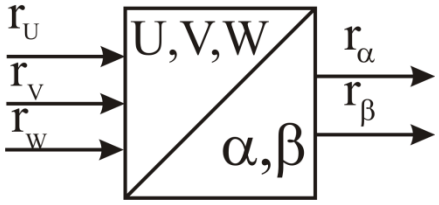

Fig. 2.4. Symbol for the transfer element "$\mathrm{UVW}-\alpha,\beta$ - coordinate transformation"

In opposite way the symbol (Fig. 2.5) and the expression of the transformation from an orthogonal two-phase α,β - system to a three-phase system is the following:

$$\begin{bmatrix} r_U \\ r_V \\ r_W \end{bmatrix} = \begin{bmatrix} 1 & 0 \\ -\frac{1}{2} & \frac{\sqrt{3}}{2} \\ -\frac{1}{2} & -\frac{\sqrt{3}}{2} \end{bmatrix} \begin{bmatrix} r_\alpha \\ r_\beta \end{bmatrix} \tag{2.19}$$

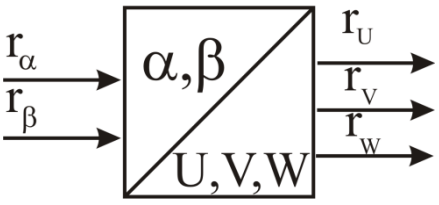

Fig. 2.5. Symbol for the transfer element "$\alpha,\beta-\mathrm{UVW}-$coordinate transformation"

2.3. Synchronous Machine

2.3.1. Introduction

Like all rotating machines, the synchronous machines are composed of two parts: the stator and the rotor. In the stator a symmetrical distributed three-phase winding is placed, whereas in the rotor a field or excitation winding or permanent magnets are located [23]. Additionally the rotor can be equipped with the so-called cage-damper winding, which exhibits a similar construction to the squirrel-cage in an asynchronous machine and serves to damp oscillations that occur during the operation when grid connected.

Synchronous machines are found in a wide spectrum of applications, from electrical energy generation in power stations to small power devices. With the development of the magnetic materials, of the power electronics and of the signal processing in digital systems, permanent magnet synchronous machines (PMSM) are used today in many applications as they exhibit several good characteristics, like high torque-density and a very good dynamic performance due to low inertia, compared to other machines. Therefore, the PMSM is primarily used in industrial servo-drive applications but also in other applications like electrical vehicles.

In the present work a PMSM is considered, whose construction and mathematic description will be explained in the following chapters.

2.3.2. Magnets for Permanent-Magnet-Synchronous-Machine

For the excitation of PMSM the following magnetic materials can be utilized:

- AlNiCo (alloy of iron with aluminum, nickel, and cobalt)
- Ferrite
- Rare-earth magnets like Samarium-Cobalt ($SmCo_5$) and Neodymium-Iron-Boron (NdFeB)

Fig. 2.6 shows the second quadrant of the magnetization characteristic curve of these materials. As depicted the magnetic material AlNiCo presents a high remanence but a small coercive field strength, because of this AlNiCo is suitable for applications with relatively small opposing demagnetizing field. - This material is used since the end of the seventies as substitute for the hard ferrite materials.

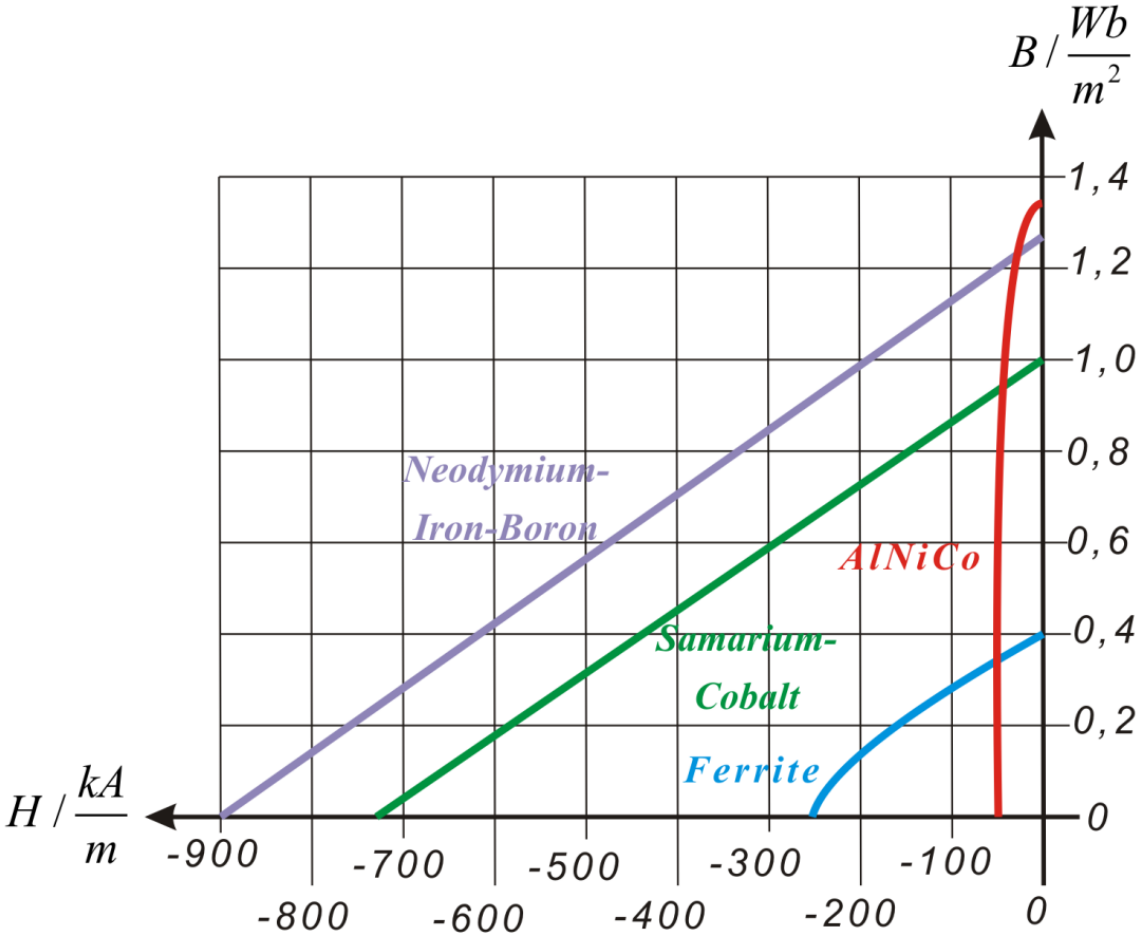

Fig. 2.6. Magnetization characteristic curve of different magnetic materials

Ferrite material presents obviously large coercive field strength in comparison with AlNiCo, but needs small remanence inductions which lead into a big volume of the machine. The advantage of the ferrite material is the cost as well as the large specific resistance value, which evolves into a small development of Eddy-currents. Ferrite materials are used in DC-actuators for example in the automobile industry (windscreen wiper motors, windows lift motors, seats adjustment motors, etc. and for the fan motors). The low torque density of the motors with ferrite materials is compensated by their low costs in some applications.

Samarium-Cobalt presents better magnetic characteristics, therefore the volume of the machines with these materials is small and they exhibit a lower moment of inertia. Many years ago, machines with SmCo magnets in the rotor were used. In the last years they were substituted with Neodymium-Iron-Boron magnets, which present also good magnetic characteristics but a lower cost in comparison with Samarium-Cobalt. The negative aspects of the Neodymium-Iron-Boron are the temperature-sensitivity and that they easily corrode.

2.3.3. Type of Construction of the Rotor of Permanent Magnet Synchronous Machines

Exist different types of construction of the rotor of the PMSM (see Fig. 2.7), which can be described as:

a) Rotor with interior recumbent radial magnet (interior-magnet rotor)
b) Rotor with surface mounted magnets
c) Rotor with interior recumbent tangential magnets (buried-magnet-rotor)

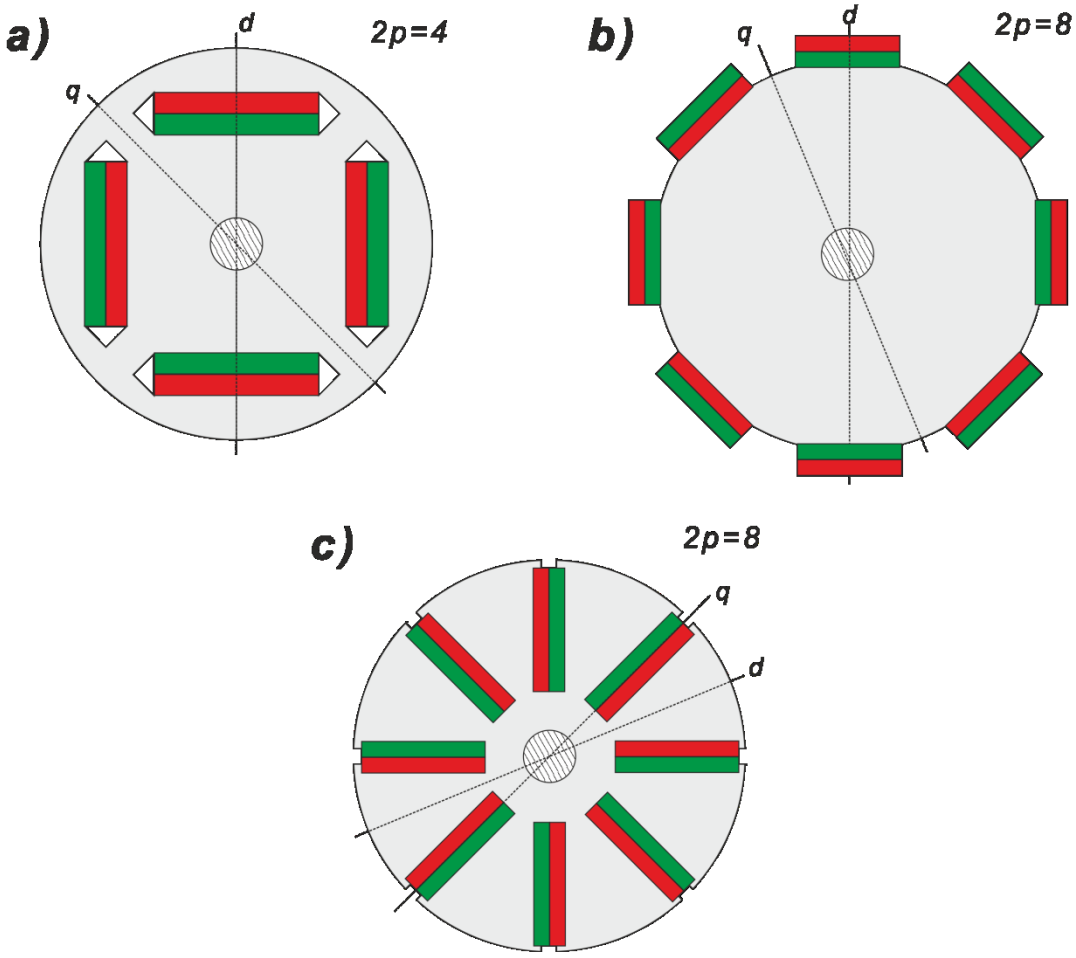

Fig. 2.7. Types of rotors for the PMSM

a) Rotor with interior recumbent radial magnet (interior-magnet rotor)

The rotor with interior recumbent radial magnet (interior-magnet rotor) presents a radial magnetization and the polarity depends on each magnet (see Fig. 2.7a). As the area of the magnet is small with respects to the area of the pole in the rotor surface, the magnetic flux density in the air gap is also small. The advantage of this type of rotor construction is the

robustness against centrifugal forces, thus these are used in high speed applications. Besides from this advantage, the field weakening operation is easier to achieve.

b) Rotor with surface mounted magnets

An easy and low-cost type of rotor construction is depicted in Fig. 2.7b, in which the magnets are placed on the rotor surface, therefore this type of machines are used in servo applications.

The magnetic resistance in the *d*- and *q*-direction are practically the same because, for the relative permeability to be valid it is assumed that:

$$\mu_{r,air} \approx \mu_{r,NdFeB} \approx \mu_{r,SmCo_5} \ll \tag{2.20}$$

By assuming a uniform air-gap the inductances in the direction *d* and *q* are also the same. These facts are used to simplify the mathematical model of this type of PMSM.

c) Special type of construction

For the case of the buried-magnet-rotors as shown in Fig. 2.7c, the permanent magnets are enclosed in deep slots. In contrast with the surface mounted magnets rotors, the buried-magnet-rotors magnetization is tangential and the rotor is anisotropic regarding its magnetics properties.

2.3.4. Model of the Synchronous Machine

The dynamic performance of a three-phase AC machine can be described by a system of ordinary differential equations that can be simplified by using the theory of space phasors explained in the chapter 2.1.

For the modelling of the synchronous machine, the following assumptions can be made:

- a two pol machine is assumed, the extension to a machine with more poles will be considered through the number of pol pairs in the latter equations
- the stator is equipped with a symmetrical distributed three-phase winding
- the stator winding is either delta or star connected with isolated neutral point, i.e. the zero sequence component does not exist
- the Eddy currents, the skin effect and the core losses are neglected in the stator as well as in the rotor of the machine

- the coil resistances are considered to be constant
- the influence of the temperature on the machine parameters as well as on the demagnetization are not taken into account
- the rotor parameters are related to the stator side
- the higher order harmonics in the air gap field are neglected and only the fundamental wave is considered in the calculation of the inductances

Fig. 2.8-2.10 show the models of a simplified two poles synchronous machine in different systems of coordinates. In all these models the rotor is supposed to have a field or excitation winding, and damper winding or a damper cage. The symmetrical damper winding is substituted in the model by a system of two orthogonal arranged short-circuited windings D and Q. Fig. 2.8 shows a representation of the synchronous machine in the three-phase UVW system. This three-phase system can be also represented by an equivalent system of two orthogonal windings α, β .

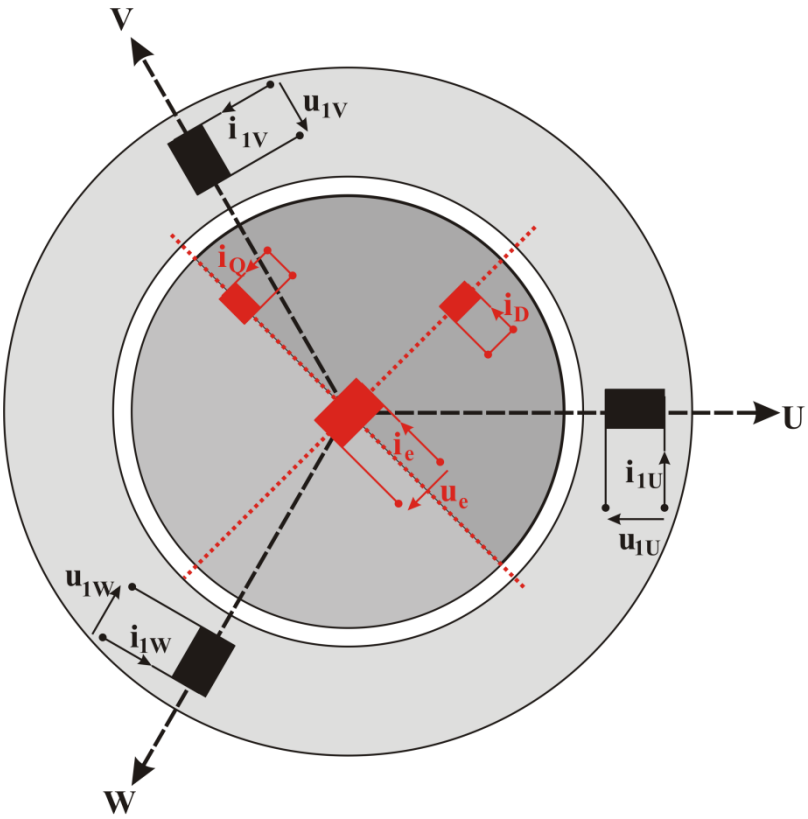

Fig. 2.8. Two-pole model of the synchronous machine in the three-phase UVW system

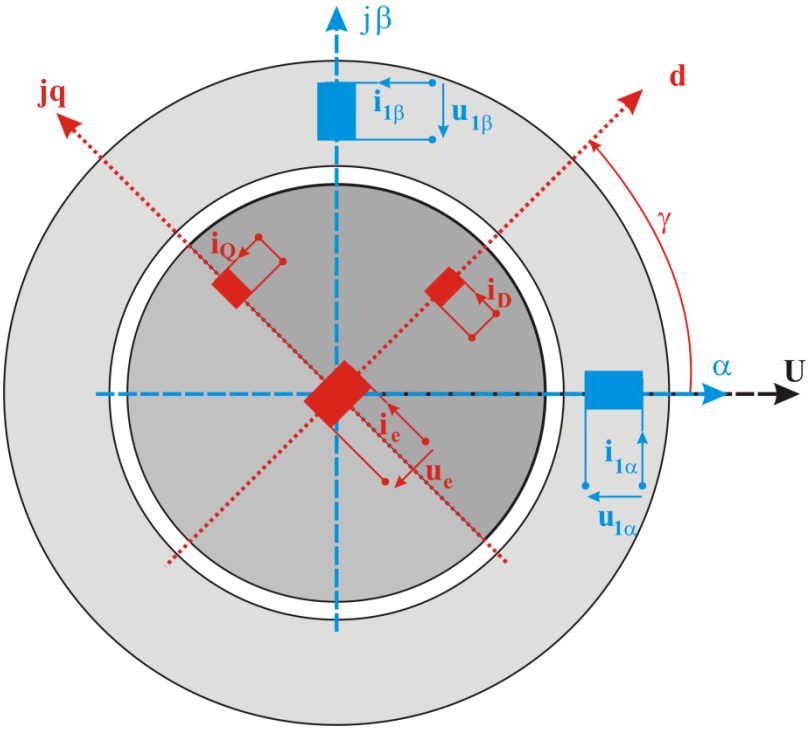

Fig. 2.9. Two-pole model of the synchronous machine in the α, β – coordinate system

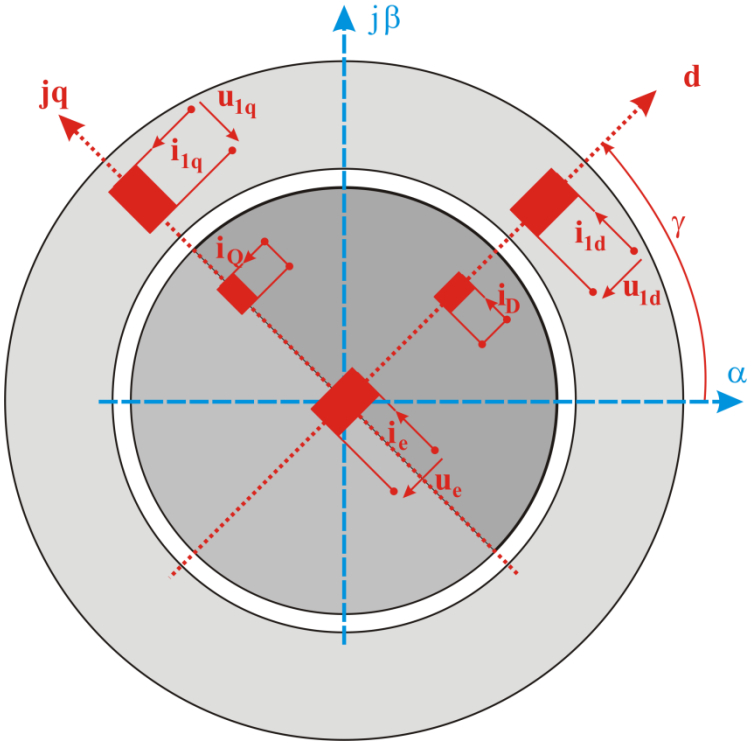

Fig. 2.10. Two-pole model of the synchronous machine in the d, q – coordinate system

The model representation of the synchronous machine in an $\alpha,\beta-$system of coordinates is shown in Fig. 2.9, in which the relative position of the rotor windings related to the $\alpha,\beta-$ stator coordinates is given by the angle γ. In the model the stator winding can be represented by an equivalent system of orthogonal windings in a reference frame d,q (see Fig. 2.10), in which the fictitious winding *d* and *q* are aligned with the axis of the field winding of the rotor. The transformation expressions between both coordinate systems were already explained in the chapter 2.2.

In the following all equations will be referred to the $d,q-$system of coordinates as it is well-known from the fundamental literature [24] [25] [1].

The voltage expressions for the synchronous machine are given by:

$$u_{1d} = R_1 \cdot i_{1d} + \frac{d\psi_{1d}}{dt} - \frac{d\gamma}{dt} \cdot \psi_{1q} \tag{2.21}$$

$$u_{1q} = R_1 \cdot i_{1q} + \frac{d\psi_{1q}}{dt} + \frac{d\gamma}{dt} \cdot \psi_{1d} \tag{2.22}$$

$$u_e = R_e \cdot i_e + \frac{d\psi_e}{dt} \tag{2.23}$$

$$0 = R_D \cdot i_D + \frac{d\psi_D}{dt} \tag{2.24}$$

$$0 = R_Q \cdot i_Q + \frac{d\psi_Q}{dt} \tag{2.25}$$

Where u_{1d} and u_{1q}, i_{1d} and i_{1q} and ψ_{1d} and ψ_{1q} are respectively the real and imaginary components of the stator voltages, stator currents and fluxes-linkage space phasors; R_1 is the stator winding resistance; u_e, i_e and ψ_e are respectively the field voltage, field current and flux-linkage space phasors; R_e is the excitation winding resistance; i_D and i_Q, ψ_D and ψ_Q are respectively the real and imaginary components of the damper-currents and -fluxes-linkage space phasors; and R_D and R_Q are respectively the resistance of the damper winding D and Q.

Due to the fact that the $d,q-$axis are orthogonal, a magnetic coupling between the *d*- and *q*-variables does not exist, however there is magnetic coupling among the coils of the windings in stator of rotor that are located in the same axis as it is shown in Fig. 2.11.

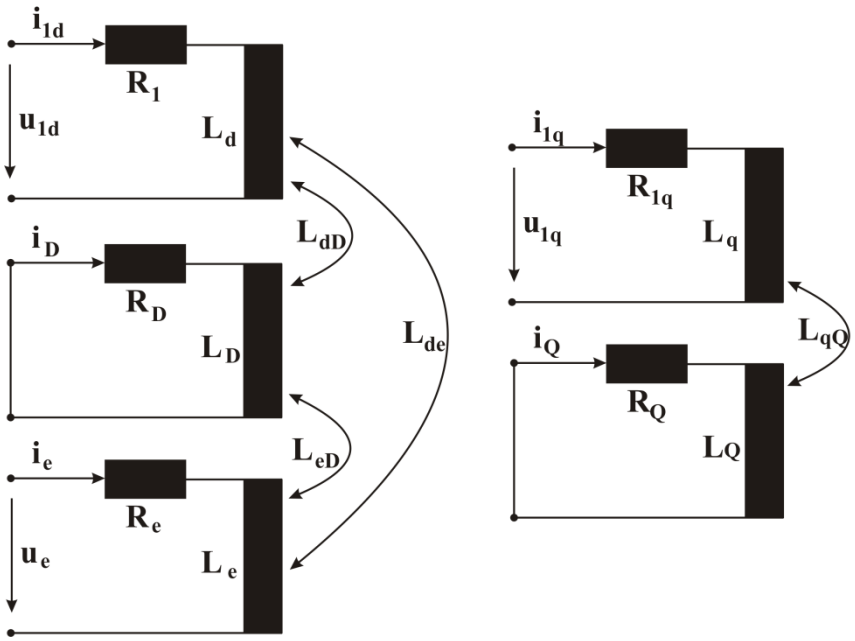

Fig. 2.11. Flux linkages in *d*- and *q*-axis

So the expressions for the flux linkages are given by:

$$\psi_{1d} = L_d \cdot i_{1d} + L_{dD} \cdot i_D + L_{de} \cdot i_e \tag{2.26}$$

$$\psi_{1q} = L_q \cdot i_{1q} + L_{qQ} \cdot i_Q \tag{2.27}$$

$$\psi_e = L_e \cdot i_e + L_{de} \cdot i_{1d} + L_{eD} \cdot i_D \tag{2.28}$$

$$\psi_D = L_D \cdot i_D + L_{dD} \cdot i_{1d} + L_{eD} \cdot i_e \tag{2.29}$$

$$\psi_Q = L_Q \cdot i_Q + L_q \cdot i_{1q} \tag{2.30}$$

Where L_d, L_q, L_D, L_Q, L_e are the self-inductances and L_{dD}, L_{de}, L_{eD}, L_{qQ} are the mutual-inductances.

In addition to the electrical and magnetic variables already described, it is necessary to know the mechanical variables i.e. the rotor position and the angular velocity in order to complete the description of the system. As explained above, the angle between the axis α and the axis d is denoted by γ, and for a machine with p pairs of poles, the mechanical angle is defined as:

$$\gamma_{mech} = \frac{\gamma}{p} \tag{2.31}$$

The electrical and the mechanical angular velocity can be written as:

$$\frac{d\gamma}{dt} = \dot{\gamma} = \omega \tag{2.32}$$

$$\frac{d\gamma_{mech}}{dt} = \dot{\gamma}_{mech} = \omega_{mech} \tag{2.33}$$

$$\dot{\gamma}_{mech} = \frac{\dot{\gamma}}{p} \qquad \text{respectively} \qquad \omega_{mech} = \frac{\omega}{p} \tag{2.34}.$$

The electromagnetic developed torque can be expressed as [24]:

$$M_e = \frac{3}{2} \cdot p \cdot \mathrm{Im}\left\{\underline{\psi}_1^* \cdot i_1\right\} \tag{2.35},$$

or in the notation of $d-$ and $q-$components:

$$M_e = \frac{3}{2} \cdot p \cdot \mathrm{Im}\left\{\psi_{1d} \cdot i_{1q} - \psi_{1q} \cdot i_{1d}\right\} \tag{2.36}.$$

In order to have a full description of the machine, it is essential to know the relationship between the mechanical system and the electrical system given by:

$$M_e - M_L = J \cdot \frac{d\omega_{mech}}{dt} = J \cdot \frac{1}{p} \cdot \frac{d^2\gamma}{dt^2} = J \cdot \frac{1}{p} \cdot \ddot{\gamma} \tag{2.37}$$

where M_L is the load torque and J is the total moment of inertia of the motor and load, the friction is neglected.

Thus, the angle γ can be calculated by the integration of:

$$\ddot{\gamma} = p \cdot \frac{M_e - M_L}{J} \tag{2.38}$$

PMSM for servo applications are built in general without damper winding and the permanent magnets are located in the rotor, so the field winding in the rotor does not exist, in consequence (see Fig. 2.12):

$$\begin{aligned} L_D = L_Q = L_{dD} = L_{dQ} = L_{eD} = L_{eQ} = 0 \\ R_D = R_Q = R_e = 0 \end{aligned} \tag{2.39}$$

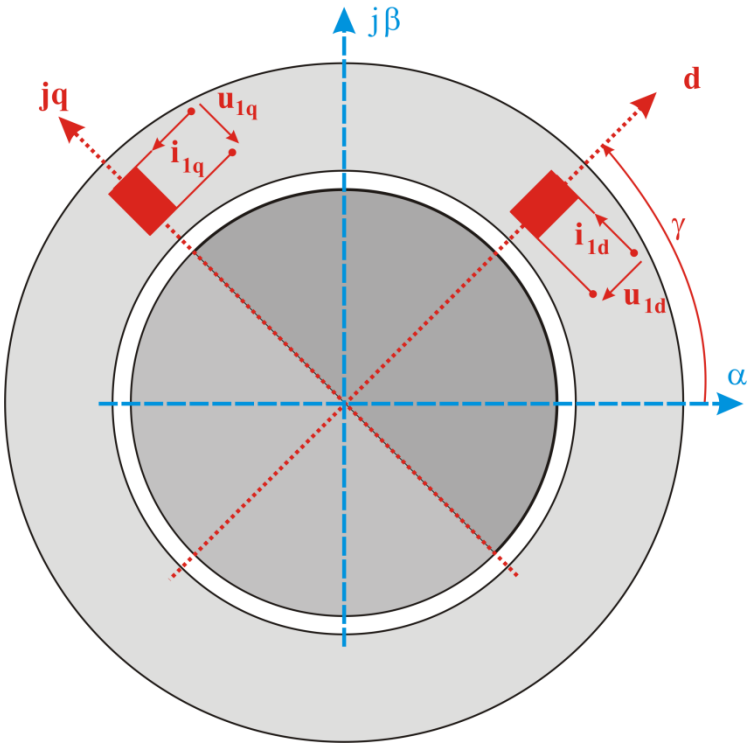

Fig. 2.12. Two-Phase model of the PMSM with non-salient-pole rotor

If a magnetic isotropic rotor of the PMSM is assumed, then L_{1d} (direct axis self-inductance) and L_{1q} (quadrature axis self-inductance) are equal, i.e. $L_{1d} = L_{1q} = L_1$.

The permanent magnet (denoted by ψ_{d0}) produces a flux in the d-axis of the rotor, which has to be added to the flux produced by the stator current in the same axis. Thus, the fluxes for a PMSM can be redefined as:

$$\psi_{1d} = L_1 \cdot i_{1d} + \psi_{d0} \tag{2.40}$$

$$\psi_{1q} = L_1 \cdot i_{1q} \tag{2.41}$$

Replacing (2.40) and (2.41) in the voltage equations of the machine, the equations that describe a PMSM are given by:

$$u_{1d} = R_1 \cdot i_{1d} + L_1 \cdot \frac{di_{1d}}{dt} - \dot{\gamma} \cdot L_1 \cdot i_{1q} \tag{2.42}$$

$$u_{1q} = R_1 \cdot i_{1q} + L_1 \cdot \frac{di_{1q}}{dt} + \dot{\gamma} \cdot L_1 \cdot i_{1d} + \dot{\gamma} \cdot \psi_{d0} \tag{2.43}$$

By using (2.40) and (2.41), the electromagnetic developed torque given by (2.36) can be rewritten as:

$$M_e = \frac{3}{2} \cdot p \cdot \left(\left(L_1 \cdot i_{1d} + \psi_{d0} \right) \cdot i_{1q} - L_1 \cdot i_{1d} \cdot i_{1q} \right) \tag{2.44}$$

$$M_e = \frac{3}{2} \cdot p \cdot \psi_{d0} \cdot i_{1q} \tag{2.45}$$

In case that the real component of the stator current $i_{1d} = 0$, the electromagnetic torque will depend only on the permanent magnet ψ_{d0} and on the imaginary current component i_{1q}, as described in (2.45). That is the basic principle for the field oriented control (FOC) for a synchronous machine, which will be explained in the following sections.

2.3.5. Model of the Synchronous Machine in the Stator-Fixed Coordinate System

An alternative reference frame to describe a synchronous machine is the stator-fixed $\alpha, \beta -$ system of coordinates, in which a direct control of the electromagnetic torque (Direct Torque Control: DTC) and of the stator flux by means of controlling the output voltage at an inverter is possible.

The voltage expressions for a three-phase PMSM in stator-fixed $\alpha, \beta -$ coordinate system are given by [25]:

$$u_{1\alpha} = R_1 \cdot i_{1\alpha} + \frac{d\psi_{1\alpha}}{dt} \tag{2.46}$$

$$u_{1\beta} = R_1 \cdot i_{1\beta} + \frac{d\psi_{1\beta}}{dt} \tag{2.47}$$

Applying the coordinate transformation explained in the chapter 2.2 to the equations (2.40) and (2.41), the flux linkages related to the $\alpha, \beta -$ coordinate system are given by:

$$\psi_{1\alpha} = L_1 \cdot i_{1\alpha} + \psi_{d0} \cdot \cos(\gamma) \tag{2.48}$$

$$\psi_{1\beta} = L_1 \cdot i_{1\beta} + \psi_{d0} \cdot \sin(\gamma) \tag{2.49}$$

From (2.48) and (2.49) is possible to describe the components of the permanent magnet flux in the $\alpha, \beta -$ coordinate system as:

$$\psi_{0\alpha} = \psi_{d0} \cdot \cos(\gamma) \tag{2.50}$$

$$\psi_{0\beta} = \psi_{d0} \cdot \sin(\gamma) \tag{2.51}$$

Thus, with (2.46)-(2.47) and (2.48)-(2.51), the expressions of the stator voltage can be rewritten as:

$$u_{1\alpha} = R_1 \cdot i_{1\alpha} + L_1 \cdot \frac{di_{1\alpha}}{dt} + \frac{d\psi_{0\alpha}}{dt} = R_1 \cdot i_{1\alpha} + L_1 \cdot \frac{di_{1\alpha}}{dt} - \frac{d\gamma}{dt} \cdot \psi_{d0} \cdot \sin(\gamma) \tag{2.52}$$

$$u_{1\beta} = R_1 \cdot i_{1\beta} + L_1 \cdot \frac{di_{1\beta}}{dt} + \frac{d\psi_{0\beta}}{dt} = R_1 \cdot i_{1\beta} + L_1 \cdot \frac{di_{1\beta}}{dt} + \frac{d\gamma}{dt} \cdot \psi_{d0} \cdot \cos(\gamma) \tag{2.53}$$

In the same way, simplifying (2.44) with (2.48)-(2.51), the expression for the electromagnetic torque in the $\alpha, \beta -$ coordinate system is given by:

$$\begin{aligned} M_e &= \frac{3}{2} \cdot p \cdot \frac{1}{L_1} \cdot \left\{ \psi_{1\beta} \cdot \psi_{d0} \cdot \cos\gamma - \psi_{1\alpha} \cdot \psi_{d0} \cdot \sin\gamma \right\} \\ M_e &= \frac{3}{2} \cdot p \cdot \frac{1}{L_1} \cdot \left\{ \psi_{1\beta} \cdot \psi_{0\alpha} - \psi_{1\alpha} \cdot \psi_{0\beta} \right\} \\ M_e &= \frac{3}{2} \cdot p \cdot \left\{ i_{1\beta} \cdot \psi_{0\alpha} - i_{1\alpha} \cdot \psi_{0\beta} \right\} \end{aligned} \tag{2.54}$$

Fig. 2.13 shows the position of the space phasors $\underline{\psi}_1$ and $\underline{\psi}_{d0}$ in the $\alpha,\beta-$plane. The angle between the α-axis and the stator flux $\underline{\psi}_1$ is denoted by φ and it is called the stator flux-angle. Using the trigonometric identity $\sin(\varphi-\gamma)=\sin(\varphi)\cdot\cos(\gamma)-\cos(\varphi)\cdot\sin(\gamma)$ on in the Fig. 2.13 and (2.54), is possible to describe the electromagnetic torque in another way as:

$$M_e=\frac{3}{2}\cdot p\cdot\frac{1}{L_1}\cdot\left|\underline{\psi}_1\right|\cdot\left|\underline{\psi}_{d0}\right|\cdot\sin(\vartheta) \tag{2.55}$$

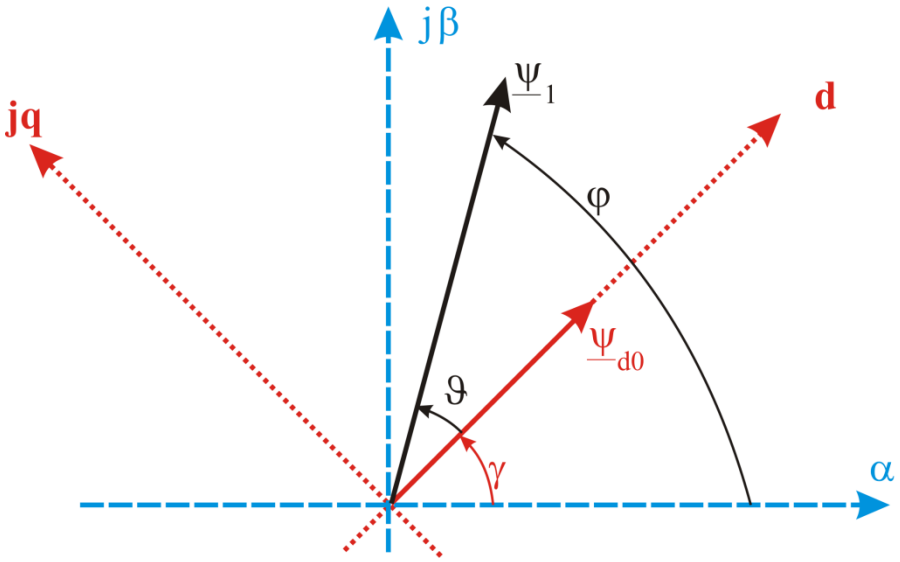

Fig. 2.13. Position of the space phasors $\underline{\psi}_1$ and $\underline{\psi}_{d0}$

Thus the electromagnetic torque depends on the magnitude of the stator- and of rotor-fluxes space phasors and the angle ϑ between both. That is the principle on which is based the "Direct Torque Control" theory for a PMSM [26].

Considering the voltage drop on the stator resistance to be negligible, the stator flux space phasor depend only on the applied stator voltage, i.e. the stator flux can be found by the integration:

$$\psi_{1\alpha}=\int\left(u_{1\alpha}-R_1\cdot i_{1\alpha}\right)dt \tag{2.56}$$

and

$$\psi_{1\phi}=\int\left(u_{1\beta}-R_1\cdot i_{1\beta}\right)dt \tag{2.57}.$$

Thus, the angle ϑ can be changed by the application of the proper stator voltage.

2.4. Control Schemes for the PMSM

Several control schemes for the PMSM have been proposed and are today well established, all with their advantages and disadvantages. Depending on their complexity the dynamical characteristics are different and an enhancement on the performance of the system usually implies a higher order of the system, the consideration of more physical effects and needs a higher computational effort of the control platform.

Most of the control schemes applied today in industrial drives are basically based on either the "Direct Torque Control"-principle (DTC) or the "Field Oriented Control"-principle (FOC).

2.4.1. Direct Torque Control Principle

The basic principle of the Direct Torque Control (DTC) consists in utilizing directly the output voltage of an inverter -and not indirectly through the currents- by selecting one of the possible space phasors (eight in the case of a two-level VSI) in order to keep the stator flux magnitude and the torque of the machine within the limits of their corresponding hysteresis bands as well as for achieving a high dynamic torque performance.

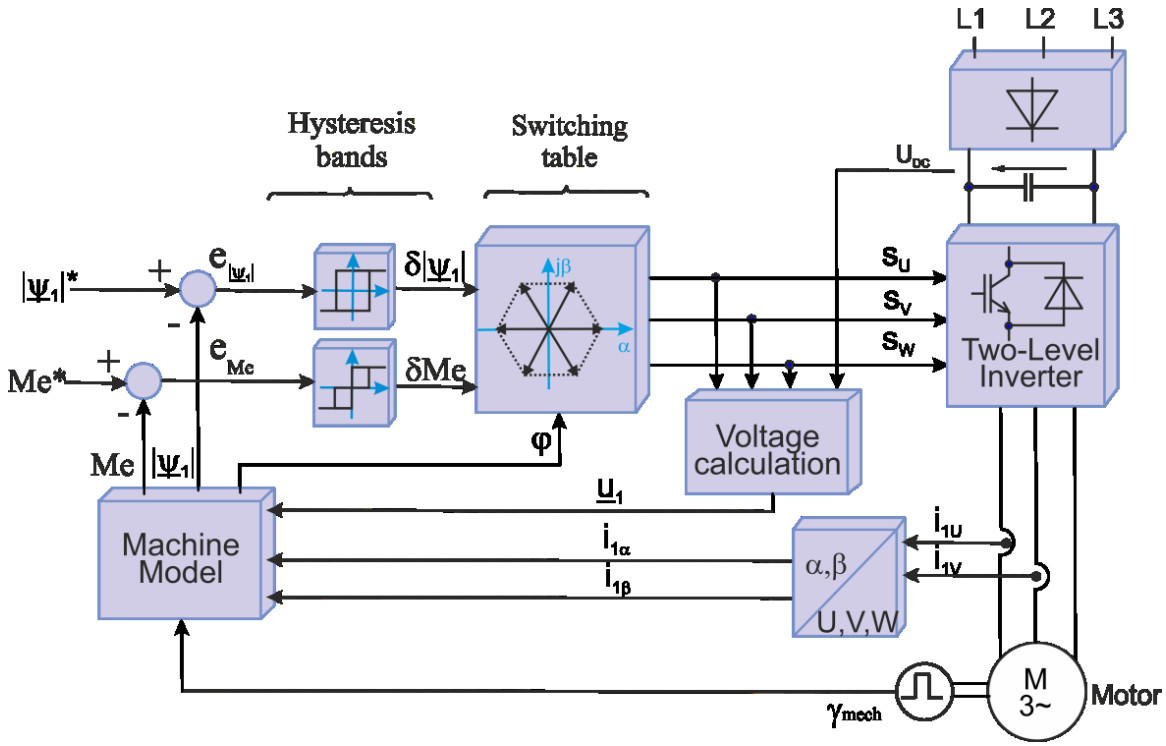

Fig. 2.14. Direct torque control scheme

A block diagram of a DTC-control is illustrated in Fig. 2.14. In the base-speed range, the reference value for the stator flux magnitude is set to its nominal value whereas the torque reference generally is obtained from a velocity controller. The reference values of the stator flux magnitude as well as the torque are compared with their actual values to obtain the corresponding control errors. Both, the torque and stator flux magnitude errors are processed in their hysteresis-band to obtain the discrete output values δM_e and $\delta\left|\underline{\psi}_1\right|$.

The discrete output values δM_e and $\delta\left|\underline{\psi}_1\right|$ of the hysteresis controller and the information of the angle φ, where the actual stator flux phasor is located, are used in a switching table to select the appropriate switching combination S_U, S_V, S_W to command the VSI.

In Fig. 2.15 the space phasor of the stator flux and of the permanent flux are shown in two different torque-operating points but with the same magnitude of the stator flux. The reactive power (caused by the current component i_d) differs in both cases. The ideal behavior without reactive power is consequently not possible for all torque-values under the constraint of constant stator flux magnitude. Thus, in order to achieve an optimal control, the stator flux reference must be adapted to the actual machine torque. This quiet complex procedure is avoided in the FOC by just controlling the current component i_d to zero.

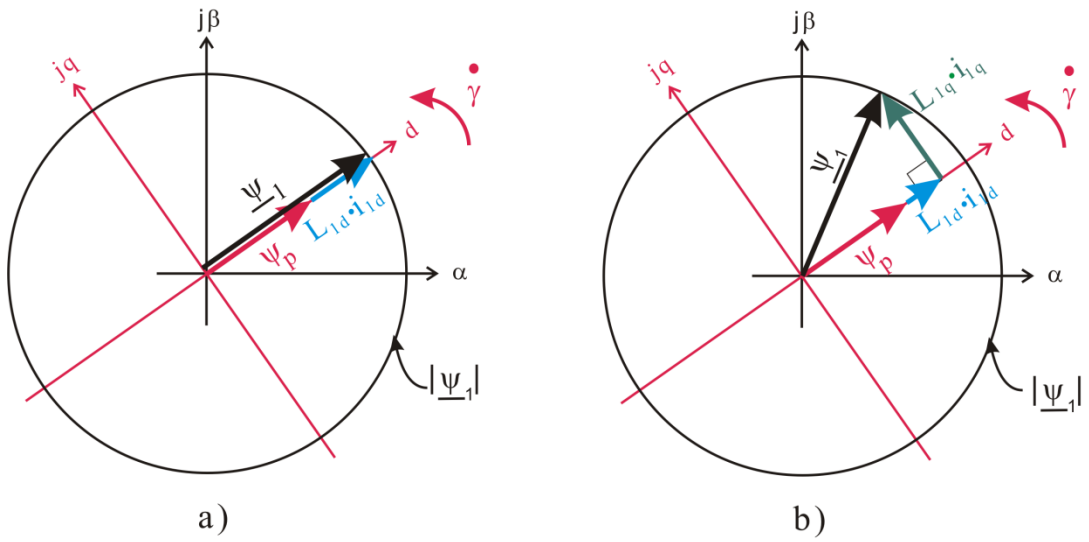

Fig. 2.15. a) Example of a stator flux space phasor for *Me*=0 b) and for *Me*≠0

2.4.2. Field Oriented Control Principle

The Field Oriented Control (FOC) principle was introduced by Blaschke [27] and Hasse [28]. The basic concept of this control is based on the advantage of working in the rotor-fixed $d,q-$ system of coordinates, where all variables become DC-quantities in steady state operation. Thus, the mathematic modelling is simplified and similar control strategies like the well-known ones for the DC-machine can be applied to the AC-machine as well.

Another advantage of the field oriented control is the simple relationship that results between i_{1d} and the magnitude of the flux space phasor $\left|\underline{\psi}_1\right|$ as well as between i_{1q} and the electromagnetic torque M_e. As stated above (2.45), the torque is given by $M_e = \frac{3}{2} \cdot p \cdot \psi_{d0} \cdot i_{1q}$ and depends only on the permanent magnet ψ_{d0} and on the imaginary current component i_{1q}, in case that the real component of the stator current $i_{1d} = 0$.

Thus, it is necessary to have a good dynamic performance of the current i_{1d}- and i_{1q}-controllers to achieve a good dynamic response of the electromagnetic torque by keeping the magnetic flux magnitude around the reference value.

The outputs of these current controllers (in i_{1d} and i_{1q}) are the reference voltages u_{1d} and u_{1q}, both are evaluated in a modulator to obtain the switching signals S_U, S_V, S_W that commands the VSI.

For the design of the current controllers, it is necessary to know the relationship between the stator voltage and the stator current. In the particular case of a PMSM, the relationships were explained by (2.42) and (2.43) and can be rewritten as:

$$u_{1d} = R_1 \cdot i_{1d} + L_1 \cdot \frac{di_{1d}}{dt} - \dot{\gamma} \cdot L_1 \cdot i_{1q} = R_1 \cdot i_{1d} + L_1 \cdot \frac{di_{1d}}{dt} + u_{rot,d} \tag{2.58}$$

$$u_{1q} = R_1 \cdot i_{1q} + L_1 \cdot \frac{di_{1q}}{dt} + \dot{\gamma} \cdot L_1 \cdot i_{1d} + \dot{\gamma} \cdot \psi_{d0} = R_1 \cdot i_{1q} + L_1 \cdot \frac{di_{1q}}{dt} + u_{rot,q} \tag{2.59}$$

As expressed by (2.58) and (2.59), there exists a coupling between both first-order differential equations, i.e. the equation of the stator voltage in each axis is coupled through a rotational voltage with its orthogonal axis stator voltage equation. Thus, the variables of coupling $u_{rot,d}$ and $u_{rot,q}$ are considered for the controllers as disturbances quantities.

For decoupling both stator voltage differential equations, the coupling variables $u_{rot,d}(t)$ and $u_{rot,q}(t)$ are computed by using the model of the machine and are added to the output of the current controllers. This way it is possible to design the current controllers without taking into account these disturbance voltages.

Fig. 2.16 shows the structure of the field oriented control. To realize the control, first it is necessary to measure the three-phase stator currents as well as the rotor position angle γ_{mech}. With this information and by using the coordinate transformation explained in the chapter 2.2, the currents i_{1d} and i_{1q} can be calculated. The current references i_{1d}* and i_{1q}* are compared with the actual measured currents i_{1d} and i_{1q}. In this way, the errors e_{i1d} and e_{i1q} are obtained. These errors are used in the current-controllers (PI-controllers), whose outputs are added to the quantities $u_{rot,d}$ and $u_{rot,q}$ resulting into the reference voltages u^*_{1d} and u^*_{1q} to be evaluated in the modulator after the coordinate transformations.

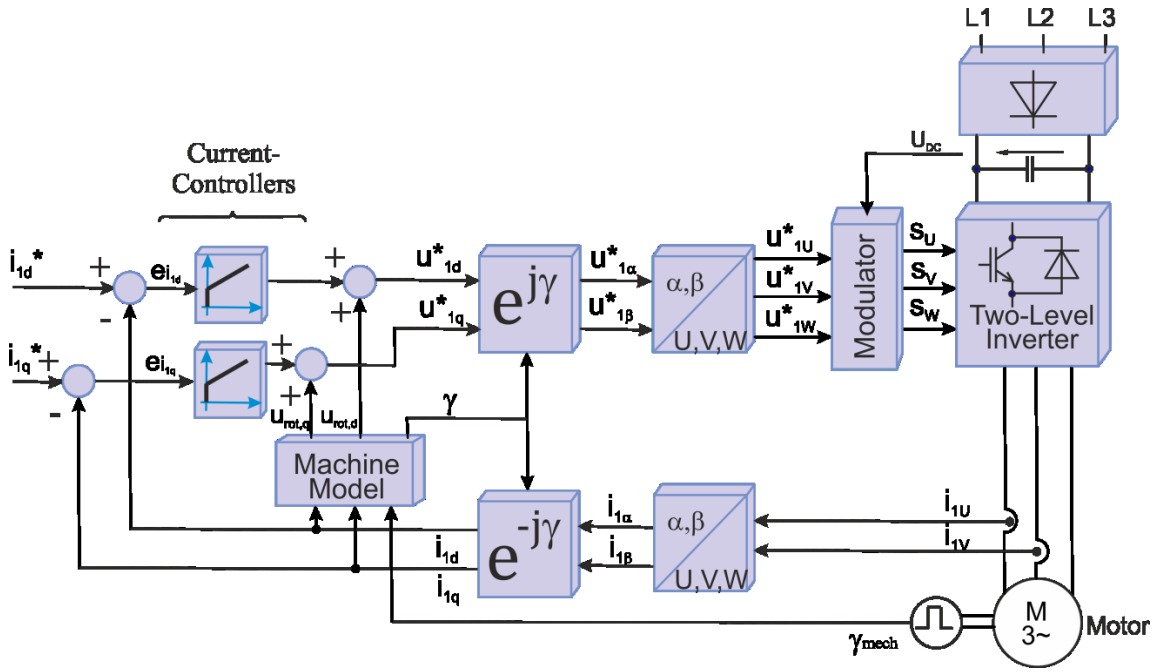

Fig. 2.16. Field oriented control Scheme

The reference value i_{1q}* is either obtained from a velocity controller or direct from a torque controller. The reference value i_{1d}* can be computed out of the desired magnetic flux magnitude. As a PMSM has a permanent magnet inside the rotor, is not necessary to generate an additional magnetic flux component from the stator side (like in the case of an IM). Therefore the reference value of i_{1d}* is generally set to zero.

2.5. Voltage Source Inverter

The power inverter that feeds an AC-Machine consists of two parts: a voltage DC-link and a three-phase Voltage Source Inverter (VSI) as illustrates Fig. 2.17.

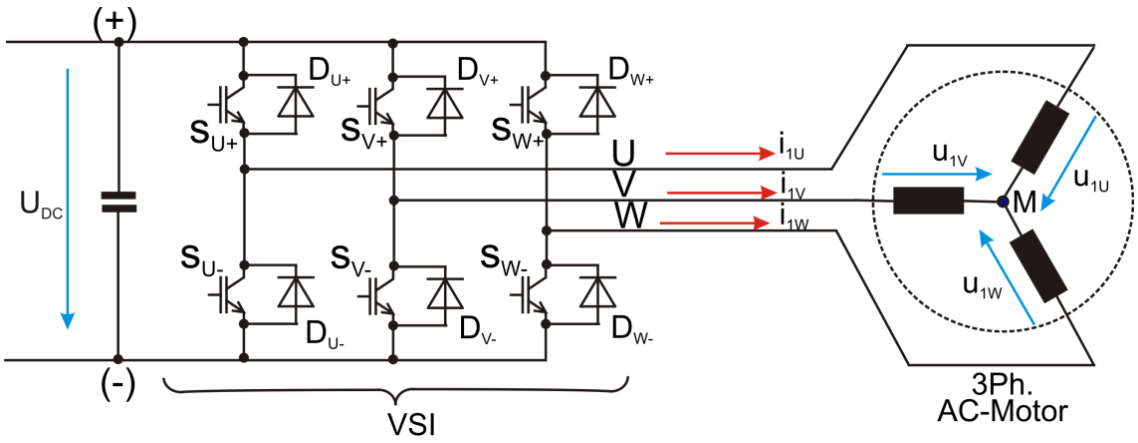

Fig. 2.17. Three-phase power inverter connected to an AC-Motor

2.5.1. Two-Level VSI

A two-level VSI consist of three pairs or half-bridges of switching power semiconductors, commonly Insulated Gate Bipolar Transistors (IGBT´s), which are denoted by S_{U+}/S_{U-}, S_{V+}/S_{V-}, S_{W+}/S_{W-}. Each IGBT has an antiparallel free-wheeling power diode with the notation D_{U+}/D_{U-}, D_{V+}/D_{V-} D_{W+}/D_{W-}. Thus, the three half-bridges can convert the DC-link voltage in three AC voltages on the corresponding phases u_{1U}, u_{1V}, and u_{1W} (see Fig. 2.17). The logical position for each phase (U, V or W) is defined as:

- (−), if the phase is connected to the negative potential, or as
- (+), if the phase is connected to the positive potential

of the DC link voltage (Fig. 2.18a). Thus, with this definition and with this VSI topology, is possible to obtain eight different combinations of switching-state of the inverter [29], respectively eight voltage space phasors $\underline{u}_0$, $\underline{u}_1$, $\underline{u}_2$, $\underline{u}_3$, $\underline{u}_4$, $\underline{u}_5$, $\underline{u}_6$, $\underline{u}_7$. The two space phasors $\underline{u}_0$ (with all phases connected to the negative potential) and $\underline{u}_7$ (with all phases connected to the positive potential) are the so-called “zero voltage space phasors” (ZP) [30] (both are redundant), the rest are called “active voltage space phasors” (AP) (see Fig. 2.18b).

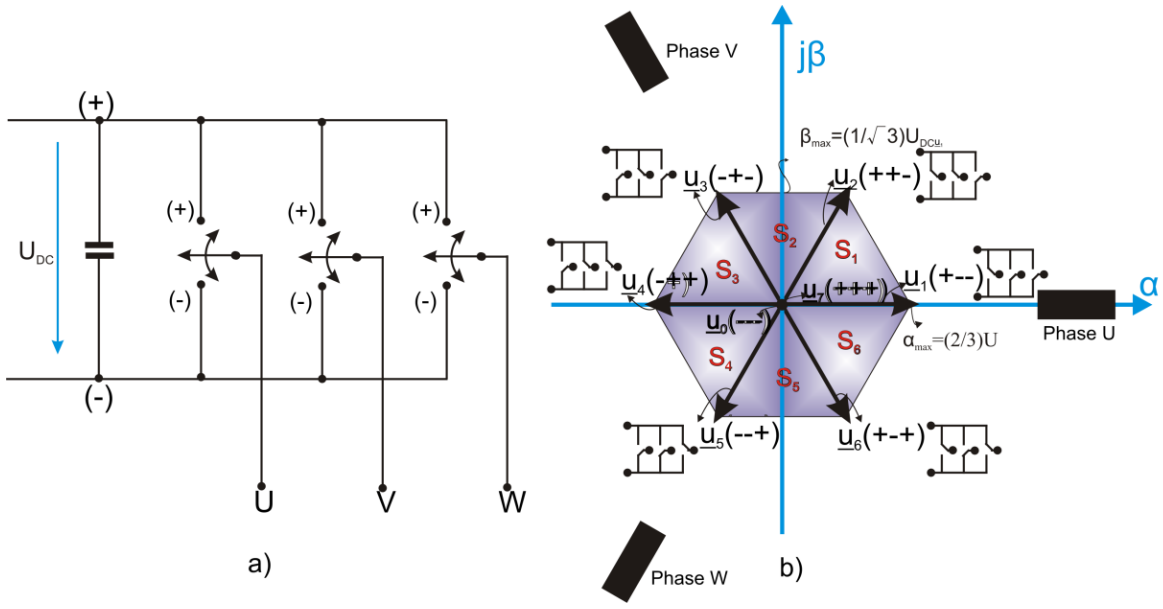

Fig. 2.18. a) Simplified scheme of a two-level VSI b) Standard voltage space phasors $\underline{u}_0 \rightarrow \underline{u}_7$ formed by the switching states of the two-level VSI

Table 2-1. Switching states and $\alpha, \beta -$ components of the eight available output space phasor voltages for a two-level VSI

	Switching-states	Components		Phasor	
Space Phasor	(uvw)	$\frac{u_\alpha}{U_{DC}}$	$\frac{u_\beta}{U_{DC}}$	$\frac{\lvert\underline{u}\rvert}{U_{DC}}$	$\angle\underline{u}$
$\underline{u}_0$	$(---)$	0	0	0	-
$\underline{u}_1$	$(+--)$	$\frac{2}{3}$	0	$\frac{2}{3}$	0°
$\underline{u}_2$	$(++-)$	$\frac{1}{3}$	$\frac{1}{\sqrt{3}}$	$\frac{2}{3}$	60°
$\underline{u}_3$	$(-+-)$	$-\frac{1}{3}$	$\frac{1}{\sqrt{3}}$	$\frac{2}{3}$	120°
$\underline{u}_4$	$(-++)$	$-\frac{2}{3}$	0	$\frac{2}{3}$	180°
$\underline{u}_5$	$(--+)$	$-\frac{1}{3}$	$-\frac{1}{\sqrt{3}}$	$\frac{2}{3}$	240°
$\underline{u}_6$	$(+-+)$	$\frac{1}{3}$	$-\frac{1}{\sqrt{3}}$	$\frac{2}{3}$	300°
$\underline{u}_7$	$(+++)$	0	0	0	-

The voltage space phasors divide the voltage phasor plane in six 60°-sextants or sectors "S1" to "S6". The Table 2-1 shows the logical switching-states of the three half-bridges as well as the eight available voltage space phasors in the stator-fixed $\alpha, \beta -$ system of coordinate.

2.5.2. Multi-Level VSI

The idea of an output voltage with several levels is a rather old concept [21], that allows one to divide the voltage phasor space in finer steps than the above mentioned 60°-sextants [31]. In comparison with the two-level VSI, multilevel topologies have the ability to synthetizes a stepped output waveform with three or more levels, in this way reducing the voltage and the current distortion. Detailed explanations about multilevel inverters can be found in the fundamental literature [32]. The multilevel VSI features can be summarized as follows:

- They produce stepped output voltages with lower distortion
- They can generate phase potentials with low common mode voltage, in this way reducing motor bearings stress [33]
- They can achieve a lower distortion of the output voltage than in a two-level inverter with the same switching frequency. This is especially important in medium voltage applications, where the switching frequency of the power switches is relatively low in order to keep the losses of the switches within allowable ranges.

Nonetheless the multilevel VSI increases the number of power semiconductor devices, as well as the complexity in the operation, the hardware and the control.

There are basically three different topologies for multilevel VSI:

- Neutral clamped topology
- Capacitive clamped inverter or flying capacitor inverter
- Series connected H-Bridge multilevel inverter

The constructive features and operation of the different multilevel VSI topologies are explained in detail in the pertinent literature [32]. A general illustration of a 3-level-, 5-level-, and a general n-level VSI with three-phase output voltages are shown in Fig. 2.19.

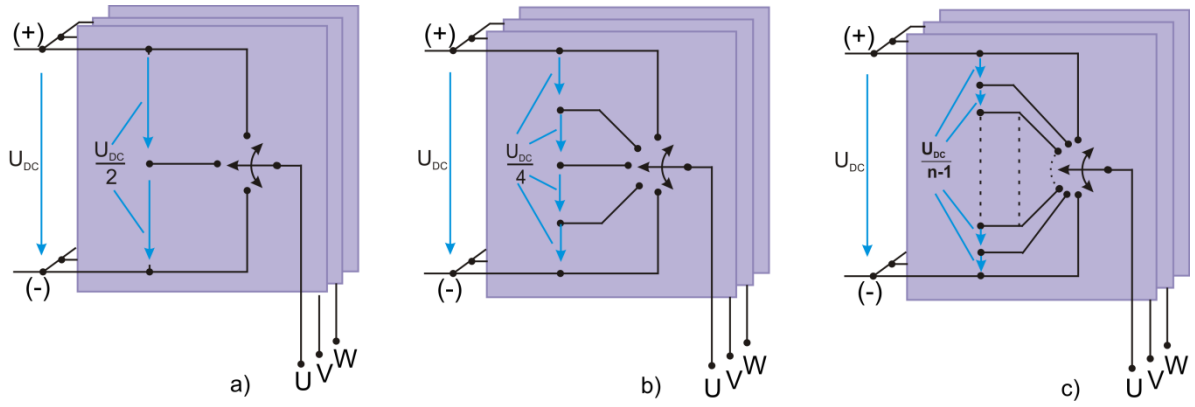

Fig. 2.19. a) 3-level VSI, b) 5-level VSI, c) n-level VSI

Similar to a two-level VSI, the possible voltage space phasor of a multilevel VSI can be represented in a stator-fixed $\alpha,\beta-$coordinate system with an hexagon voltage limit. Fig. 2.20 illustrates as example the cases of different multilevel VSI´s, in which each cross-point represent a voltage space phasor of the multilevel VSI. In the same way each voltage space phasor has its α - and β -components (Table 2-2 shows the values for a 3-level VSI). Obviously, by increasing the number of levels of the VSI, the number of possible voltage space phasors as well as the system complexity increase. In general for a $N_{output\text{-}Phases}$ VSI with N_{levels}, the total number of switching-states ($N_{switching\_states}$) can be calculated by means of:

$$N_{switching\_states} = \left(N_{levels}\right)^{N_{output-Phases}} \tag{2.60}$$

particularly for the cases of a 3-level- and a 5-level- VSI´s, the number of switching-states is 27 (3^3) and 125 (5^3) respectively. Yet, because of topology of the multilevel VSI several redundant switching-states exist, thus the real number of different voltage space phasors in the case of a three-phase multilevel VSI can be calculated by [32]:

$$N_{voltage\_space\_phasors} = 1 + 6 \cdot \sum_{i}^{levels-1} i \tag{2.61}$$

for instance a two-level VSI has 8 (2^3) possible switching-states and 7 valid possibilities of voltage space phasors $(1+6\cdot(1))$; a three-levels VSI has 27 switching-states and 19 possible voltage space phase phasors $(1+6\cdot(1+2))$; a five-levels VSI has 125 switching-states and 61 possible voltage space phasors $(1+6\cdot(1+2+3+4))$, and so on.

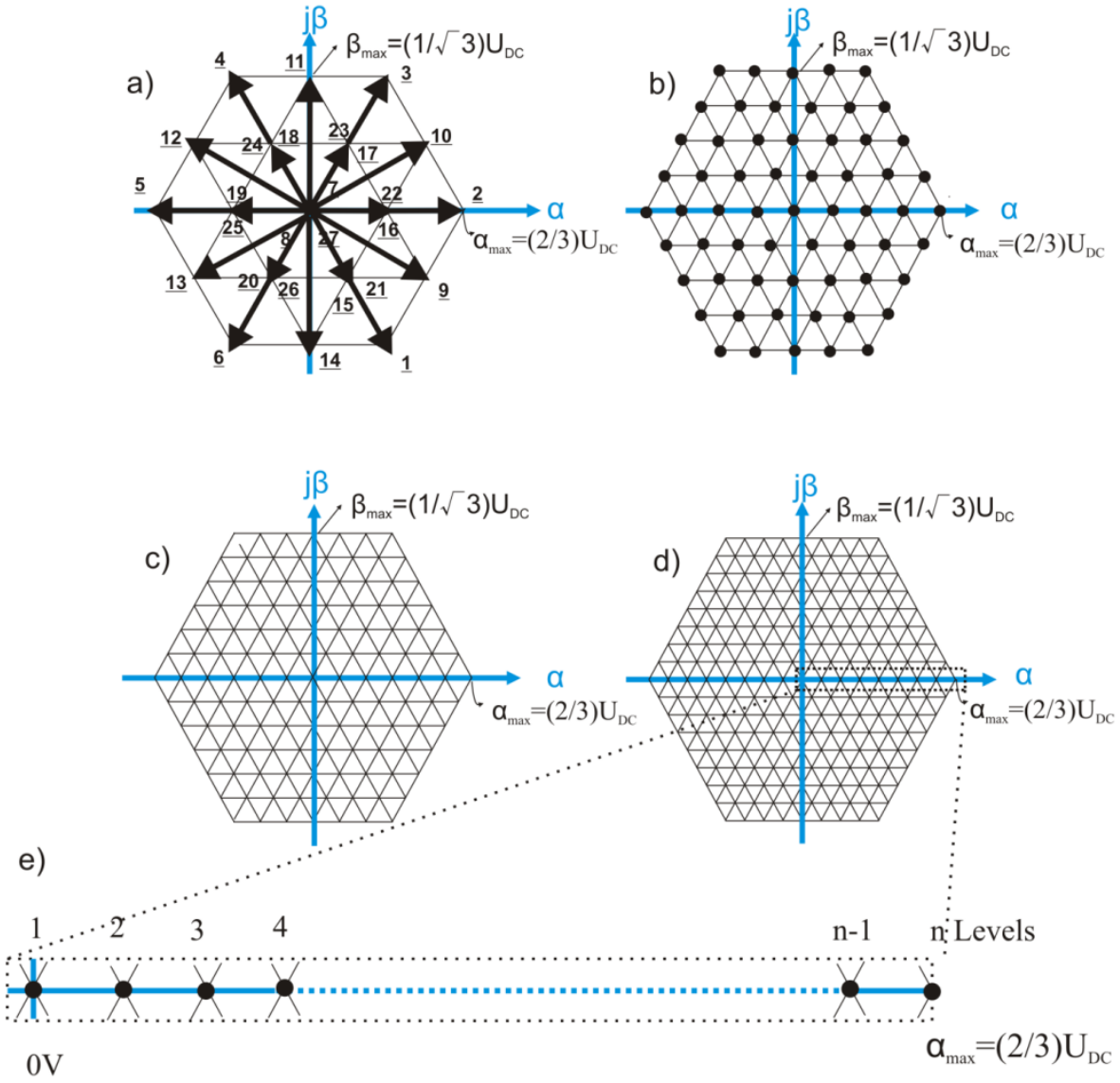

Fig. 2.20. Examples for the output voltages of multilevel VSI in stationary reference frame αβ a) 3-level; b) 5-level; c) 7-level; d) n-level; e) Division of the maximal value in (n-1) parts to build n-levels

Table 2-2 Switching states and $\alpha, \beta -$ components of the eight available output space phasor voltages for a 3-level VSI

	Switching-states	Components		Phasor	
Space Phasor	(uvw)	$\frac{u_\alpha}{U_{DC}}$	$\frac{u_\beta}{U_{DC}}$	$\frac{\lvert\underline{u}\rvert}{U_{DC}}$	$\angle\underline{u}$
$\underline{u}_1$	$(+-+)$	$1/3$	$-1/3$	$2/3$	300°
$\underline{u}_2$	$(+--)$	$2/3$	0	$2/3$	0°
$\underline{u}_3$	$(++-)$	$1/3$	$1/\sqrt{3}$	$2/3$	60°
$\underline{u}_4$	$(-+-)$	$-1/3$	$1/\sqrt{3}$	$2/3$	120°
$\underline{u}_5$	$(-++)$	$-2/3$	0	$2/3$	180°
$\underline{u}_6$	$(--+)$	$-1/3$	$-1/\sqrt{3}$	$2/3$	240°
$\underline{u}_7$	$(+++)$	0	0	0	-
$\underline{u}_8$	$(---)$	0	0	0	-
$\underline{u}_9$	$(+-0)$	$1/2$	$-\sqrt{3}/6$	$1/\sqrt{3}$	330°
$\underline{u}_{10}$	$(+0-)$	$1/2$	$\sqrt{3}/6$	$1/\sqrt{3}$	30°
$\underline{u}_{11}$	$(0+-)$	0	$1/\sqrt{3}$	$1/\sqrt{3}$	90°
$\underline{u}_{12}$	$(-+0)$	$-1/2$	$\sqrt{3}/6$	$1/\sqrt{3}$	150°
$\underline{u}_{13}$	$(-0+)$	$-1/2$	$-\sqrt{3}/6$	$1/\sqrt{3}$	210°
$\underline{u}_{14}$	$(0-+)$	0	$-1/\sqrt{3}$	$1/\sqrt{3}$	270°
$\underline{u}_{15}$	$(+0+)$	$1/6$	$-\sqrt{3}/6$	$1/3$	300°
$\underline{u}_{16}$	$(+00)$	$1/3$	0	$1/3$	0°
$\underline{u}_{17}$	$(++0)$	$1/6$	$\sqrt{3}/6$	$1/3$	60°
$\underline{u}_{18}$	$(0+0)$	$-1/6$	$\sqrt{3}/6$	$1/3$	120°
$\underline{u}_{19}$	$(0++)$	$-1/3$	0	$1/3$	180°
$\underline{u}_{20}$	$(00+)$	$-1/6$	$-\sqrt{3}/6$	$1/3$	240°
$\underline{u}_{21}$	$(0-0)$	$1/6$	$-\sqrt{3}/6$	$1/3$	300°
$\underline{u}_{22}$	$(0--)$	$1/3$	0	$1/3$	0°
$\underline{u}_{23}$	$(00-)$	$1/6$	$\sqrt{3}/6$	$1/3$	60°
$\underline{u}_{24}$	$(-0-)$	$-1/6$	$\sqrt{3}/6$	$1/3$	120°
$\underline{u}_{25}$	(-00)	$-1/3$	0	$1/3$	180°
$\underline{u}_{26}$	$(--0)$	$-1/6$	$-\sqrt{3}/6$	$1/3$	240°
$\underline{u}_{27}$	(000)	0	0	0	-

2.6. Space Phasor Modulation

Some control schemes for electrical machines, which do not directly command the switching-states of a VSI (for example the field oriented control) need to modulate their control output voltage signals. A common modulation method is the so-called space phasor modulation (SPM).

The space phasor modulation technique applies the space phasor theory to each voltage phasor, inside of the hexagon-voltage-limits of the VSI.

As already explained in section 1, in a two-level VSI topology six active-space phasors and two redundant zero-space phasors are possible. Fig. 2.21 shows an equivalent structure of a two-level VSI, where voltages of the output terminals (denoted by U, V, and W) are referred to a fictitious neutral-point "0". Table 2-1 is complemented with the values of the voltage with respect to the fictitious neutral-point "0", as well as with the phase-to-phase voltage and with the voltage on the machine, as Table 2-3 shows.

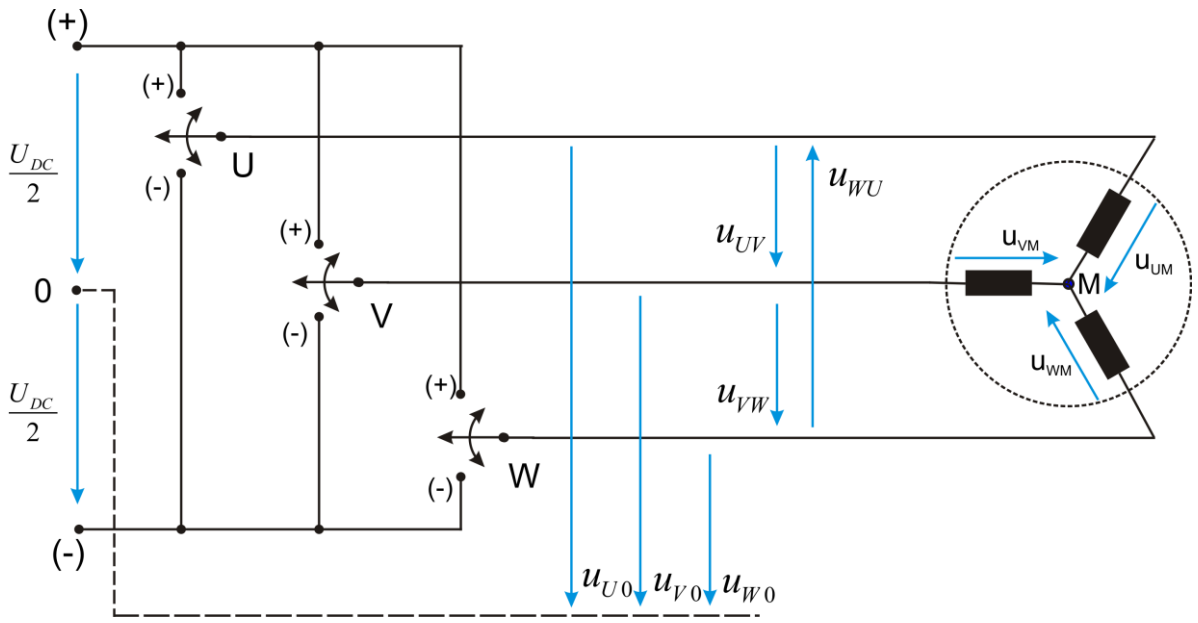

Fig. 2.21. Equivalent circuit of the three-phase VSI from Fig. 2.17

The space phasor modulation (SPM) synthetizes a voltage space phasor $\underline{u}_s$ located inside of one sector (S_1 to S_6) using the three nearest voltage space phasors of the VSI (two active space phasors and one zero-phasor).

Table 2-3. Voltage characteristic of the space phasors for a two-level VSI

	Switching-states	Output Inverter Voltage			Phase-to-phase Inverter Voltage			Motor Voltage				
Space Phasor	(uvw)	$\frac{u_{U0}}{U_{DC}}$	$\frac{u_{V0}}{U_{DC}}$	$\frac{u_{W0}}{U_{DC}}$	$\frac{u_{UV}}{U_{DC}}$	$\frac{u_{VW}}{U_{DC}}$	$\frac{u_{WU}}{U_{DC}}$	$\frac{u_{UM}}{U_{DC}}$	$\frac{u_{VM}}{U_{DC}}$	$\frac{u_{WM}}{U_{DC}}$	$\frac{\lvert\hat{u}\rvert}{U_{DC}}$	$\angle\underline{u}$
$\underline{u}_0$	$(---)$	$-\frac{1}{2}$	$-\frac{1}{2}$	$-\frac{1}{2}$	0	0	0	0	0	0	0	-
$\underline{u}_1$	$(+--)$	$\frac{1}{2}$	$-\frac{1}{2}$	$-\frac{1}{2}$	1	0	-1	$\frac{2}{3}$	$-\frac{1}{3}$	$-\frac{1}{3}$	$\frac{2}{3}$	0°
$\underline{u}_2$	$(++-)$	$\frac{1}{2}$	$\frac{1}{2}$	$-\frac{1}{2}$	0	1	-1	$\frac{1}{3}$	$\frac{1}{3}$	$\frac{2}{3}$	$\frac{2}{3}$	60°
$\underline{u}_3$	$(-+-)$	$-\frac{1}{2}$	$\frac{1}{2}$	$-\frac{1}{2}$	-1	1	0	$-\frac{1}{3}$	$\frac{2}{3}$	$-\frac{1}{3}$	$\frac{2}{3}$	120°
$\underline{u}_4$	$(-++)$	$-\frac{1}{2}$	$\frac{1}{2}$	$\frac{1}{2}$	-1	0	1	$-\frac{2}{3}$	$\frac{1}{3}$	$\frac{1}{3}$	$\frac{2}{3}$	180°
$\underline{u}_5$	$(--+)$	$-\frac{1}{2}$	$-\frac{1}{2}$	$\frac{1}{2}$	0	-1	1	$-\frac{1}{3}$	$-\frac{1}{3}$	$\frac{2}{3}$	$\frac{2}{3}$	240°
$\underline{u}_6$	$(+-+)$	$\frac{1}{2}$	$-\frac{1}{2}$	$\frac{1}{2}$	1	-1	0	$\frac{1}{3}$	$-\frac{2}{3}$	$\frac{1}{3}$	$\frac{2}{3}$	300°
$\underline{u}_7$	$(+++)$	$\frac{1}{2}$	$\frac{1}{2}$	$\frac{1}{2}$	0	0	0	0	0	0	0	-

Fig. 2.22 shows as an example a voltage space phasor $\underline{u}_s$ located in the sector S_1 and the generation of the SPM using their nearest VSI-voltage space phasors $\underline{u}_1$, $\underline{u}_2$ and $\underline{u}_0$ or $\underline{u}_7$. So, $\underline{u}_s$ can be calculated by means of:

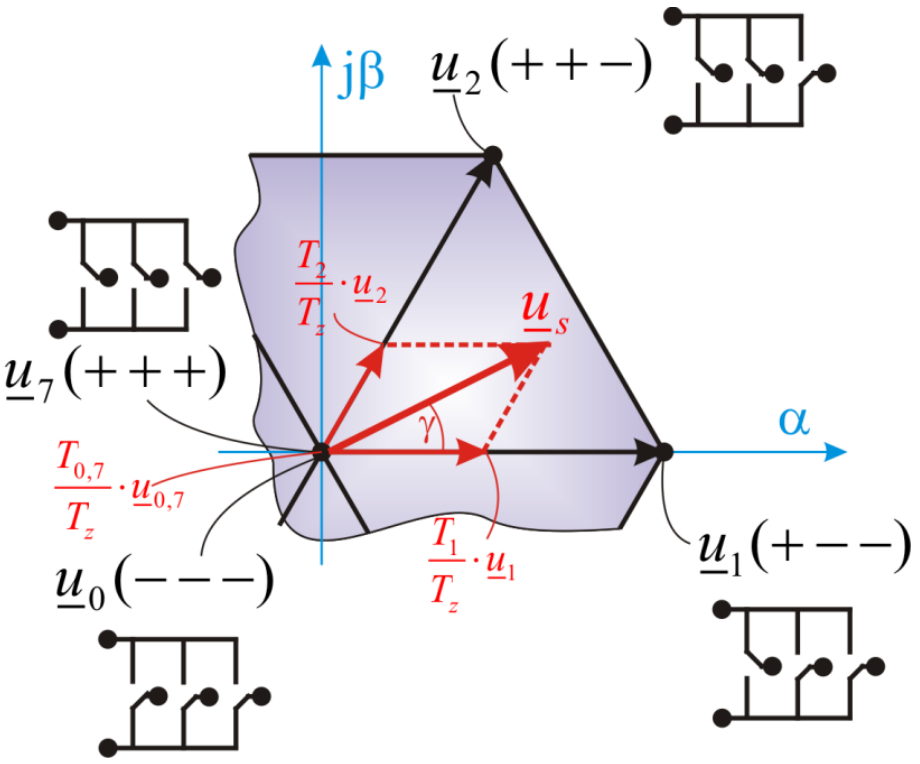

Fig. 2.22. Example of the generation of the output voltage by using Voltage Space Phasor Modulation

$$\underline{u}_s = u \cdot e^{j\gamma} = \frac{T_1}{T_z} \cdot \underline{u}_1 + \frac{T_2}{T_z} \cdot \underline{u}_2 + \frac{T_{0,7}}{T_z} \cdot \underline{u}_{0,7}$$
$$\underline{u}_s = \frac{T_1}{T_z} \cdot \frac{2}{3} \cdot U_{DC} + \frac{T_2}{T_z} \cdot \frac{2}{3} \cdot U_{DC} \cdot e^{j\frac{\pi}{3}} \tag{2.62}$$

where

$$\frac{T_1}{T_z} = \frac{2}{\sqrt{3}} \cdot \frac{u}{U_{DC}} \cdot \sin\left(\frac{\pi}{3} - \gamma\right) \tag{2.63}$$

$$\frac{T_2}{T_z} = \frac{2}{\sqrt{3}} \cdot \frac{u}{U_{DC}} \cdot \sin(\gamma) \tag{2.64}$$

$$T_{0,7} = T_z - T_1 - T_2 \tag{2.65}$$

With T_z the cycle time and $\frac{T_1}{T_z}$, $\frac{T_2}{T_z}$ and $\frac{T_{0,7}}{T_z}$ are the duty cycles of their respective nearest voltage space phasors $\underline{u}_1$ and $\underline{u}_2$, and $\underline{u}_0$ or $\underline{u}_7$. Fig. 2.23 shows the switching patterns of the voltage space phasors in the sector S_1. The procedure is similar in the others five sectors.

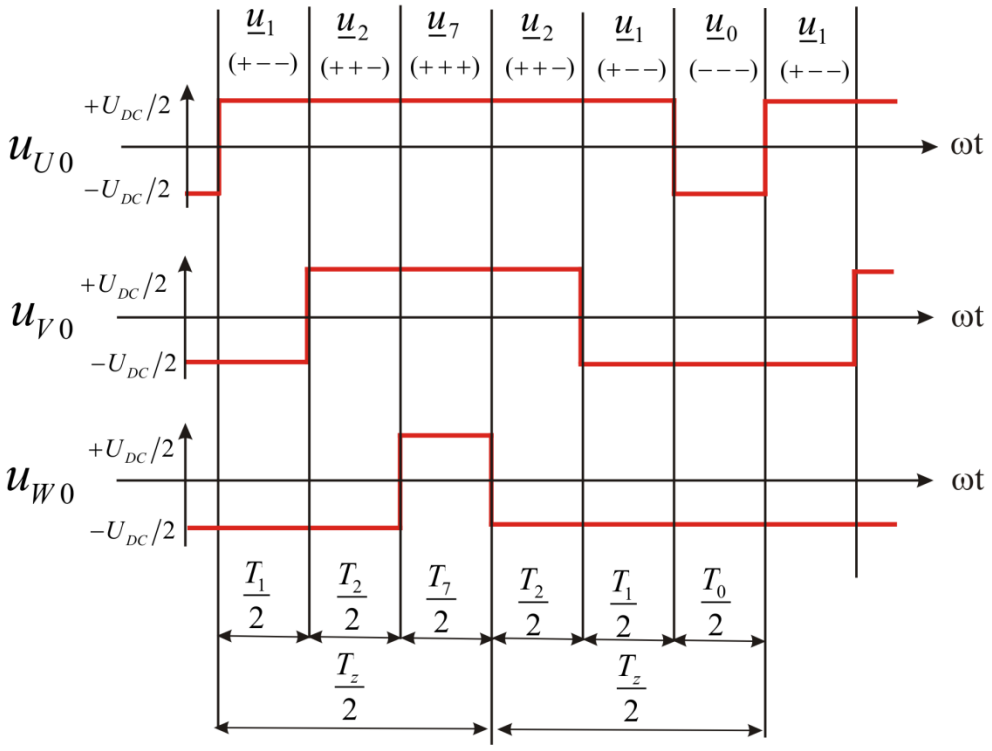

Fig. 2.23. Switch patterns of the space phasors in the sector S_1

2.7. Sinusoidal Pulse Width Modulation

Another common method for synthesizing the output voltage of a VSI is the sinusoidal Pulse Width Modulation (PWM), in which the reference voltage signal (in steady state a sinusoidal-waveform) is compared with a triangular carrier signal with constant period T_s, for obtaining the driver signals of the inverter. Fig. 2.24 shows the scheme and the output voltage waveforms of a PWM for a one-phase VSI; the fundamental harmonic of the output pulsed voltage waveform of the VSI corresponds to the sinusoidal reference

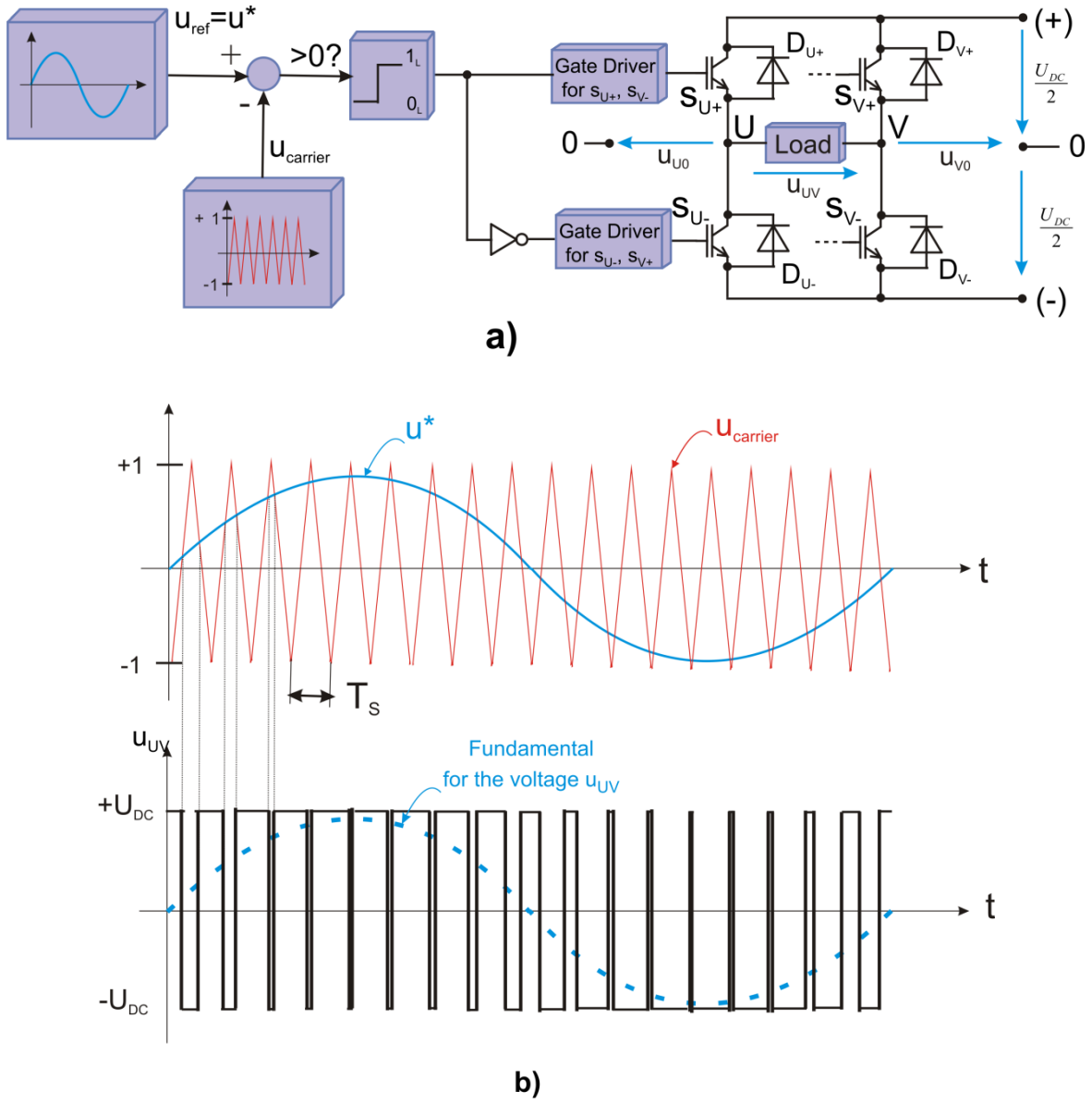

Fig. 2.24: a) Scheme of a one-phase-VSI sine-PWM; b) PWM waveform for a one-phase VSI

In the case of a three-phase VSI, the reference voltage space phasor must be transformed from the stator-fixed α, β – coordinate system to the three-phase system previously (as

already explained in section 2.2), and after that each phase is compared with a triangular carrier, generating the switching-states for each half-bridge of the three-phase VSI. Fig. 2.25 shows a scheme of a three-phase sine-PWM.

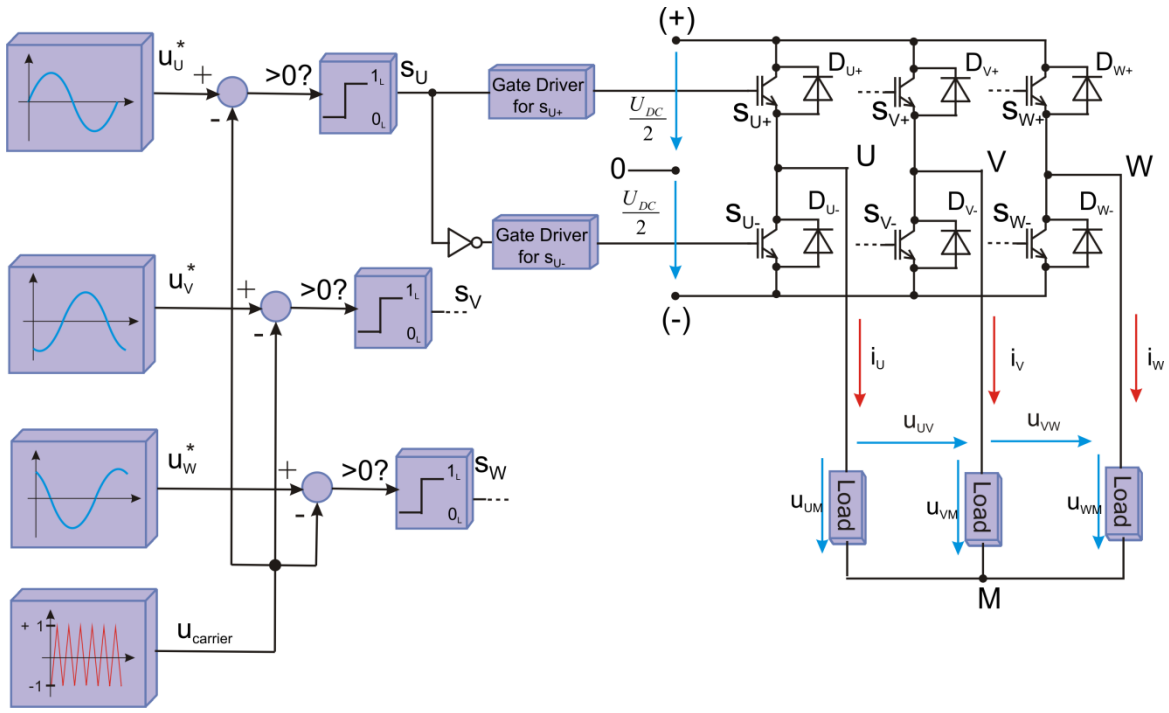

Fig. 2.25. Scheme of a three-phase PWM

In the fundamental literature [34] is shown that a sinusoidal fundamental with an additional injected third-harmonic instead of a pure sinusoidal function as reference for the modulation of a two-level VSI leads to identical results as the space vector modulation (both produce identical mean values of the output voltages). Yet the difference between both methods is in the treatment of the zero space phasor. Fig. 2.26 illustrates the formation principle of a sine PWM with 3rd-harmonic injection and also the reference waveforms for the phases *u, v* and w, and the phase-to-phase waveform *uv*.

Because of the above mentioned advantages of the sinusoidal-PWM with 3rd-harmonic injection technique, in the laboratory set-up a sinusoidal-PWM with 3rd-harmonic injection technique for the calculation of the switching-states to drive the VSI was used.

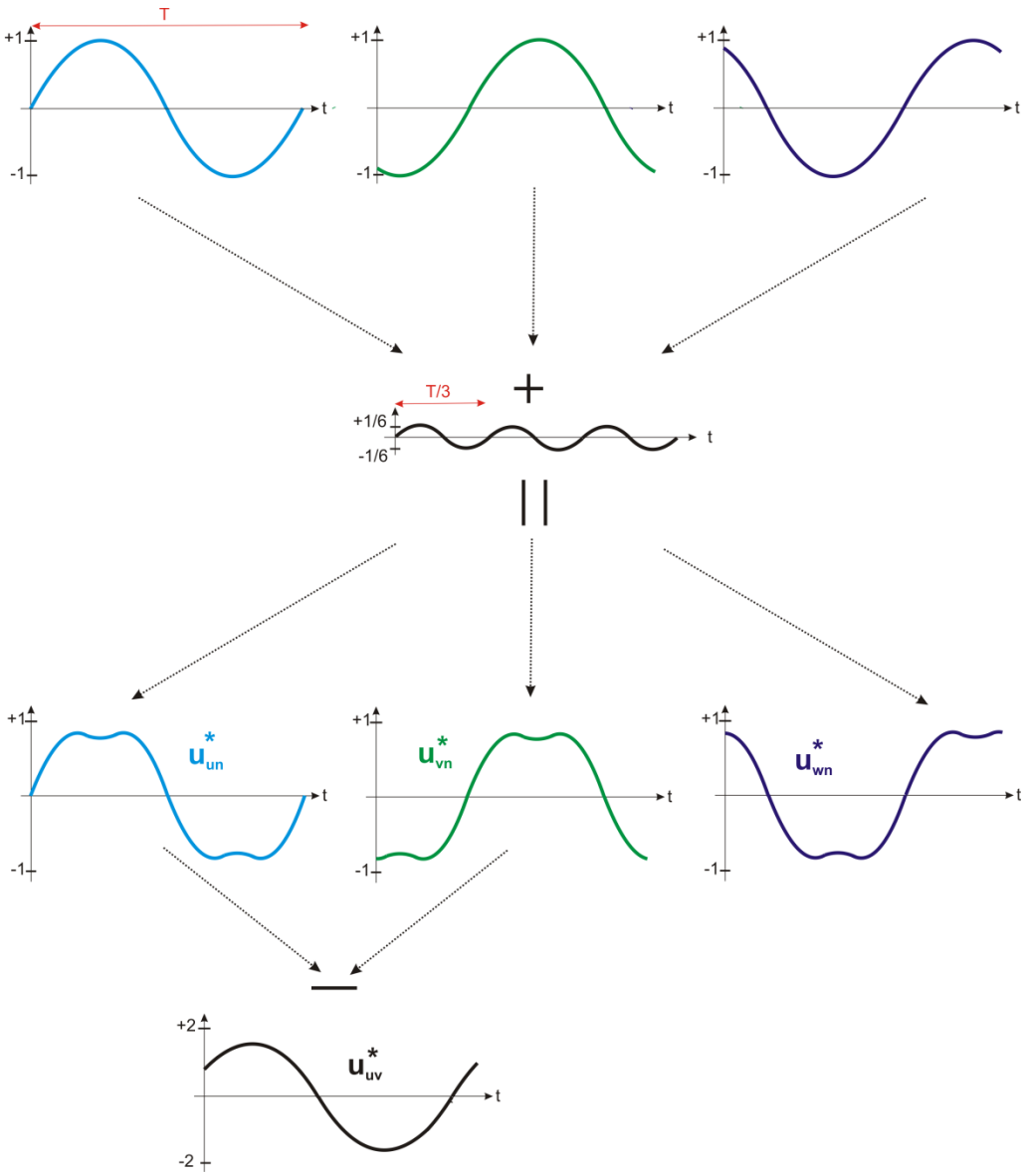

Fig. 2.26. Third-harmonic injection waveform and references for u_{un}*, u_{vn}* and u_{uv}*

2.8. Summary of the Chapter

This chapter summarizes some fundamental concepts that will be used in the present project. A brief description of the space phasor theory and coordinate transformation, the modelling and control of a PMSM, topologies and operation of voltage source inverters and also the space phasor modulation as well as the PWM principles are presented.

3. PREDICTIVE CONTROL FOR THE SYSTEM LC FILTER- PMSM

3.1. Predictive Control Principle

The idea of predictive control as a mathematical concept came up in the early 20th century, but it took until the seventies for its introduction by Richalet, Cutler and Ramaker [35] as a new control strategy to be applicable in the chemical industry as an alternative to the conventional control schemes.

Later in the eighties, Garcia, Prett, Morari, Clarke et al. introduced at the same time different schemes and styles of predictive control as well as different techniques to solve the optimization task associated with this kind of control [36]. These schemes and styles were improved and developed subsequently by Maciejowski [6], Camacho [7], Soeterboerk [35], Grimble [36], et al. to be a suitable control principle for several different industry applications. Morari and Camacho in [4] and [5] respectively explain in detail the past, present and the future of the predictive control. Nowadays, predictive control is an alternative control technique and has become an attractive and interesting topic to research.

3.1.1. Principle

Although there are different classes of predictive control schemes, in general predictive control is based on the model of a system or process to control, i.e. the dynamic model of the process is explicitly used to design the controller [35]. Thus, the predictive controller is composed by a mathematic process-model, a cost function, and an optimization of the cost function.

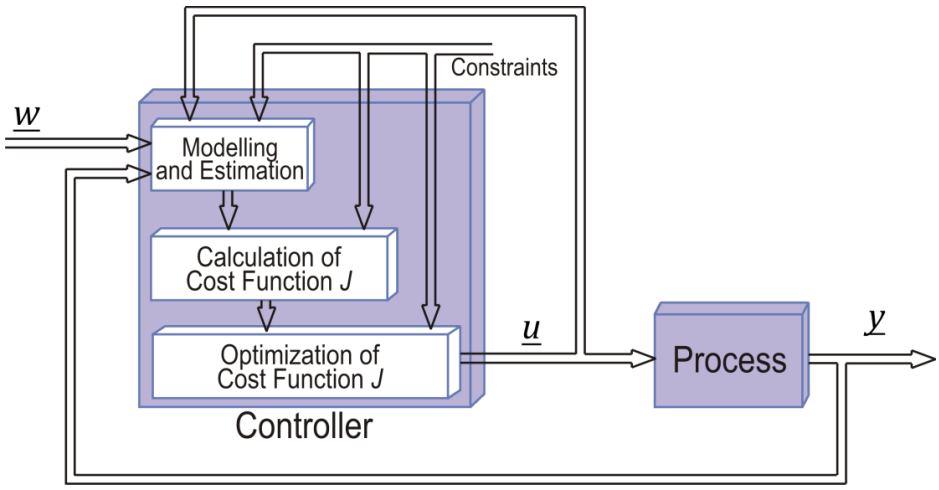

Fig. 3.1. Predictive control principle

The predictive control principle can be described as follows: based on the desired process-output $\underline{w}$ (set-point or trajectory reference), the controller computes, by means of the system mathematic model as well as by means of the optimization of a cost function *J,* the manipulated controller-output $\underline{u}$ to be applied to the process in order to obtain the process-output $\underline{y}$ (see Fig. 3.1). The limitations of the process or of the actuators must be taken into account as constraints in the model and in the optimization.

In general, the principle of predictive control is similar to the principle of the conventional control (for instance a PID controller). The main difference is that predictive control works with the future output error (the difference between the future desired output and the future estimated output): $\underline{e}(k+n) = \underline{w}(k+n) - \underline{y}(k+n)$, in contrast to the conventional controllers that work with the actual error $\underline{e}(k) = \underline{w}(k) - \underline{y}(k)$.

Theoretically predictive controllers can be designed in continuous time (the mathematic model as well as the optimization), however for implementation, the predictive controllers are mostly programmed in digital systems. Therefore the predictive control is designed and implemented in discrete time. Thus, the following explanations of the predictive control operation refer to a discrete time.

For a discrete-time SISO system (single-input single-output), where *w* is the desired output signal or reference trajectory, *y* is the real output signal or real trajectory, *u* is the controller signal, and t_k is each *k* instant (*Ts* is the sample time and is the difference between a pair of instants t_{k+n} and t_{k+n+1}), the strategy to achieve the predictive control can be described as follows:

- Based on the values of the reference-, of the output- and of the controller-signals up to the instant t_k, and on the mathematic model of the system, the predictive controller estimates the next value or future value of the controller *u(k+1)* by means of an optimization of the cost function *J*.
- Based on the estimation of the values of the controller *u(k+1)* and of the reference *w(k+2)*, the output signal is computed for the instant t_{k+2}, i.e. $y(k+2)$, subsequently, the values of the variables at the instant t_{k+2} are used in the predictive controller to estimate a the future value for the next instant t_{k+3}, i.e. *u(k+3)*.
- This procedure is repeated for all times steps within the prediction horizon N_H.

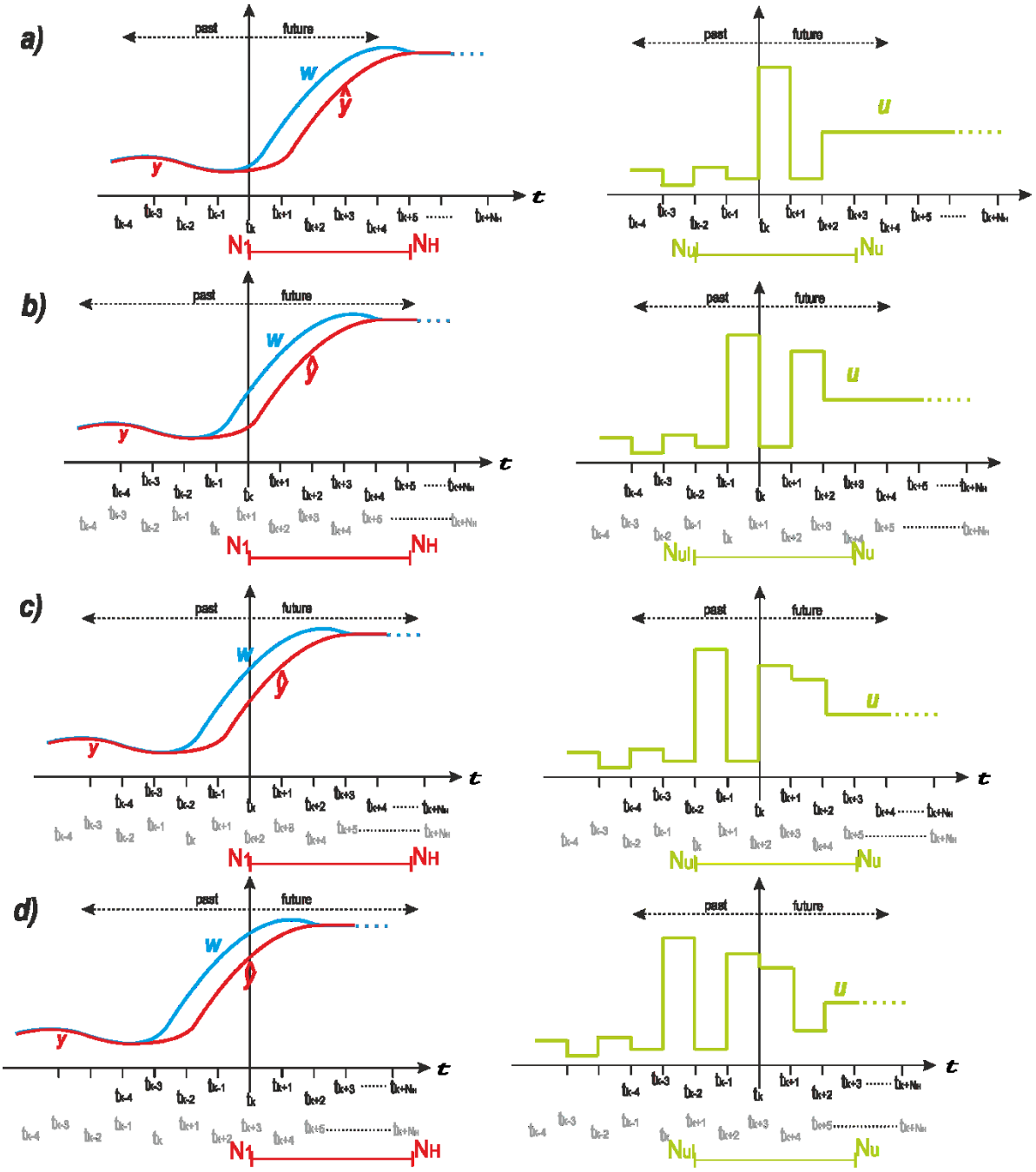

Fig. 3.2. Example of the Receding-Horizon-Control (RHC) for the instants a) t_k, b) t_{k+1}, c) t_{k+2}, d) t_{k+3}

This is the principle of Receding-Horizon-Control (RHC) as illustrated by Fig. 3.2, which shows the reference, the output signals as well as the control signal at the instants t_k, t_{k+1}, t_{k+2}, and t_{k+3} with the shifted forward horizon [9]. Fig. 3.2b shows the correction at the instant t_{k+1} for the control signal in order to compensate a wrong future output $y(k+2)$. The corrections and compensations for the control signal at the instants t_{k+2}, and t_{k+3} are shown in Fig. 3.2c and d. This is one of the advantages of predictive control, in each new instant is

possible to compensate and correct the future errors by the RHC, in other words a feedback mechanism is activated [35], as illustrates Fig. 3.2.

The explanation is the same for all variables in the case of a MIMO system (multiple-input, multiple-output).

It is important to have an exact model of the process as the whole procedure of predictive control is reiterated. In fact, any kind of model that describes the relationships between the input- and the output-signals of a process can be used. In this way there are many different possibilities: transfer-function model, impulse-response model, step-response model, state-space model, nonlinear model, etc., furthermore disturbances can be included.

The prediction horizon value $N_{H\,\mathrm{can}}$ be selected by using the mathematic model of the system for the calculation of the instant, when the steady-state of the system is reached and the controller output remains constant. The optimization, the estimation of the control- and real output-signals demands a higher computational effort. Therefore by selecting an adequate prediction horizon value N_H and a good optimization method, the computational effort can be reduced.

3.1.2. Cost Function

The cost function of the predictive control has different forms depending on the applications. In general, the mathematical expression of the cost function of a predictive control for a MIMO system that takes into account the principle expressed in the section 3.1.1 can be written as:

$$J\left(N_L, N_H, N_{uL}, N_u\right) = \sum_{i=1}^{n} \sum_{j=N_L}^{N_H} \left(\delta_i(j) \cdot \left(w_i\left(t_k + j\right) - y_i^p\left(t_k + j \middle| t_k\right) \right)^2 \right) + \sum_{i=1}^{m} \sum_{j=N_{uL}}^{N_u - 1} \left(\lambda_i(j) \cdot \left(\Delta u_i\left(t_k + j - 1\right) \right)^2 \right) \tag{3.1}$$

where:

- n and m are positive integers and represent the order of the output and control vectors of the MIMO system respectively,
- $\underline{y} = [\ y_1 \quad y_2 \quad \ldots \quad y_n\ ]^T$ is the output vector,

- y_i are the elements of the vector $\underline{y}$; the predicted values of the elements of the vector $\underline{y}$ are marked with the symbol superscript ^{p}.
- $\underline{w} = [\ w_1 \quad w_2 \quad \dots \quad w_n\ ]^T$ is the reference vector (set-point or reference trajectory),
- w_i are the elements of the vector $\underline{w}$;
- $\underline{u} = [\ u_1 \quad u_2 \quad \dots \quad u_m\ ]^T$ is the control vector,
- Δu_i are the elements of the vector $\Delta\underline{u}$, where $\Delta\underline{u}$ is the past control error, i.e. the difference between two control vectors at consecutive instants.

The first part of the cost function is known as the predicted error, i.e. the error between the references- and the estimated output-signals, and the second part is known as the penalization due to the control effort or the control error. Depending on the applications and constraints, the second part of the cost function is not taken into account [7].

$\delta_i(j)$ and $\lambda_i(j)$ are parameters representing the weights for the prediction error and for the control error respectively, which are positive real numbers. In general these weights are always constants, but in some applications, depending on the control topic, these weights are not constant, i.e. they take different values in each instant t_k, therefore the nomenclature… .

N_L and N_H are the lower value and the higher value of the prediction horizon respectively, and N_{uL} and N_u are the limits of the control horizon.

If only the prediction-errors, i.e. the errors between the references- and the estimated output-signals for the computation of (3.1), are taken into account, the limits for the sums i.e. for the horizon still have to be defined. If the error in the steady state or in the far future should have a higher weight in the minimization, a high-value can be chosen for N_L, obtaining thus a good steady state response. This condition occurs in applications with delays and processes with dead-time. In contrast, if the near future of the system is of relevance for the behavior of the system, low values are selected for N_L, sometimes $N_L=1$, thus a good dynamic response in the transitions as well as in steady state is achieved. In real cases is often $N_L=1$, which represents an evaluation of the cost function beginning with the instant t_k, while N_H is selected according to the explanation in section 3.1.1.

If the actuator of the process has constraints or the parameters of the modeled system are wrong, then differences between the reference and the output signals can occur and in those cases N_{uL} and N_u can be taken into account. The value of N_u can be lower or equal to N_H. The N_{uL} and N_u values are selected for the function depending on how important the past control-errors are and penalize the cost function due to the control effort. Some authors called this control effort integral action [37]. If this penalization due to the control effort has no influence on the cost function, the second part of the cost function (3.1) is not considered.

3.1.3. Optimization

The control signal is obtained from the optimization and minimization of the cost function J, thus:

$$\underline{u}_{opt} = \min_{\underline{u}} J \tag{3.2}$$

is the optimal control signal under the conditions of the cost function J and its minimization, i.e. the future error is minimized, then the predictive control can be classified as a feed-forward control.

For the optimization, different procedures and strategies exist, for example least-squares, dynamic programming, geometrical solution, piecewise-affine, set of points-solutions, etc., all with their advantages and disadvantages especially in real-time applications.

3.1.4. Constraints

The constraints of the whole system must be also taken into account. Thus, the output signals as well as the control signals have operative constraints, i.e. they have a range of operation defined by:

$$\begin{cases} y_{i\min} \le y_i^p(k) \le y_{i\max} \\ u_{i\min} \le u_i^p(k) \le u_{i\max} \end{cases} \tag{3.3}$$

These constraints have to be used in the modelling as well as in the cost function of the predictive control.

3.1.5. Relationship with other Controllers

As a basic concept, predictive control is a type of Model-Based-Control, however there are other controllers which are also model-based, e.g. optimal control, H_2-, H_∞-controllers, LQ-controller, dead-beat-controller, etc. Soeterboek explains in [35] the relationship between predictive control and LQ-controller and pole-placement. Grimble in [36] explains the relations between H_2-, H_∞-controllers and other controllers (e.g. predictive control) from the point of view of industrial applications.

Essentially all model-based control schemes imply structures similar to cost functions in the optimal control cost function. The difference is the length of the prediction horizon. For example, optimal control has an infinity prediction horizon, the LQ-controller has a quasi-infinity prediction horizon and predictive control has a limited and short prediction horizon, etc. All model-based control schemes have their properties and strategies of optimization, however infinity and a quasi-infinity prediction horizon are ideal cases, in which it is assumed that the reference as well as the control signals, the disturbance, etc. will not change in the future and therefore predictive control offers a good and realistic alternative of model-based control.

3.1.6. Properties, Advantages and Disadvantages of the Predictive Control

Based on the above explanations, the following properties and advantages of the predictive control can be mentioned:

- The concept of prediction, the idea of the cost function and the influence of the weights are easy and intuitive to understand.
- The cost function can be easily modified and offers a flexible way to consider other aspects that are not taken into account by the conventional controllers.
- The predictive control is not only applicable to SISO systems but also to MIMO systems.
- With predictive control it is possible to include nonlinear parts of the process and of the system.
- Disturbance can be also taken into account in the predictive control as explained by Grimble in [36]

- Constraints can be included in the model as well as in the optimization of the predictive control.
- Predictive control is a feed-forward controller, i.e. predictive control is an open-loop method but with stability in comparison with other open-loop-controllers. Comments and mathematical analysis of the stability of the predictive control are explained very well by Morari in [4], by Grimble in [36], and by Mikleš et al in [38].

As already mentioned above, the predictive control is a variant of model-based control, which means that the predictive control demands a good knowledge of the parameters of the whole system. This point is the big disadvantage of the predictive control. If the parameters of the system are wrong, the modelling is also erroneous, as a consequence the control signals are also incorrect, creating thus a permanent steady state control error, yet by using an additional on-line adaptive parameter tuning the control can be improved and this disadvantage can be corrected.

Another drawback of the predictive control is the great computational effort in the optimization that is necessary for finding an optimum control signal $\underline{u}_{opt}$. The high number of calculations is due to the fact, that predictive control takes into account all possibilities to the minimization, i.e. the number of possibilities taken into account for the calculation and for the minimization of the cost function is infinite. Therefore, one main goal of the presented work is to propose a very simple method to minimize the cost function making an implementation with low computational effort possible. In the next sections the proposed method will described in detail.

3.1.7. Predictive Control Applied to Power Electronics and Control Drive Systems

Section 3.1.1 already explained that predictive control, in all different classes and schemes, has a variety of industry applications, but it is used in particular in the petrochemical industry. The success of the application of the predictive control in the petrochemical industry was due to the fact that the time constants in their processes are often in the magnitude of seconds or minutes, thus for the implementation of predictive control, fast computing hardware was not required.

In contrast, applications that need fast calculations also need fast control hardware. This is the case with power electronics converters and applications in motor drives. Therefore, predictive control was not extensively applied to power converter applications due to the small time constants and the difficulty of the implementation. Thanks to the development and advance of digital systems, nowadays it is possible to implement and run sophisticated applications like predictive control on power converters, with switching frequencies up 50kHz, i.e. with a period of 20µs.

Rodriguez and Cortes in [8] and Kennel and Linder in [9] explain the applications of predictive control to power converters in a very good and comprehensive manner. They explain that in general, there are two styles of predictive control schemes. In the case of the DC/AC converters or inverters, the predictive control can be realized with the help of a modulator but there is also the possibility of a realization without modulator, in which the control delivers the switching-pattern for the inverter.

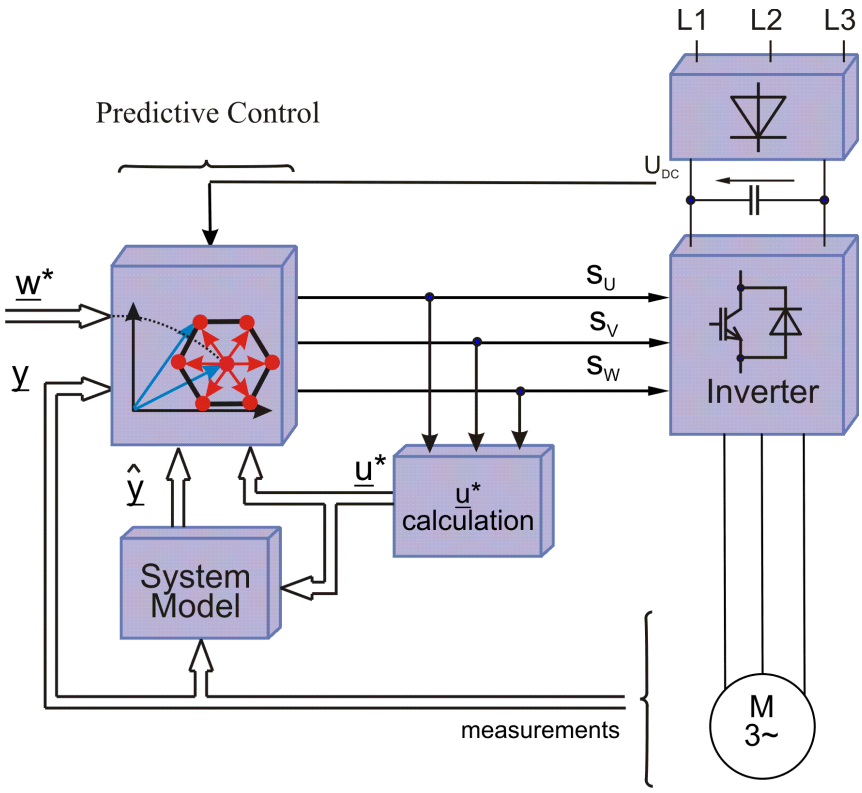

Fig. 3.3. Predictive control scheme with finite set control

The direct generation of the switching-pattern of the inverter (see Fig. 3.3) has the advantage that modulator is not required yet the controller has only a finite control set (the number of possible solutions depends on the number of levels in the inverter, for example

eight possibilities in the case of a two-level inverter). Furthermore, the individually driving of each power switch of the inverter allows the operation with variable switching frequency of the inverter.

The alternative predictive control scheme uses an additional block, a modulator (see Fig. 3.4) for the generation of the switching signals. The advantage of this scheme is the possibility to work with a continuous control set, i.e. the possibilities of control are infinite. The disadvantage of this scheme is that the operation of the fixed carrier frequency in the modulator prevents a minimization of the switching losses.

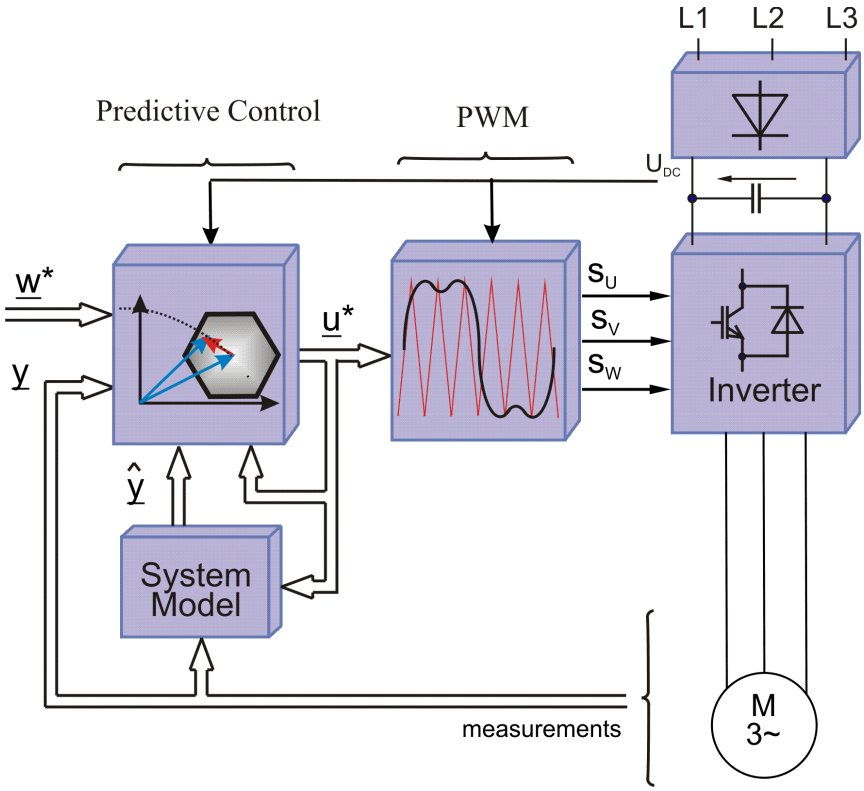

Fig. 3.4. Predictive control scheme with continuous set control

Rodriguez, et al. in [8] focused on a predictive control scheme with just a finite control set without modulator whereas other authors like Morari [16] [17], et al. focused their research on a predictive control with a continuous control set with modulator.

For a good performance of the predictive control, e.g. a minimum ripple of the torque, an infinity or continuous control set is recommended. In other words in the case of an inverter, an operation with all voltage space phasors that are possible with the inverter should be the

goal. Therefore, in the present project the scheme with PWM is selected. For the optimization a novel technique is proposed which will be explained in the next sections.

3.1.8. Selection of the Cost Functions in Power Electronics and Drive Systems

In section 3.1.2 the general mathematical definition of a cost function for a predictive control was already enounced. The cost function *J* expressed by (3.1) can be rewritten as *g* to be used in power electronics and drive applications and can be described as follows [8], i.e.:

$$g = \sum_{i=1}^{n} \left(w_i e_i^2 \right) \tag{3.4}$$

Where

$$e_i = x_i^* - x_i^p \tag{3.5}$$

is the error between the reference and the prediction of the variable x_i, and *n* is the number of variables to be taken into account in the cost function *g*. The symbol * denotes the reference value and the superscript p represents the prediction value of the variable x_i.

w_i is the weight for each error e_i and is used also to normalize the different variables x_i. In order to give a non-dimensional per-unit perception of all variables x_i, normalization is necessary, thus each variable x_i is divided by the base value x_i^N, i.e. the error e_i is re-defined as a per-unit error:

$$e_i = \frac{x_i^* - x_i^p}{x_i^N} \tag{3.6}.$$

Further the range of values of the weights w_i are: $w_i \in [0,1]$, and they determine the high-importance (values close or equal to 1) or the low-importance (values close or equal to 0) of the variable x_i in the cost function *g*.

The quadratic terms in the cost function increase the sensibility to the error e_i. Instead of a quadratic cost function a linear one can be used and (3.4) can be redefined as:

$$g = \sum_{i=1}^{n} \left(w_i \left| e_i \right| \right) \tag{3.7}$$

In order to consider the trajectory of the variable x_i between the instants t_k and t_{k+1} (and not only the prediction value at t_{k+1}), the following expression (described by the integral value of the error e_i) defines a trajectory cost function:

$$g = \sum_{i=1}^{n} \left(\int_{t_k}^{t_{k+1}} \left(w_i \left| e_i \right| \right) dt \right) \tag{3.8}$$

Some authors, for instance Laczynski and Mertens in [39] suggest a trajectory cost function considering not only the interval between the instants t_k and t_{k+1}, but also considering the past, the present and the future in the computation of the cost function, i.e. the integration interval is defined between the values at the instant t_{k-L} and t_{k+H}, with *L* and *H* being integer numbers and representing the number of instants before and after of the present instant t_k, in other words:

$$g = \sum_{i=1}^{n} \left(\int_{t_{k-L}}^{t_{k+H}} \left(w_i \left| e_i \right| \right) dt \right) \tag{3.9}$$

The different cost functions applied in power electronics and drives usually only have one prediction horizon. The main reason for this practice is that predictive control by definition is Receding-Horizon-Control (RCH), i.e. the predictive control is adjusted, corrected and controlled in each instant. Although a large prediction-horizon is possible, it implies more computational effort, therefore in the present work just one prediction-horizon is used.

3.1.9. Constraints in Cost Functions Applied in Power Electronics and Drives

As already mentioned in section 3.1.4, the constraints of the system must be taken into account in the modelling as well as in the calculation of the cost function. In the case of power electronics and drive applications, the constraints can be found in the physical limits (maximum values of current and voltages) of the electrical machine and the converter. For the case of electrical drives, the inverter limitations have to be included into the cost function, in particular the current limit [8]. Thus, the cost function (3.4) including the electrical drive constraints can be expressed as:

$$g = \sum_{i=1}^{n} \left(w_i e_i^2 \right) + f_{Lim} \left(i_1^p \right) \tag{3.10}$$

where i_1^p is the predicted stator current value, and f_{Lim} is defined as:

$$f_{Lim} \left(i_1^p \right) = \begin{cases} \infty, if \left| i_1^p \right| > i_{\max} \\ 0, if \left| i_1^p \right| \le i_{\max} \end{cases} \tag{3.11}$$

Generalizing, any constraint can be then included into the cost function, so (3.10) can be rewritten as:

$$g = \sum_{i=1}^{n} \left(w_i e_i^2 \right) + \sum_{j=1}^{n_{Const}} \left(f_{Lim} \left(j^p \right) \right) \tag{3.12}$$

where j is any constraint variable, n_{Const} is the number of constraints and the value of f_{Lim} is defined also as:

$$f_{Lim} \left(j^p \right) = \begin{cases} \infty, if \left| j^p \right| > j_{\max} \\ 0, if \left| j^p \right| \le j_{\max} \end{cases} \tag{3.13}$$

3.2. The System LC Filter – PMSM

In the present investigation a symmetrical 3-phase PMSM is used, consequently a 3-phase sine-wave filter with the capacitors in delta connection is selected (see Fig. 3.5a). For the mathematic modelling of the filter the equivalent circuit of the 3-phase LC-Filter, as shown in Fig. 3.5b is used.

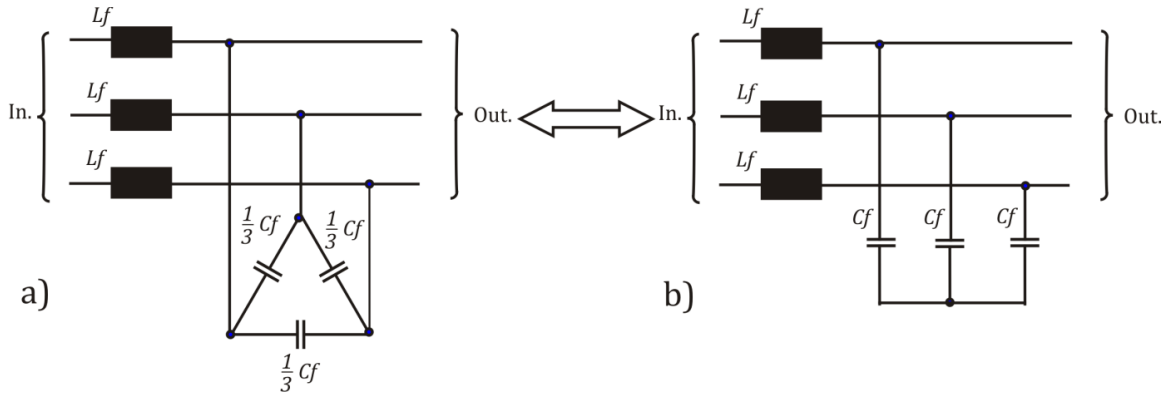

Fig. 3.5. a) Used LC-filter b) Equivalent circuit

The whole analyzed system consists of a 3-phase PMSM, a 3-phase two-level inverter and a 3-phase sine-wave filter (LC-filter) as shown in Fig. 3.6.

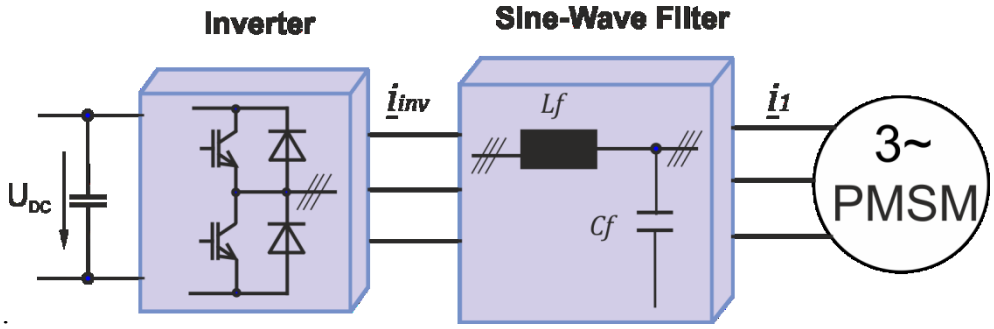

Fig. 3.6. System "LC-Filter-PMSM"

3.2.1. State-Space Model of the System LC Filter - PMSM

In order to describe the examined system, the equations for the PMSM are augmented by the addition of the LC-filter equations. For the equations of the LC-filter in the rotor coordinate system d,q follows:

$$\begin{aligned} u_{inv\_d} &= R_f i_{inv\_d} + L_f \frac{di_{inv\_d}}{dt} - \dot{\gamma} L_f i_{inv\_q} + u_{1d} \\ u_{inv\_q} &= R_f i_{inv\_q} + L_f \frac{di_{inv\_q}}{dt} + \dot{\gamma} L_f i_{inv\_d} + u_{1q} \end{aligned} \tag{3.14}$$

$$\begin{aligned} i_{inv\_d} &= i_{1d} + C_f \frac{du_{1d}}{dt} - \dot{\gamma} C_f u_{1q} \\ i_{inv\_q} &= i_{1q} + C_f \frac{du_{1q}}{dt} + \dot{\gamma} C_f u_{1d} \end{aligned} \tag{3.15}$$

L_f, R_f and C_f are the inductance, resistance and capacitance of the filter respectively; the angular velocity $\dot{\gamma} = p\Omega$, where $\dot{\gamma}$ and Ω are the rotor electrical and the mechanical velocity respectively, p is the numbers of pole pairs; u_{1d}, u_{1q}, and i_{1d}, i_{1q} are the real and imaginary components of the stator voltage and current space phasors of the PMSM and u_{inv_d}, u_{inv_q}, and i_{inv_d}, i_{inv_q} are the real and imaginary components of the space phasors of the inverter voltage and current.

The equations of the PMSM in the rotor reference frame d,q have been already described in the section 2.3.4, however to complete the mathematical description of the system "LC-Filter-PMSM" (2.42) and (2.43) can be rewritten as:

$$\begin{aligned} u_{1d} &= R_1 i_{1d} + L_1 \frac{di_{1d}}{dt} - \dot{\gamma} L_1 i_{1q} \\ u_{1q} &= R_1 i_{1q} + L_1 \frac{di_{1q}}{dt} + \dot{\gamma} L_1 i_{1d} + \dot{\gamma} \psi_p \end{aligned} \tag{3.16}$$

where ψ_p is the permanent magnet flux linkage, R_1 is the resistance of the stator winding, $L_1 = L_{1d} = L_{1q}$ is the inductance of the machine. A magnetic isotropic rotor of the PMSM is assumed and L_{1d} (direct axis self-inductance), L_{1q} (quadrature axis self-inductance) are therefore equal.

By rearranging (3.14)-(3.16), the state-space representation of the electrical part of the system "LC-Filter-PMSM" can be written as:

$$\dot{\underline{x}} = A\underline{x} + B\underline{u} + \underline{S} \tag{3.17}$$

$$\underline{y} = C\underline{x} \tag{3.18}$$

where the state vectors and the state space matrices are:

$$\underline{x} = \begin{bmatrix} i_{inv\_sd} & i_{inv\_q} & u_{1d} & u_{1q} & i_{1d} & i_{1q} \end{bmatrix}^T \tag{3.19},$$

$$\underline{y} = \begin{bmatrix} i_{inv\_d} & i_{inv\_q} \end{bmatrix}^T \tag{3.20},$$

$$\underline{u} = \begin{bmatrix} u_{inv\_d} & u_{inv\_q} \end{bmatrix}^T \tag{3.21},$$

$$B = \begin{bmatrix} 1/L_f & 0 & 0 & 0 & 0 & 0 \\ 0 & 1/L_f & 0 & 0 & 0 & 0 \end{bmatrix}^T \tag{3.22},$$

$$C = \begin{bmatrix} 1 & 0 & 0 & 0 & 0 & 0 \\ 0 & 1 & 0 & 0 & 0 & 0 \end{bmatrix} \tag{3.23},$$

$$A = \begin{bmatrix} -\frac{R_f}{L_f} & \dot{\gamma} & -\frac{1}{L_f} & 0 & 0 & 0 \\ -\dot{\gamma} & -\frac{R_f}{L_f} & 0 & -\frac{1}{L_f} & 0 & 0 \\ \frac{1}{C_f} & 0 & 0 & \dot{\gamma} & -\frac{1}{C_f} & 0 \\ 0 & \frac{1}{C_f} & -\dot{\gamma} & 0 & 0 & -\frac{1}{C_f} \\ 0 & 0 & \frac{1}{L_1} & 0 & -\frac{R_1}{L_1} & \dot{\gamma} \\ 0 & 0 & 0 & \frac{1}{L_1} & -\dot{\gamma} & -\frac{R_1}{L_1} \end{bmatrix} \tag{3.24},$$

and $$\underline{S} = \begin{bmatrix} 0 & 0 & 0 & 0 & 0 & -\frac{\dot{\gamma}\psi_p}{L_1} \end{bmatrix}^T \tag{3.25}.$$

These equations are the base for the development of the control strategy.

3.2.2. Observer Model

The control of the augmented system of high order resulting from the connection of the sine-wave filter and the PMSM demands the knowledge of all state variables. The 3-phase inverter currents are measured and three inverter voltages can be obtained from the switching state and the measured DC-link voltage, but in addition the voltage and currents of the machine and the current of the capacitors are necessary for the realization of the control.

Due to cost, size and reliability issues, additional sensors are avoided but a Luenberger observer is used to estimate the non-measured state variables (Fig. 3.7 shows the Luenberger observer scheme). In the present work, the observer is capable of delivering the currents of the machine and thus allows the field-oriented control scheme of the PMSM with LC-filter. Yet the observer demands the knowledge of all the system parameters.

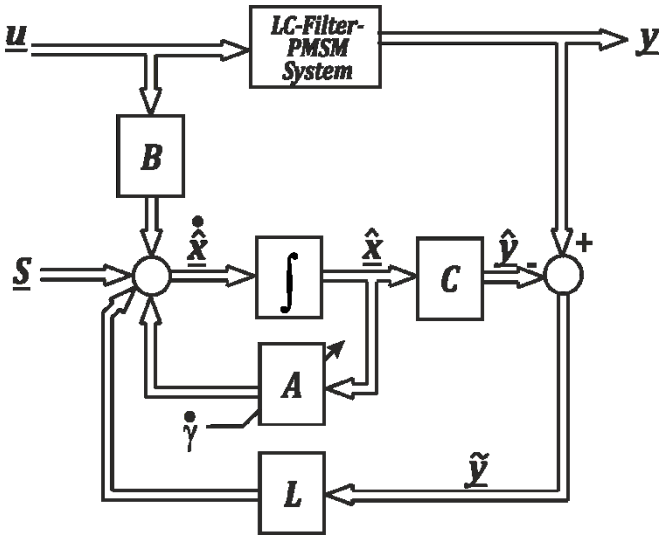

Fig. 3.7. General structure of a Luenberger observer

The Luenberger observer is described by its state space equations as:

$$\dot{\underline{x}} = A\underline{\hat{x}} + B\underline{u} + \underline{S} + L\underline{\tilde{y}} \tag{3.26}$$

where $\underline{\tilde{y}}$ is the error, i.e. the difference between the measured inverter current space phasor $\underline{y} = \underline{i}_{inv}$ and its estimated space phasor $\underline{\hat{y}}$, i.e.:

$$\underline{\tilde{y}} = C\left(\underline{x} - \underline{\hat{x}}\right) = \begin{bmatrix} i_{inv\_d} - \hat{} \\ i_{inv\_q} - \hat{} \end{bmatrix} \tag{3.27}$$

The states estimated with the observer are marked with the symbol "^". L is the observer gain matrix with simple constant gain values according to [40]:

$$L = \begin{bmatrix} k_{i_{inv\_d}} & k_{i_{inv\_q}} & k_{u_{l\_d}} & k_{u_{l\_q}} & k_{i_{l\_d}} & k_{i_{l\_q}} \\ -k_{i_{inv\_q}} & k_{i_{inv\_d}} & -k_{u_{l\_q}} & k_{u_{l\_q}} & -k_{i_{l\_q}} & k_{i_{l\_d}} \end{bmatrix}^T \tag{3.28}$$

3.3. Numerical Integration

In order to avoid interferences in the system, decoupling between the maximum frequency f_m of the PMSM, the resonance frequency of the LC-filter f_r and the switching frequency of the inverter f_{sw} should be well-preserved. In particular it is desirable to have a relationship

$f_m<f_r<f_{sw}$. Yet, interdependence occurs between the time of the numerical integration (the same as the switching time or sample time T_s) and the resonance time constant.

By applying the conventional implicit Euler method for the particular system LC-Filter-PMSM, the sample time has to be chosen far below the resonance time constant to ensure the stability of the numerical integration. In the present case, the sample time has to be set lower than 1µs, which cannot be realized with the available DSP control platform. Therefore, a low-order implicit method for the numerical integration of this complex system, like the traditional Euler fails and it does not deliver correct results especially during the transients.

In [40] a symmetric Euler method as solver system is proposed. This method is a combination between implicit and explicit numerical integration methods but in the present investigation did not yield satisfactory results.

After a simulation study with different methods, the Runge-Kutta implicit fourth-order method was selected because it ensures the stability of the numerical integration even with higher sample times (for example up 200µs).

In [41] different numerical methods for numerical solving i.e. integration systems of first-order ordinary differential equations (ODE´s) are explained: implicit, explicit, as well as high-order methods like the Runge-Kutta numerical integration.

For the present investigation, in which the system LC-Filter-PMSM is analyzed, the solution of (3.17) by using the Runge-Kutta fourth-order method was chosen and can be described in the following steps:

The discretization of the state space equations (3.26) at the instants t_k is:

$$\dot{\underline{x}}(k) = A\underline{\hat{x}}(k) + B\underline{u}(k) + \underline{S} + L\tilde{\dot{}} \tag{3.29}$$

The first the slope at t_k is assumed to be:

$$\underline{slp}_1 = \dot{\underline{x}}(k) = A\underline{\hat{x}}(k) + B\underline{u}(k) + \underline{S} + L\tilde{\dot{}} \tag{3.30}$$

Intermediate values can be obtained by:

$$\underline{slp}_2 = A\left(\underline{\hat{x}}(k) + \frac{1}{2}T_s \cdot \underline{slp}_1\right) + B\underline{u}(k) + \underline{S} + L\tilde{\underline{\cdot}} \tag{3.31}$$

$$\underline{slp}_3 = A\left(\underline{\hat{x}}(k) + \frac{1}{2}T_s \cdot \underline{slp}_2\right) + B\underline{u}(k) + \underline{S} + L\tilde{\underline{\cdot}} \tag{3.32}$$

$$\underline{slp}_4 = A\left(\underline{\hat{x}}(k) + T_s \cdot \underline{slp}_3\right) + B\underline{u}(k) + \underline{S} + L\tilde{\underline{\cdot}} \tag{3.33}.$$

Then it is possible to calculate the states variables at the instant t_{k+1} by combining the values obtained above, i.e.:

$$\underline{\hat{x}}(k+1) = \underline{\hat{x}}(k) + \frac{1}{6}T_s \cdot \left(\underline{slp}_1 + 2 \cdot \underline{slp}_2 + 2 \cdot \underline{slp}_3 + \underline{slp}_4\right) \tag{3.34}$$

The Runge-Kutta algorithm delivers the numerical integration of (3.17) at every sampling instant.

3.4. Control Strategy of the Predictive Control for the System PMSM-LC Filter

3.4.1. Principle of Operation

The predictive torque control is based on a cost function that minimizes the electromagnetic torque error by minimizing the errors of the currents i_{1q} and i_{1d}. For the evaluation of the cost function, a first estimate of the voltage space phasor that should be applied to the system in each point of operation is carried out. This is done by using the equations of the mathematical model of the whole system enhanced by a Luenberger observer and based on the measured inverter currents and on the shaft position. A superimposed velocity controller delivers the reference value for i_{1q}, and the i_{1d} reference value is set to zero. Fig. 3.8 shows a scheme of the predictive torque control for the system PMSM-LC filter.

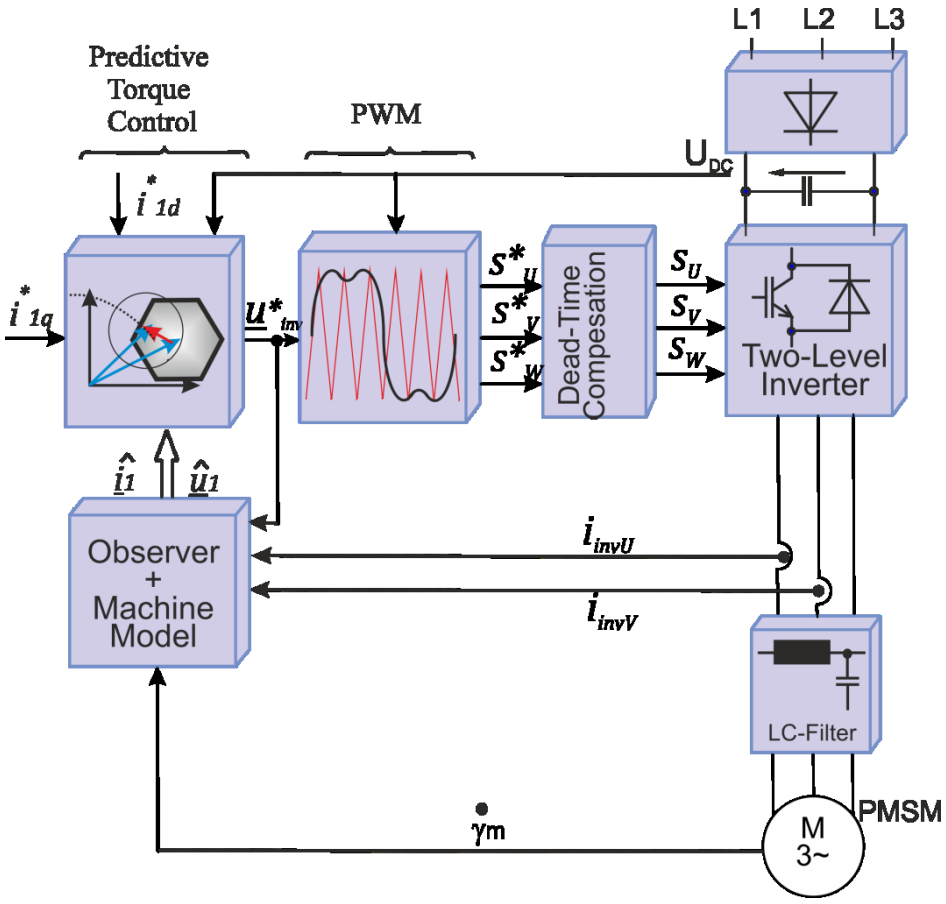

Fig. 3.8. Structure of the predictive torque control of a PMSM-drive

In the next step the predictive control demands the minimization of a cost function. The cost function is minimized by defining a mesh of voltage space phasors that corresponds to the output states of a "virtual" multilevel inverter with a high number of levels (>3). The center of this mesh with a finite number of elements corresponds to the first calculated value of the reference voltage. For the minimization only the points belonging to the mesh are considered. Based on this assumption the minimization procedure selects the voltage space vector that produces the minimum value of the cost function out of a finite number of states close to the first estimate. The voltage space phasor chosen in this way is then used for the calculation of the switching commands in a conventional space phasor modulation, which in the present work, is realized by using a sinus PWM with third harmonic injection as explained in the section 2.7. Finally these switching signals are sent to a real two-level inverter. The influence of the inverter dead-time is compensated according to [42].

The proposed scheme results in an easy implementation and delivers good dynamics in the torque behavior. Fig. 3.9 shows the flow diagram of the predictive torque control as described before.

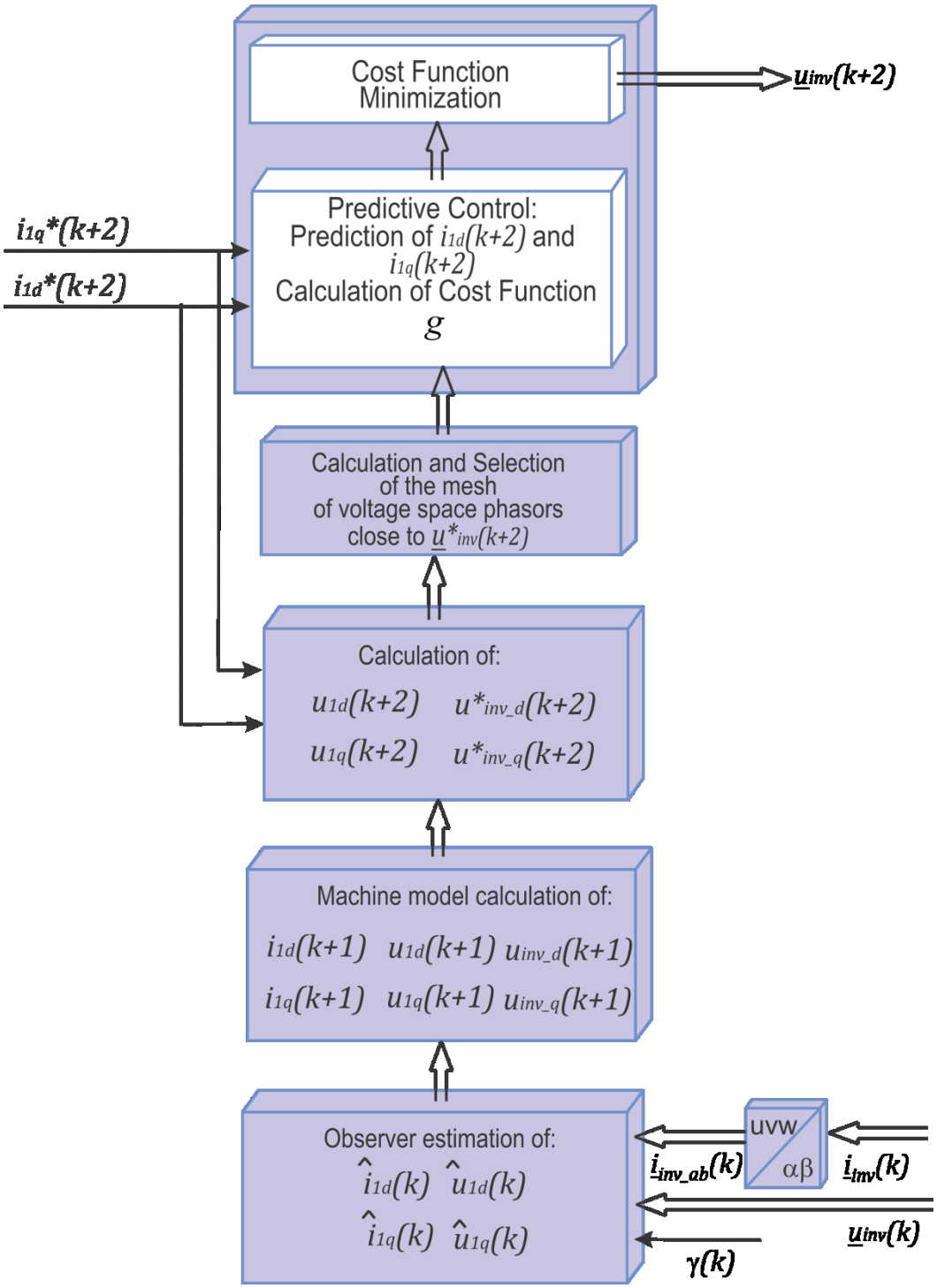

Fig. 3.9. Predictive torque control flow diagram

3.4.2. Ideal Voltage Space Phasor Reference

The mechanical time constant of the system is determined by the inertia of the machine and is usually large compared to the sampling time, hence it can be assumed that during the short sampling time the mechanical velocity of the machine does not change, i.e. $\dot{\gamma}(k+2) = \dot{\gamma}(k+1) = \dot{\gamma}(k) = \dot{\gamma}$. Thus for a discrete time step T_s it is possible to find the voltage space phasor that will be applied to the machine in the next sampling time t_{k+2} in order to reach the targets of the current references i^*_{1q} and i^*_{1d} in the next steps:

$$\begin{aligned} u_{1d}(k+2) &= R_1 i_{1d}(k+1) + L_1 \frac{i^*_{1d} - i_{1d}(k+1)}{Ts} - \dot{\gamma} L_1 i_{1q}(k+1) \\ u_{1q}(k+2) &= R_1 i_{1q}(k+1) + L_1 \frac{i^*_{1q} - i_{1q}(k+1)}{Ts} + \dot{\gamma} L_1 i_{1d}(k+1) + \dot{\gamma} \psi_p \end{aligned} \tag{3.35}$$

The inverter current in t_{k+2} can then be expressed by:

$$\begin{aligned} i_{inv\_d}(k+2) &= i^*_{1d} + C_f \frac{u_{1d}(k+2) - u_{1d}(k+1)}{Ts} - \dot{\gamma} C_f u_{1q}(k+1) \\ i_{inv\_q}(k+2) &= i^*_{1q} + C_f \frac{u_{1q}(k+2) - u_{1q}(k+1)}{Ts} + \dot{\gamma} C_f u_{1d}(k+1) \end{aligned} \tag{3.36}$$

With these machine voltages and inverter current space phasors it is also possible to calculate the inverter voltage space phasor which has to be applied to the whole system "LC-filter-PMSM":

$$\begin{aligned} u^*_{inv\_d}(k+2) &= R_f i_{inv\_d}(k+1) + L_f \frac{i_{inv\_d}(k+2) - i_{inv\_d}(k+1)}{Ts} - \dot{\gamma} L_f i_{inv\_q}(k+1) + u_{1d}(k+1) \\ u^*_{inv\_q}(k+2) &= R_f i_{inv\_q}(k+1) + L_f \frac{i_{inv\_q}(k+2) - i_{inv\_q}(k+1)}{Ts} + \dot{\gamma} L_f i_{inv\_d}(k+1) + u_{1d}(k+1) \end{aligned} \tag{3.37}$$

3.4.3. Cost function and optimization

The calculation so far corresponds to a pure model-based open loop control, to a feed forward control or to a deadbeat control. The system can be complemented by using an additional conventional control or an optimization by means of a cost function. In the present work, the possibility of an optimum control is examined focusing on a simple calculation of the cost function. The following simple cost function considers the error of the stator currents

in *d* and *q* reference frame and does not yield any significant enhancement in performance as long as the system is operated in the linear region. Yet it permits assigning a different weight to the dynamics of the currents i_{1d} and i_{1q}.

As the electromagnetic torque is direct proportional to the current i_{1q} a cost function at instant t_{k+2} defined by:

$$g = \left(\frac{i_{1_q}^{*}(k+2) - i_{1_q}^{p}(k+2)}{i^{N}} \right)^2 + w \left(\frac{i_{1_d}^{*}(k+2) - i_{1_d}^{p}(k+2)}{i^{N}} \right)^2 + f_{Lim}\left(i_{1_q}^{p}(k+2)\right) + f_{Lim}\left(i_{1_d}^{p}(k+2)\right) + f_{Lim}\left(i^{p}(k+2)\right) \tag{3.38}$$

with $$f_{Lim}\left(i_{1_q}^{p}\right) = \begin{cases} \infty, if \left|i_{1_q}^{p}\right| > i_{\max} \\ 0, if \left|i_{1_q}^{p}\right| \le i_{\max} \end{cases}, f_{Lim}\left(i_{1_d}^{p}\right) = \begin{cases} \infty, if \left|i_{1_d}^{p}\right| > i_{\max} \\ 0, if \left|i_{1_d}^{p}\right| \le i_{\max} \end{cases}, f_{Lim}\left(i_{1}^{p}\right) = \begin{cases} \infty, if \left|i_{1}^{p}\right| > i_{\max} \\ 0, if \left|i_{1}^{p}\right| \le i_{\max} \end{cases} \tag{3.39}$$

and $$i_{1}^{p} = \sqrt{\left(i_{1_d}^{p}\right)^2 + \left(i_{1_q}^{p}\right)^2} \tag{3.40}$$

is chosen. It contains the errors of the current components and the weight *w*. The weight *w* can be used for adjusting the dynamic behavior of the control, which is a different with respect to a simple feed-forward, open-loop control or a model based control. Besides, other constraints can be considered as it will be explained in the following chapters. As current constraints $i_{\max}$ the maximum current of the inverter is considered.

3.4.4. Virtual Multilevel Inverter and Mesh with Voltage Space Phasors as Finite Set

For the evaluation of the cost function a two level inverter is used yet a multilevel inverter with an arbitrary number of levels is assumed. The discrete voltage levels of this "virtual" inverter are emulated in order to allow easy selection of the values close to the ideal voltage space phasor reference and to apply them for minimization of the cost function in the predictive control.

In order to emulate the discrete voltage steps, the maximal value of the inverter output is first normalized and then discretized to divide the whole plane in triangles resembling the structure of a multilevel inverter with its possible space phasors in the corners of each triangle (see Fig. 3.10).

The "ideal voltage space phasor reference" $\underline{u}^{*}_{inv}\left(k+2\right)$ that is estimated with (3.37) is now located in one of the triangles of the possible outputs of the virtual multilevel inverter and the points in its neighborhood build a mesh of voltage space phasors that are found through an algebraic transformation as proposed by Correa in [21], i.e. changing from α,β to α',β' coordinates through the transformation matrix [T]:

$$\begin{bmatrix} u'_{inv\_\alpha} \\ u'_{inv\_\beta} \end{bmatrix} = [T] \begin{bmatrix} u_{inv\_\alpha} \\ u_{inv\_\beta} \end{bmatrix} = \frac{n-1}{U_{DC}} \begin{bmatrix} 3/2 & -\sqrt{3}/2 \\ 0 & \sqrt{3} \end{bmatrix} \begin{bmatrix} u_{inv\_\alpha} \\ u_{inv\_\beta} \end{bmatrix} \tag{3.41}$$

where

$$[T] = \begin{bmatrix} 3/2 & -\sqrt{3}/2 \\ 0 & \sqrt{3} \end{bmatrix} \tag{3.42}$$

and U_{DC} is the DC link voltage, or DC inverter input voltage and n represent the number of levels of the virtual multilevel inverter. u_{inv_α}, u_{inv_β}, u'_{inv_α} and u'_{inv_β} are respectively the components of a inverter voltage space phasor in α,β and α',β' coordinate system.

For example Fig. 3.10 shows the triangle-corner voltage space phasor $\underline{u}^{*}_{inv_k} = u^{*}_{inv_k\_\alpha} + j \cdot u^{*}_{inv_k\_\beta}$ in a α,β coordinate system with its equivalent $\underline{u}^{*}_{inv\_k} = \underline{k}$, its transformation and equivalent to the α',β' coordinate system is $\underline{u}^{*'}_{inv\_k} = \underline{k}'$ (here k is a integer number and represent one of the voltage space phasor of the mesh near to the ideal voltage reference).

Within this system of coordinates, it is extremely easy to find the space phasors close to the computed one by using the floor function in C-language. Thus the space phasor $\underline{u}^{*'}_{inv\_1}$ of the mesh is defined as:

$$\underline{u}^{*'}_{inv\_1} = \underline{1}' = \lfloor \mathrm{Re}\left\{\underline{u}^{*'}_{inv}\right\} + j\,\mathrm{Im}\left\{\underline{u}^{*'}_{inv}\right\} \rfloor \tag{3.43}$$

where the operator ⌊ ⌋ defines the "greatest integer smaller value than or equal to". The other mesh voltage space phasor points are calculated based on 1' by adding an integer multiple of the discrete voltage step in the real axis α' as well as in the imaginary axis β' on the α', β' – reference frame, for instance as it is shown in the Fig. 3.10 the voltage space phasors 2', 3', etc. Fig. 3.10a also shows an example for a 16-points mesh, and Fig. 3.10b for a 4-points mesh.

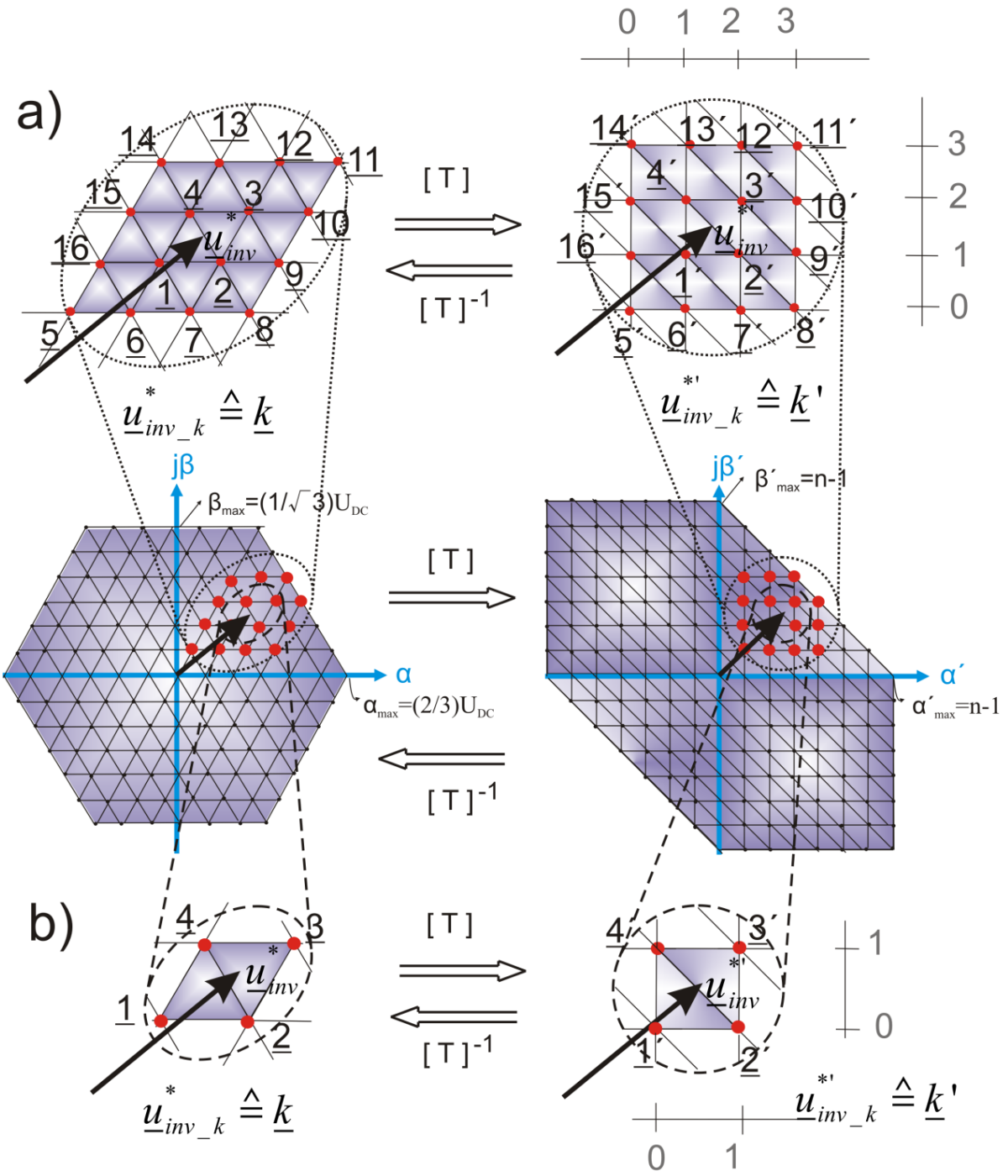

Fig. 3.10. Algebraic transformation of coordinate reference to find a mesh of a) 16-points, b) 4-points

3.4.5. Inverter Voltage Limit

In the cost function (3.38) of the predictive control for the system PMSM-LC-filter the current constraint is already included, but the inverter voltage limit (the space voltage space phasor points of the hexagon-limit in the plane of α, β – reference frame) was not taken into account until now.

In the section 3.1.9 it is suggested to include the inverter voltage constraint in the modelling, thus in the present work the inverter voltage limit is included in the model of the whole system as well as in the minimization/optimization of the cost function of the predictive controller.

If the operation of the system is in the linear region (that means, in the interior of the modulation circle), the points of the inverter voltage limits are no taken into account. The system works in this particular case (in linear region) as a pure model-based controller, actually as a dead beat control.

The inverter voltage limit is important in the case that "ideal voltage space phasor reference" u_{inv}^{*} is located either in the non-linear region (region between the internal and external circles) or outside of all (outside of the external circle).

In the case that the "ideal voltage space phasor reference" u_{inv}^{*} is located in the above-mentioned non-linear region, the suggested mesh of voltage space phasor points near to the first reference is generated, and then the minimization procedure is applied but just only with the points inside of the inverter voltage limit (see Fig. 3.11). The other mesh points outside will be not taken into account for the minimization of the cost function.

If the voltage space phasor points of the mesh near the first "ideal voltage space phasor reference" u_{inv}^{*} are located outside the external circle, then this reference u_{inv}^{*} is truncated to its cross-point with the hexagon-limit (denoted by u_{inv}^{**}), after that with this new point in the hexagon another mesh of voltage space phasor points close to the computed one is generated and finally the minimization procedure is applied to the last set of points as well (see Fig. 3.12).

In this way the proposed controlled scheme is ensured to operate in all regions (linear and non-linear), which is an advantage in comparison to conventional controllers.

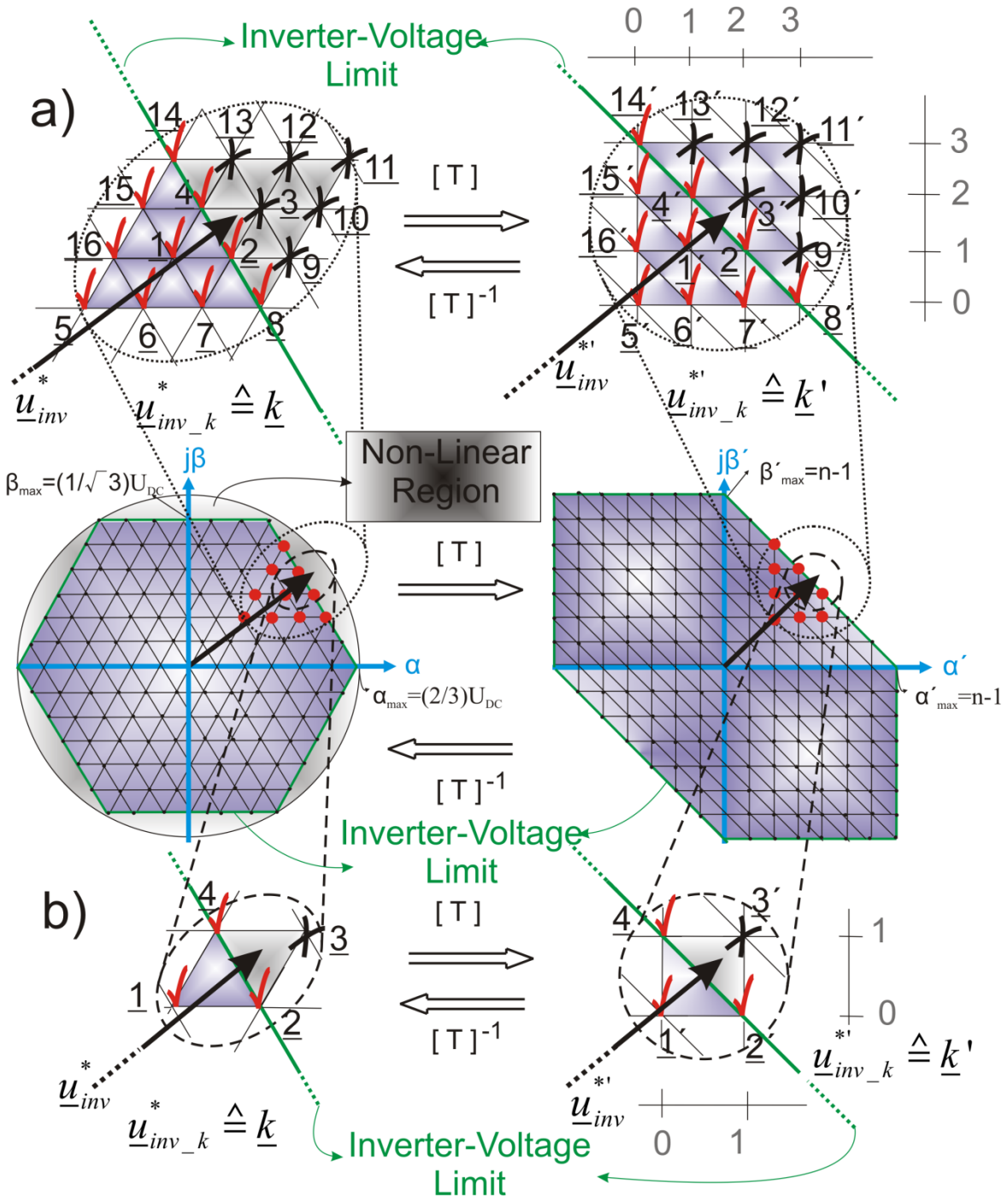

Fig. 3.11. An example for the ideal voltage reference in the non-linear region and mesh with voltage space phasor points inside and outside of the inverter voltage limits

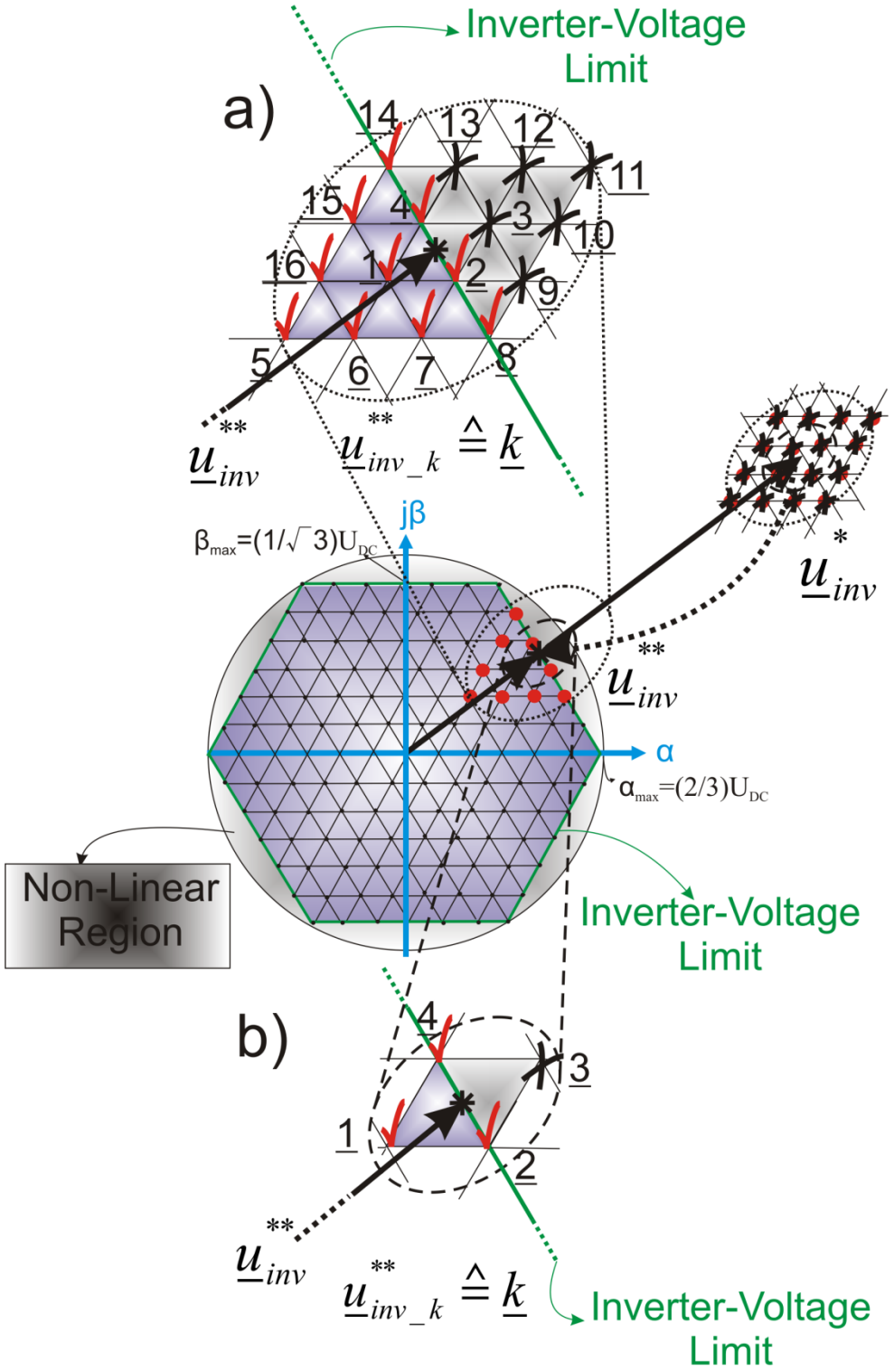

Fig. 3.12. Mesh of point near to the "ideal voltage space phasor reference" $\underline{u}^{*}_{inv}$ located outside the external circle

3.4.6. Enhanced Cost Function

Although the utilized cost function (3.38) works very good even in the case of voltage values in the non-linear region and outside of the external circle, it does not deliver appropriate voltage values if the parameters of the system are wrong and the desired results are not optimal.

In all technical systems, the parameters are not constant due to different physical effects like temperature, humidity, etc. An alternative is to add an on-line adaptive parameter tuning as it will be explained in the next sections. Another alternative that can also work in combination with the on-line adaptive parameter tuning is the applications of an enhanced cost function within the predictive control as it was already indicated in section 3.1.8.

If the system parameters are wrong, a trajectory cost function is proposed in order to improve the behavior of the system. Thus, a trajectory cost function takes into account the history of the system by summing up the past errors. For the systems PMSM-LC-filter such a cost function can be defined according to (3.9) as:

$$g = \int_{t_{k-L}}^{t_{k+H}} \left(\left|e_{iq}\right|\right) dt + w \int_{t_{k-L}}^{t_{k+H}} \left(\left|e_{id}\right|\right) dt \tag{3.44}$$

where

$$e_{iq} = \left| \frac{i_{1q}^{*} - i_{1q}^{p}}{i^{N}} \right| \tag{3.45}$$

and

$$e_{id} = \left| \frac{i_{1d}^{*} - i_{1d}^{p}}{i^{N}} \right| \tag{3.46}.$$

By considering an interval of integration that contains the three past steps before the actual sampling point and by applying a trapezoidal integration, the expression (3.44) can be redefined as:

$$
\begin{aligned}
g = {} & w_q e_{iq}(k+2) + w_d e_{id}(k+2) + \\
& w_{\Sigma q}\left(\frac{e_{iq}(k-1)+e_{iq}(k)}{2}\cdot T_s + \frac{e_{iq}(k)+e_{iq}(k+1)}{2}\cdot T_s + \frac{e_{iq}(k+1)+e_{iq}(k+2)}{2}\cdot T_s \right) + \\
& w_{\Sigma d}\left(\frac{e_{id}(k-1)+e_{id}(k)}{2}\cdot T_s + \frac{e_{id}(k)+e_{id}(k+1)}{2}\cdot T_s + \frac{e_{id}(k+1)+e_{id}(k+2)}{2}\cdot T_s \right)
\end{aligned}
\tag{3.47}
$$

where w_q, w_d, $w_{\Sigma q}$ and $w_{\Sigma d}$ are the weights of the predicted currents in *q* and *d*, and of the integration of the currents in *q* and *d* respectively. Rearranging (3.47), it can be rewritten as:

$$
\begin{aligned}
g = {} & w_q e_{iq}(k+2) + w_d e_{id}(k+2) + \\
& w'_{\Sigma q}\cdot\frac{T_s}{2}\left(e_{iq}(k-1) + 2e_{iq}(k) + 2e_{iq}(k+1) + e_{iq}(k+2) \right) + \\
& w'_{\Sigma d}\cdot\frac{T_s}{2}\left(e_{id}(k-1) + 2e_{id}(k) + 2e_{id}(k+1) + e_{id}(k+2) \right)
\end{aligned}
\tag{3.48}
$$

In this way a kind of I-control behavior can be obtained that reduces the steady state error in case of a model with inaccurate parameters.

Another possibility to improve the basic cost function is by including an "integral-action" in the model as well as in the cost function as suggested by Cannon in [37]. For a system expressed by the following steady-space representation:

$$
\begin{cases}
\underline{x}^p(k+1) = A\underline{x}(k) + B\underline{u}^*(k) \\
\underline{y}^p(k+1) = C\underline{x}^p(k+1)
\end{cases}
\tag{3.49}
$$

with $\underline{x}$, $\underline{u}^*$ and $\underline{y}$ being the state, input and output vectors and A, B, C being the system, input and output matrices. The control signal $\underline{u}^*(k)$ and the predicted values $\underline{x}^p(k+1)$ as well as $\underline{y}^p(k+1)$ for next instant t_{k+1} can be obtained by means of an optimization. If some system parameters are wrong, a permanent output error with respect to a reference $\underline{y}^*$ is persistent, i.e.:

$$
\underline{e}_y(k) = \underline{y}^*(k) - \underline{y}^m(k)
\tag{3.50}
$$

where $\underline{y}^m(k)$ is the measured value of the output $\underline{y}$ sampled at the instant t_k.

Then, for the calculated optimal control signal at the instant t_{k+1} is suggested to do an adjustment adding an integral-action given by:

$$\underline{u}^{**}(k+1) = \underline{u}^{*}(k+1) + K_I \cdot \int_{t_{k-L}}^{t_k} \left(\underline{e}_y(t)\right) dt \tag{3.51}$$

with K_I being an integral gain and L being an integer number they represent the number of past instants of the error $\underline{e}_y$ to be taken into account in the integration. If after a few steps in steady state the reference is reached then $\underline{e}_y \to 0$, i.e. an integral part of the expression becomes zero as well as the correction done in (3.51).

For the case of a cost function, similarly to (3.1) it is suggested to considerer the second part, i.e. to add the penalization due to the control effort. Should the cost functions be applied to control drives as in (3.7), a new expression adding the penalization due to the control effort can be redefined as:

$$g = \sum_{i=1}^{n}\left(w_i e_i^2\right) + \sum_{j=1}^{m}\left(w_j \sum_{uL}^{uH} \Delta u_j\right) \tag{3.52}$$

where n is the number of variables included in the prediction, m is the number of variables for considering the control-effort, and uL and uH are the limits of the control-effort horizon.

The applications of the integral-action procedure for the system LC-Filter-PMSM, the expressions (3.49)-(3.51) become:

$$\begin{aligned} u_{inv\_d}^{**}(k+2) &= u_{inv\_d}^{*}(k+2) + K_{Id} \cdot \int_{t_{k-L}}^{t_k} \left(e_{id}^{m}(t)\right) dt \\ u_{inv\_q}^{**}(k+2) &= u_{inv\_q}^{*}(k+2) + K_{Iq} \cdot \int_{t_{k-L}}^{t_k} \left(e_{iq}^{m}(t)\right) dt \end{aligned} \tag{3.53}$$

where K_{Id} and K_{Iq} are integral gains and

$$e_{id}^{m} = i_{1d}^{*} - i_{1d}^{m} \tag{3.54}$$

and $$e_{iq}^{m} = i_{1q}^{*} - i_{1q}^{m} \tag{3.55}$$

are the control errors.

If $L=k$, the second term of (3.53) is an integral that considers the whole past of the system beginning with t=0. So, (3.53) can be rewritten as:

$$\begin{aligned} u_{inv\_d}^{**}(k+2) &= u_{inv\_d}^{*}(k+2) + K_{Id} \cdot \int_{0}^{t_k} \left(e_{id}^{m}(t) \right) dt \\ u_{inv\_q}^{**}(k+2) &= u_{inv\_q}^{*}(k+2) + K_{Iq} \cdot \int_{0}^{t_k} \left(e_{iq}^{m}(t) \right) dt \end{aligned} \tag{3.56}$$

With these new "ideal voltage space phasor reference", the predictive control is applied in the linear region as well as the non-linear region and outside the external circle.

The cost function used in the experimental test is obtained by adding the penalization due to the control effort and is given by:

$$\begin{aligned} g = w_q \left(\frac{i_{1_q}^{*}(k+2) - i_{1_q}^{p}(k+2)}{i^N} \right)^2 + w_d \left(\frac{i_{1_d}^{*}(k+2) - i_{1_d}^{p}(k+2)}{i^N} \right)^2 + \\ w_{uq} \frac{1}{u^N} \sum_{j=-2}^{0} \left(\Delta u_q^{**}(k-j) \right) + w_{ud} \frac{1}{u^N} \sum_{j=-2}^{0} \left(\Delta u_d^{**}(k-j) \right) \end{aligned} \tag{3.57}$$

where w_q, w_d, w_{uq} and w_{ud} are the weights of the predicted currents in *q* and *d*, and of the control-efforts in *q* and *d* respectively.

$$\Delta u_q^{**}(k-j) = u_q^{**}(k-j) - u_q^{**}(k-j-1) \tag{3.58}$$

and $$\Delta u_d^{**}(k-j) = u_d^{**}(k-j) - u_d^{**}(k-j-1) \tag{3.59}$$

are the difference between control signals of two consecutive instances. If in steady state the reference trajectory is reached, this control effort becomes zero.

3.5. Summary of the Chapter

This chapter explains the main concepts of predictive control and its overall principles, features, advantages, disadvantages. The cost function and optimization of the predictive control, with special attention dedicated to the application of predictive control in power electronics and drives.

In a second part of the chapter, the state-space model of the system PMSM-LC-Filter is described and an observer is introduced for obtaining the variables that are not measured. It is also explained that simple single-step numerical integration fails to deliver correct results and a high order solver like Runge-Kutta becomes necessary.

Besides, a novel predictive control with a continuous control set for the system PMSM-LC filter is proposed. Its principle of operation, the calculation of an ideal voltage space phasor reference, the use of a virtual multilevel inverter and a mesh of points near to the first reference for the reduction of the computational effort in the minimization of the cost function are explained.

The inverter voltage limit as well as the current constraints are also considered in the cost function and in the calculation of the minimization. This is done to guarantee the operation of the proposed predictive control in linear- and nonlinear-regions.

Finally, the performance of the proposed predictive control is improved by adding an “I-control” part and an “integral action” in the calculation of the ideal space phasor voltage reference as well as in the minimization of the cost function of the predictive control. In this way, the steady state error is reduced in case of a model with erroneous parameters.

4. SENSORLESS CONTROL, ON-LINE PARAMETER IDENTIFICATION AND ADAPTIVE TUNING

4.1. Sensorless Control

4.1.1. Introduction

Mechanical sensors for the measurement of the angular position of the shaft in electrical drives with an encoder, are sensitive to influences of the environment, such as temperature, humidity, noise, etc. and also lead to high mechanical and electrical installation effort. For all these reasons the control of the drive without a mechanical rotor position sensor has become an interesting topic of research.

Thus, the motivations for eliminating the rotor position sensor is the reduction of hardware complexity, of the length of the machine, of the maintenance requirements and of the cost, as well as the elimination of sensor cables and interface cards, which increase noise immunity leading to better reliability.

Holtz in [43] describes the state of the art of sensorless AC-Drives. Kubota [44] and Quang [30] explain several methods of control without speed or rotor position sensor and Luomi and Hinkkanen et al. in [45] and [13] improve the full- and reduced-order observer and signal injection methods for the implementation in encoder-less drives.

In general, the methods for sensorless-control of electrical machines are classified in fundamental wave-models and in signal-injection-techniques. Both need to extend the mathematical models in the control, but especially the signal-injection techniques require a more complex control scheme. The fundamental-wave model methods are based either on observer structures or on the voltage-model of the machine.

The estimated rotor position is necessary for the coordinate transformations between the stator-fixed- and an arbitrary-reference frame in the field oriented control and for the control of the mechanical velocity.

4.1.2. Observer Based Methods

Based on the Luenberger observer structure mentioned in the section 3.2.2, the output error $\tilde{y}$ between the output y- and the observer-output signals $\hat{y}$, is not only used for the estimation of the state vector x but also to estimate the angular velocity $\dot{\gamma}$. Fig. 4.1 shows an observer structure that takes the angular velocity estimation into account.

The estimation of the angular velocity is obtained by means of a PI compensator. Thus, the estimation of the angular velocity expression is given by [30]:

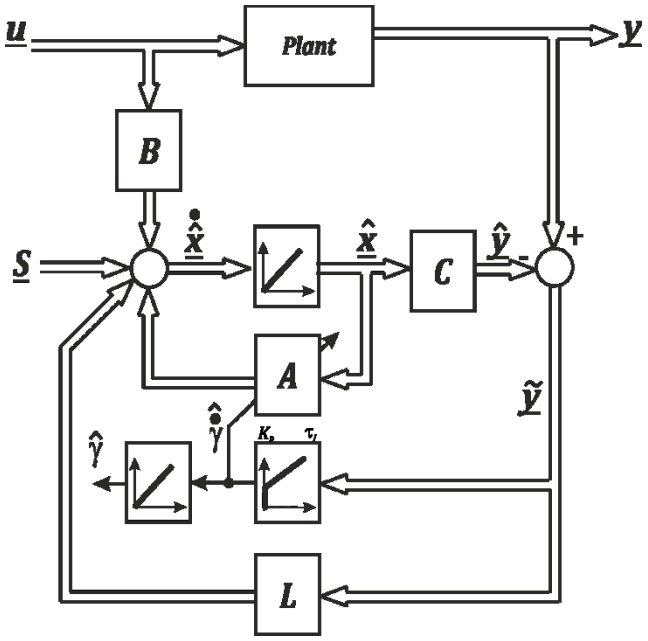

Fig. 4.1. Structure of a Luenberger observer with angular velocity and rotor position estimation

$$\dot{\gamma} = K_P \cdot e_\omega + K_I \int e_\omega dt \tag{4.1}$$

where K_P and K_I are the gain matrices. If the output vector corresponds to the stator current, the estimation of the angular velocity is expressed as:

$$\dot{\gamma} = K_P \cdot e_{\omega i} + K_I \int e_{\omega i} dt \tag{4.2}$$

with $e_{\omega i} = f\left(\tilde{\quad} \quad \tilde{\quad}\right.$, (4.3)

The estimated rotor position γ is found by the integration of the estimated angular velocity $\dot{\gamma}$. A similar concept based on the voltage model of the machine is explained in the following.

4.1.3. Voltage Model Method

Feuersänger et al. in [46] improve the method proposed by Barinberg et al. in [47] to estimate the angular-velocity and rotor position for the sensorless control of PMSM-Drives. The method is based on the voltage model of the machine in the $d, q-$coordinates and consists firstly to find the voltage error $\Delta\underline{u}_1$ between the machine voltage and the calculated voltage value that is computed by the model of the machine with the current measurements and the parameters of the machine. With this voltage error and under some conditions, the rotor position and the angular velocity can be estimated. The voltage error is defined as:

$$\Delta\underline{u}_1 = \underline{u}_1^* - \underline{u}_1^{\text{model}} = \begin{cases} \Delta u_{1d} = u_{1d}^* - u_{1d}^{\text{model}} \\ \Delta u_{1q} = u_{1q}^* - u_{1q}^{\text{model}} \end{cases} \tag{4.4}$$

$\underline{u}_1^{\text{model}}$ is the expressions already presented in (2.42) and (2.43) and is derived from the mathematic model of a PMSM, thus (4.4) can be rewritten as:

$$\begin{aligned} \Delta u_{1d} &= u_{1d}^* - R_{1d} \cdot i_{1d} - L_{1d} \cdot \dot{i}_{1d} + \dot{\gamma} \cdot L_{1q} \cdot i_{1q} \\ \Delta u_{1q} &= u_{1q}^* - R_{1q} \cdot i_{1q} - L_{1q} \cdot \dot{i}_{1q} - \dot{\gamma} \cdot L_{1d} \cdot i_{1d} - \dot{\gamma} \cdot \psi_P \end{aligned} \tag{4.5}$$

Should all machine parameters be correct and should the machine currents, the angular velocity and rotor position be measured with an encoder, then the errors Δu_{1d} and Δu_{1q} become ideally zero.

In contrast, in the sensorless operation an angular position error $\Delta\gamma$ cannot be avoided:

$$\Delta\gamma = \gamma - \gamma \tag{4.6}$$

where γ and γ are the estimate and real rotor position respectively. Thus, another reference frame, aligned with the estimated but erroneous angle γ can be defined and designated in the

$d,q-$system of coordinates. In this new reference frame, considering that the machine does not exhibit strong variations in L_{1d} and L_{1q} ($\Delta L \ll L_{1d}$) the estimated machine voltage can be approximated as [47]:

$$\begin{aligned}
u_{1d}^{*} &= R_{1d}\cdot i_{1d} + \left(L_{1d} - 2\cdot\Delta L\cdot\sin^2(\Delta\gamma)\right)\cdot\dot{i}_{1d} + \Delta L\cdot\dot{\gamma}\cdot\sin(2\Delta\gamma)\cdot i_{1d} \\
&-\Delta L\cdot\sin(2\Delta\gamma)\cdot\dot{i}_{1q} - \left(L_{1q} + 2\cdot\Delta L\cdot\sin^2(\Delta\gamma)\right)\cdot\dot{\gamma}\cdot i_{1q} + \psi_P\cdot\dot{\gamma}\cdot\sin(\Delta\gamma) \\
u_{1d}^{*} &\approx R_{1d}\cdot i_{1d} + L_{1d}\cdot\dot{i}_{1d} - \dot{\gamma}\cdot L_{1q}\cdot i_{1q} + \psi_P\cdot\dot{\gamma}\cdot\sin(\Delta\gamma) \\
u_{1q}^{*} &= R_{1q}\cdot i_{1q} + \left(L_{1q} + 2\cdot\Delta L\cdot\sin^2(\Delta\gamma)\right)\cdot\dot{i}_{1q} - \Delta L\cdot\sin(2\Delta\gamma)\cdot\dot{\gamma}\cdot i_{1q} \\
&-\Delta L\cdot\sin(2\Delta\gamma)\cdot\dot{i}_{1q} + \left(L_{1d} + 2\cdot\Delta L\cdot\sin^2(\Delta\gamma)\right)\dot{\gamma}\cdot i_{1d} + \psi_P\cdot\dot{\gamma}\cdot\cos(\Delta\gamma) \\
u_{1q}^{*} &\approx R_{1q}\cdot i_{1q} + L_{1q}\cdot\dot{i}_{1q} + \dot{\gamma}\cdot L_{1d}\cdot i_{1d} + \psi_P\cdot\dot{\gamma}\cdot\cos(\Delta\gamma)
\end{aligned} \tag{4.7}$$

with u_{1d}^{*} and u_{1q}^{*}, being the machine voltages, R_{1d} and R_{1q}, being the stator resistance values and L_{1d} and L_{1q} being the stator inductance values in the dq-coordinate system, and i_{1d} and i_{1q} being the stator currents transformed with the estimated rotor angle γ in the $d,q-$ coordinate system and $\Delta L = \left(L_{1d} - L_{1q}\right)/2$.

For small angle errors $\Delta\gamma$, the machine voltages u_{1d}^{*} and u_{1q}^{*} in the estimated frame are practically the same as u_{1d}^{*} and u_{1q}^{*} in the real *dq*-frame, the same applies to the machine parameters and to the current, in other words $u_{1d}^{*} \cong u_{1d}^{*}$, $u_{1q}^{*} \cong u_{1q}^{*}$, $R_{1d} = R_{1d}$, $R_{1q} = R_{1q}$, $L_{1d} = L_{1d}$, $L_{1q} = L_{1q}$, $i_{1d} = i_{1d}$, $i_{1q} = i_{1q}$, thus (4.7) can be approximated as:

$$\begin{aligned}
u_{1d}^{*} &\approx u_{1d}^{*} \\
u_{1d}^{*} &\approx R_{1d}\cdot i_{1d} + L_{1d}\cdot\dot{i}_{1d} - \dot{\gamma}\cdot L_{1q}\cdot i_{1q} + \psi_P\cdot\dot{\gamma}\cdot\sin(\Delta\gamma) \cong R_{1d}\cdot i_{1d} + L_{1d}\cdot\dot{i}_{1d} - \dot{\gamma}\cdot L_{1q}\cdot i_{1q} + \psi_P\cdot\dot{\gamma}\cdot\sin(\Delta\gamma) \\
u_{1q}^{*} &\approx u_{1q}^{*} \\
u_{1q}^{*} &\approx R_{1q}\cdot i_{1q} + L_{1q}\cdot\dot{i}_{1q} + \dot{\gamma}\cdot L_{1d}\cdot i_{1d} + \psi_P\cdot\dot{\gamma}\cdot\cos(\Delta\gamma) \cong R_{1q}\cdot i_{1q} + L_{1q}\cdot\dot{i}_{1q} + \dot{\gamma}\cdot L_{1d}\cdot i_{1d} + \psi_P\cdot\dot{\gamma}\cdot\cos(\Delta\gamma)
\end{aligned} \tag{4.8}$$

In the same way, the voltage error (4.5) can be rewritten as:

$$\Delta u_{1d} \approx u_{1d}^{*} - R_{1d} \cdot i_{1d} - L_{1d} \cdot \dot{i}_{1d} + \dot{\gamma} \cdot L_{1q} \cdot i_{1q} \cong u_{1d}^{*} - R_{1d} \cdot i_{1d} - L_{1d} \cdot \dot{i}_{1d} + \dot{\gamma} \cdot L_{1q} \cdot i_{1q}$$
$$\Delta u_{1q} \approx u_{1q}^{*} - R_{1q} \cdot i_{1q} - L_{1q} \cdot \dot{i}_{1q} - \dot{\gamma} \cdot L_{1d} \cdot i_{1d} - \dot{\gamma} \cdot \psi_P \cong u_{1q}^{*} - R_{1q} \cdot i_{1q} - L_{1q} \cdot \dot{i}_{1q} - \dot{\gamma} \cdot L_{1d} \cdot i_{1d} - \dot{\gamma} \cdot \psi_P \quad (4.9)$$

Replacing (4.8) in (4.9) yields:

$$\Delta u_{1d} \cong \psi_P \cdot \dot{\gamma} \cdot \sin(\Delta\gamma)$$
$$\Delta u_{1q} \cong \psi_P \cdot \left(\dot{\gamma} \cdot \cos(\Delta\gamma) - \dot{\gamma} \right) \quad (4.10)$$

By assuming small angle errors $\Delta\gamma$, the trigonometric terms can be approximated as $\sin(\Delta\gamma) \cong \Delta\gamma$ and $\cos(\Delta\gamma) \cong 1$, and (4.10) can be simplified:

$$\Delta u_{1d} \cong \psi_P \cdot \dot{\gamma} \cdot \Delta\gamma$$
$$\Delta u_{1q} \cong -\psi_P \cdot \Delta\dot{\gamma} \quad (4.11)$$

With both voltage errors available, a rotor position and angular velocity estimation is proposed in [46] using the control structure illustrated in Fig. 4.2, with $1/\tau_\omega$ being the corner frequency of the controller response in the bode diagram.

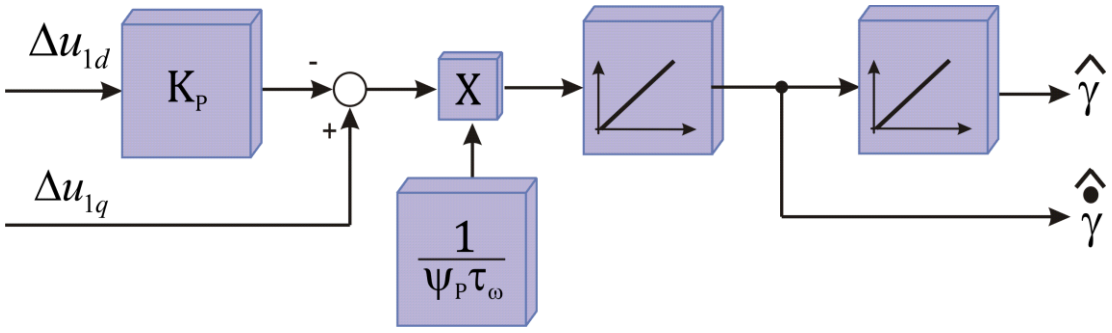

Fig. 4.2. Rotor position and angular velocity estimation

It is important to mention that the rotor position and angular velocity estimation work properly if all machine parameters correspond to their real values, otherwise the performance of the sensorless control decreases. It is well known that stator resistance and permanent magnet flux are influenced by temperature, which means both parameters are not constant, and therefore an on-line parameter identification and adaptive parameter tuning is necessary, which will be explained in the next section.

It is also important to include a compensation of the dead-time effects on the output voltage of the inverter in the control scheme, because the inverter dead-times generate voltage errors causing interference in the proposed solution and in consequence a bad performance of the sensorless-control. To eliminate the inverter nonlinearities due to the inverter dead-times, a compensation according to [42] is implemented in the present work.

The voltage errors Δu_{1d} and Δu_{1q} are calculated for the systems LC-Filter-PMSM, by using the machine voltage reference space phasor $\underline{u}_1$ described in (3.35) and the estimated machine voltage space phasor obtained by the Luenberger observer found in (3.26), i.e. the voltage errors are expressed as:

$$\begin{aligned} \Delta u_{1d} &= u_{1d}^{*} - u_{1d}^{\text{model}} = u_{1d} - u_{1d}^{\text{model}} \Rightarrow \Delta u_{1d}(k) = u_{1d}(k) - u_{1d}(k) \\ \Delta u_{1q} &= u_{1q}^{*} - u_{1q}^{\text{model}} = u_{1q} - u_{1q}^{\text{model}} \Rightarrow \Delta u_{1q}(k) = u_{1q}(k) - u_{1q}(k) \end{aligned} \tag{4.12}$$

4.2. On-Line PMSM Parameter Identification and Adaptive Tuning

To insure a good performance of the control an online parameter adaption is necessary. This requires knowing the exact values of the system parameters. Especially in the sensorless control, in which the estimation of the rotor position strongly depends on the accuracy of the machine parameters, the adaptive parameter tuning becomes crucial.

Inductances depend on the machine currents but not on the temperature. Therefore a look up table that considers the dependency of the inductances on the saturation is the better choice. As stated before resistance and flux strongly depend on the temperature. A temperature rise of 100K leads to an 40% increase of the stator resistance in a cooper winding ($\alpha_{Cu} \cong 0{,}39\%/K$). In the case of a PMSM the permanent flux value decreases if the temperature is increased. The change depends on the used magnetic material. For NdFeB-magnets, the variation is of approximately -12% for a $\Delta\vartheta$ of 100K.

In [30] [48] [49] [50] several methods to identify and real-time adapt the parameters of electrical machines are presented, however these methods identify only one parameter, either resistance or flux, but not both parameters at the same time, which is insufficient because both are temperature dependent.

Therefore, in the following an enhanced on-line parameter identification and adaptive parameter tuning for PMSM-control schemes based on [51] is proposed. This method can simultaneously identify both parameters: stator resistance and permanent magnetic flux and can operate in high dynamic applications that are often not taken into consideration in other identification methods that are known form the literature.

4.2.1. Enhanced On-line PMSM Adaptive Parameter Tuning

By assuming that the rotor position is identified or measured correctly the voltage errors Δu_{1d}^{Param} and Δu_{1q}^{Param} can be computed based on the wrong model parameters as follows:

$$\Delta u_{1d}^{Param} = u_{1d}^{\text{model}} - u_{1d}^{real} = -\Delta R_1 \cdot i_{1d} - \Delta L_{1d} \cdot \frac{di_d}{dt} + \Delta L_{1q} \cdot \dot{\gamma} \cdot i_{1q} \tag{4.13}$$

$$\Delta u_{1q}^{Param} = u_{1q}^{\text{model}} - u_{1q}^{real} = -\Delta R_1 \cdot i_{1q} - \Delta L_{1q} \cdot \frac{di_q}{dt} - \Delta L_{1d} \cdot \dot{\gamma} \cdot i_{1d} - \Delta \psi_P \cdot \dot{\gamma} \tag{4.14}$$

where $\Delta R_1 = R_1^{\text{model}} - R_1^{real}$, $\Delta \psi_P = \psi_P{}^{\text{model}} - \psi_P{}^{real}$ and $\Delta L_{1d\_or\_1q} = L_{1d\_or\_1q}^{\text{model}} - L_{1d\_or\_1q}^{real}$.

Thus, the machine voltage errors computed by using the wrong model parameters are given by:

$$\Delta u'_{1d} = \Delta u_{1d} + \Delta u_{1d}^{Param} \cong \psi_P \cdot \dot{\gamma} \cdot \Delta\gamma - \Delta R_1 \cdot i_{1d} - \Delta L_{1d} \cdot \frac{di_d}{dt} + \Delta L_{1q} \cdot \dot{\gamma} \cdot i_{1q} \tag{4.15}$$

$$\Delta u'_{1q} = \Delta u_{1q} + \Delta u_{1q}^{Param} \cong -\psi_P \cdot \Delta\dot{\gamma} - \Delta R_1 \cdot i_{1q} - \Delta L_{1q} \cdot \frac{di_q}{dt} - \Delta L_{1d} \cdot \dot{\gamma} \cdot i_{1d} - \Delta \psi_P \cdot \dot{\gamma} \tag{4.16}$$

Eq. (4.16) does not depend on the rotor position error $\Delta\gamma$ and can therefore be used for the sensorless control as well as for the on-line parameter identification, due to the large difference of the time-constants influencing the change of the parameters (several minutes) and the angular velocity error variation (several milliseconds).

For the parameter identification, $\Delta u'_{1d}$ cannot be used because it depends not only on the model parameter errors but also on the rotor position error $\Delta\gamma$. Thus, a decoupling of both is not possible as the position error can be nonzero even under steady state conditions. In the opposite case, for $\Delta u'_{1q}$ these restrictions do not appear, because $\Delta u'_{1q}$ depends only on the angular velocity error $\Delta\dot{\gamma}$ with zero average value as long as the sensorless control is stable.

This voltage error $\Delta u'_{1q}$ is a function of both temperature dependent machine parameters R_1 and ψ_P. Under special conditions, these two parameters can be identified based on this voltage error $\Delta u'_{1q}$. Therefore, for sensor- as well as for sensorless-operation and for the on-line parameter identification the voltage error $\Delta u'_{1q}$ is used.

Equations (4.13) and (4.14) are overdetermined, because there are only two equations for four unknown variables (R_1, ψ_P, L_{1d}, L_{1q}). Therefore, some simplifications are necessary in order to decouple the effects of these four unknown variables.

On the one hand, terms containing derivatives can be neglected because their average value is zero and they are not significant in the dynamic of the on-line identification due to their large thermal time-constant. On the other hand, if only the operation of the machine in the base speed range but not in the field weakening area is considered, the flux generating current i_{1d} is zero and (4.13) and (4.14) become:

$$\Delta u_{1d}^{Param} \cong \Delta L_{1q} \cdot \dot{\gamma} \cdot i_{1q} \tag{4.17}$$

and

$$\Delta u_{1q}^{Param} \cong -\Delta R_1 \cdot i_{1q} - \Delta \psi_P \cdot \dot{\gamma} \tag{4.18}.$$

As already stated, the voltage error Δu_{1d}^{Param} can only be used in operations with encoder. In that case this equation can be used to identify the value of the inductance L_{1q}, however the inductances of the machine are not dependent on the temperature, so the on-line identification for the inductances is not necessary. The values of the inductances L_{1d} and L_{1q} measured with conventional tests at standstill are sufficient for the control if the iron is not extremely saturated. In case of a high saturated machine a simple table (L vs. i) can be used for the correction of the values.

The voltage error Δu_{1q}^{Param} is used to identify the stator resistance R_1 and the permanent flux linkage ψ_P. Both parameters depend on the temperature and therefore a decoupling is necessary. Feuersänger, et al. in [51] propose a procedure for this decoupling. For high velocity operation, the value of the flux-error has relevance, whereas in high current but low

speed operation, the resistance-error is significant, i.e. if the machine is operated in two different operating points, two formulas can be obtained:

$$\Delta u_{1q}^{Param}{}_1 = f\left(i_{1q1}, \dot{\gamma}_1\right) = -\Delta R_1 \cdot i_{1q1} - \Delta\psi_P \cdot \dot{\gamma}_1 \tag{4.19}$$

And $$\Delta u_{1q}^{Param}{}_2 = f\left(i_{1q2}, \dot{\gamma}_2\right) \cong -\Delta R_1 \cdot i_{1q2} - \Delta\psi_P \cdot \dot{\gamma}_2 \tag{4.20}.$$

with i_{1q1} and $\dot{\gamma}_1$ being the current and the and the angular velocity in operating point "1", and i_{1q2} and $\dot{\gamma}_2$ being the current and the angular velocity in operating point "2".

Now, there are in principle two equations and the parameters can be identified by following formulas:

$$\Delta R_1 = \frac{\Delta u_{1q}^{Param}{}_1 \cdot \dot{\gamma}_2 - \Delta u_{1q}^{Param}{}_2 \cdot \dot{\gamma}_1}{\dot{\gamma}_1 \cdot i_{1q2} - \dot{\gamma}_2 \cdot i_{1q1}} \tag{4.21}$$

$$\Delta\psi_p = \frac{\Delta u_{1q}^{Param}{}_2 \cdot i_{1q1} - \Delta u_{1q}^{Param}{}_1 \cdot i_{1q2}}{\dot{\gamma}_1 \cdot i_{1q2} - \dot{\gamma}_2 \cdot i_{1q1}} \tag{4.22}$$

It is important to mention that this very simple approach is only valid if the stator resistance R_1 and the permanent flux ψ_P do not change notably between both operation points or in other words, the temperature should not have changed significantly between the two operation points. Otherwise the parameter identification procedure will fail. Therefore, the following approach can only be applied if the machine changes its operation points with a duration lower than the thermal machine time constant.

The disadvantage of the proposed method is the necessity of two consecutive operating points. Hence, a different structure as depicted in Fig. 4.3 is proposed, in which the condition of decoupling is carried out by means of two weighted integrators. With this approach the operation under arbitrary load torque- and angular velocity-profiles is possible.

Both integral (I)-controllers for the adaption of the parameters R_1 and ψ_P try to reduce the voltage error Δu_{1q}^{Param}. In order to avoid a cross coupling between both branches, the influence of the region of operation is considered by weights that change their values depending on the actual point of operation.

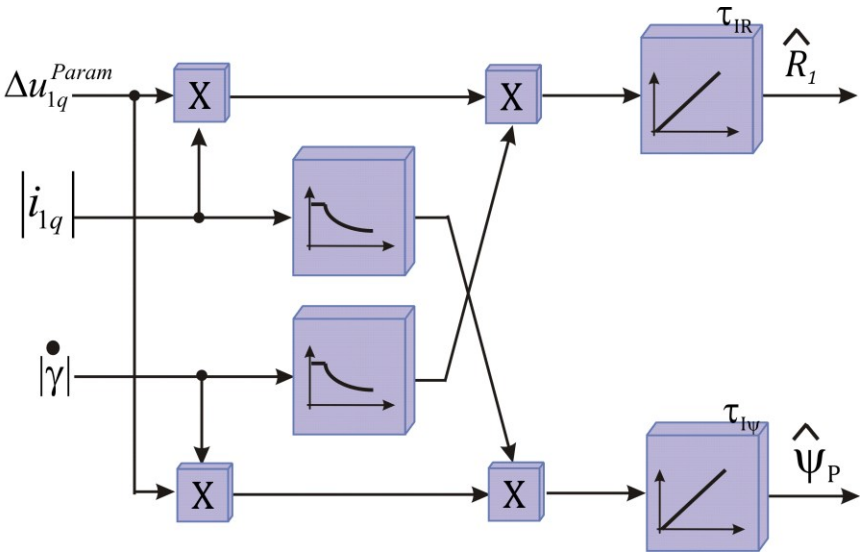

Fig. 4.3. Decoupling of the voltage error Δu_{1q}^{Param}

In the proposed scheme, the gain in the channel for the adaption of the resistance error ΔR_1 is increased in operating points with a high current, whereas gain for the adaption of the permanent flux error $\Delta\psi_P$ is increased in operating points with a high velocity. The identification of the stator resistance is achieved by the following procedure:

- The voltage error Δu_{1q}^{Param} is multiplied with the stator current i_{1q} to increase the gain in the channel of the adaptive resistance tuning for higher current values
- After that, the multiplication result is weighted to reduce it for high angular velocity values, otherwise it is kept constant for lower velocity operation (<10% of its nominal value).

As a result, the value of the stator resistance is stabilized quickly in the operating points with high currents and low angular velocity.

The identification procedure of the permanent flux works in the opposite way:

- The voltage error Δu_{1q}^{Param} is first multiplied with the angular velocity $\dot{\gamma}$ to increase the gain in the channel of the adaptive permanent flux tuning for higher velocity values
- The result of the multiplication is weighted for changing torque (or its equivalent: i_{1q}), i.e. the gain in this channel is gradually reduced for higher current values (>10% i_N) otherwise it is kept constant.

Thus, in both control loops (for R_1 and for ψ_P), the resulting gains are high if the actual operating point is in favor of an adaptive tuning of the corresponding parameter, and the resulting gains are low if the adaptive tuning of the parameter has no sense.

In real dynamic applications (process of a working machine) the speed as well as the torque changes regularly, and the conditions for the above presented parameter adaption method are fulfilled.

In the present work which examines the system PMSM -LC-Filter, including the sensorless control technique mentioned above, the procedure is identical with the difference that some variables are not measured but estimated by the Luenberger observer, thus (4.17) and (4.18) for the on-line adaptive parameter tuning of the system PMSM-LC filter can be rewritten as:

$$\Delta u_{1d}^{Param} \cong \Delta L_{1q} \cdot \dot{\gamma} \cdot \hat{} \tag{4.23}$$

and $$\Delta u_{1q}^{Param} \cong -\Delta R_1 \cdot \hat{} \qquad \dot{\gamma} \tag{4.24}.$$

And in the same way, the full expressions for the sensorless control and on-line adaptive parameter tuning of the system PMSM- LC-Filter are given by:

$$\Delta u'_{1d} = \Delta u_{1d} + \Delta u_{1d}^{Param} \cong \psi_P \cdot \dot{\gamma} \cdot \Delta\gamma - \Delta R_1 \cdot \hat{} \qquad \hat{} \qquad at \qquad \hat{} \tag{4.25}$$

$$\Delta u'_{1q} = \Delta u_{1q} + \Delta u_{1q}^{Param} \cong -\psi_P \cdot \Delta \dot{\gamma} - \Delta R_1 \cdot \hat{} \qquad \frac{d\hat{}}{dt} - \Delta L_{1d} \cdot \dot{\gamma} \cdot i_{1d} - \Delta\psi_P \cdot \dot{\gamma} \tag{4.26}$$

Fig. 4.4 shows the complete scheme including the predictive-sensorless control and the on-line adaptive parameter tuning. The parameters of the LC-Filter are not adapted, so the

filter-inductances and capacitances are supposed to be constant and the ohmic resistance is not relevant because its contribution to the voltage error is lower than 1V meaning that it can be neglected.

To validate the proposed on-line parameter identification and adaptive parameter tuning method, the system PMSM-LC filter was tested in a highly dynamic process. To emulate this process a coupled system motor-load is set-up in laboratory in which a torque- and a speed-profile are applied (torque-profile for the load and speed-profile for the motor) operating on the following criteria:

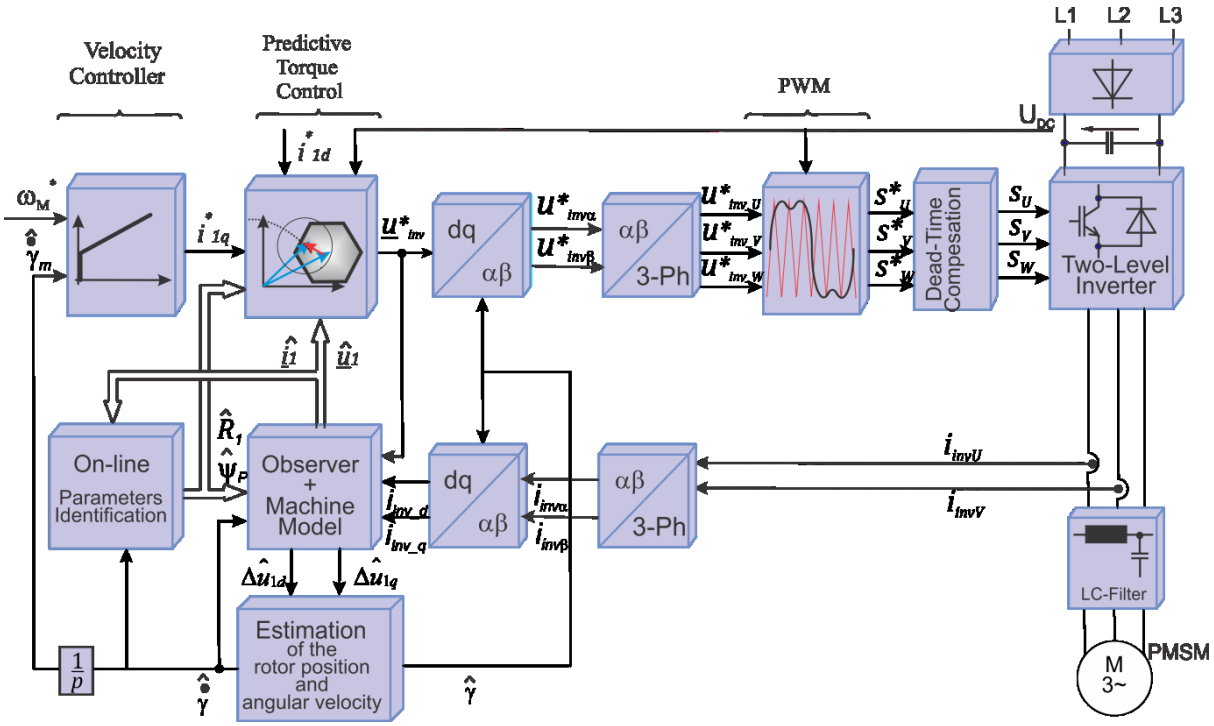

Fig. 4.4. Sensorless predictive torque control scheme with on-line adaptive parameter tuning

- Constant speed but changing torque and vice versa,
- lower speed with high torque and
- lower torque with high speed.

The torque- and speed-profiles and the laboratory results will be shown in the chapter of experimental results.

4.3. Summary of the Chapter

In this chapter, the methods for sensorless control in drives with PMSM were presented as far as they are relevant for the present work. In addition a method for the on-line adaptive parameter tuning of the PMSM was discussed.

In the case of the sensorless control, different techniques were mentioned and the scheme based on the voltage model of the machine, which is applied in the present project, was studied in depth.

Besides for the utilized sensorless control a novel on-line adaptive parameter tuning method is presented that allows the correction of changes in the values of the stator resistance as well of the permanent magnet flux under certain operation conditions

The presented methods of sensorless control and of parameter adaption were extended to the case of predictive control for a PMSM drive with sine-wave filter.

5. LABORATORY SET-UP AND EXPERIMENTAL RESULTS

5.1. Experimental Set-up

The proposed ideas and principles for the predictive control of the system LC-Filter-PMSM explained in the chapters three and four were verified through experiments carried out on a laboratory set-up which is illustrated in the Fig. 5.1 with all its components.

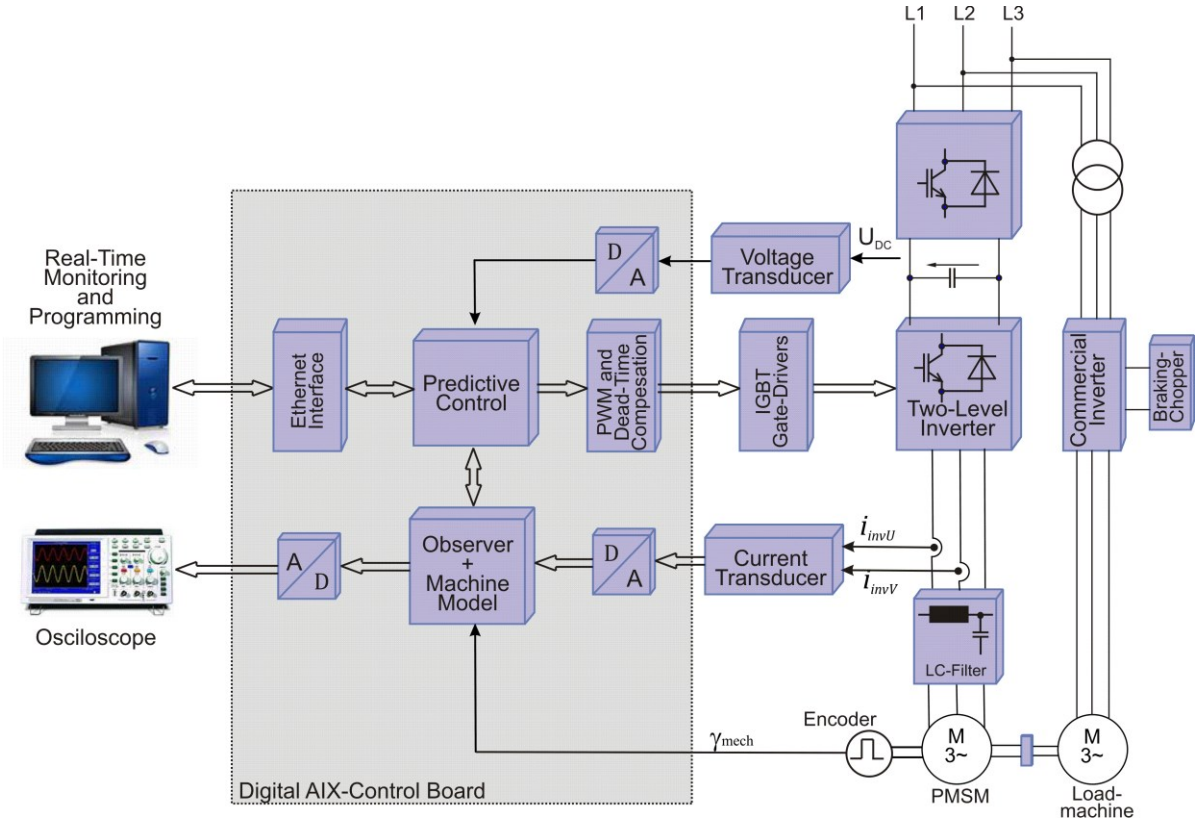

Fig. 5.1. General scheme of the experimental set-up

For the digital control a commercial board "AIX-Control" (AIX-2010-Power Control System) is used which contains four slot´s and one back-plane distributed and described as follow:

- The backplane interconnects all four modules and also provides some additional I/O-extensions.
- Slot 1: Processor Module. In this slot, the core of the whole digital system is located, i.e. here a FPGA is situated (user programmable, but also with some pre-programmed blocks) which is interconnected with two DSP´s units (one for the control and the other for the system and communications). This slot 1

also contains the DAC´s and ADC´s, and is connected with the main-plug which is the interface for: the analog I/O signals, the digital I/O signals, the global signals and the system signals (start, stop, reset, internal I^2C-bus, etc.).

- Slot 2: Communication module. Here the Ethernet interface is located and interconnects the digital AIX-control board with an external PC where the real-time monitoring as well as the programming of the FPGA is possible.
- Slot 3: converter interface module. It is a user adaptable platform containing all functions required for driving one inverter with up to four phases.
- Slot 4: universal I/O-module with up to eight analog outputs and high-speed digital-inputs and –outputs, which are used for general purposes as well as the encoder interface.

For the measurement of the mechanical angular position of the shaft an incremental encoder with 2048 increments per revolution and a reference mark are used.

The currents of the machine are measured with two Hall-effect current transducers.

The inverter that is used is a Eupec-IGBT-Power-Module Series FF-300R12-KF2 and it is mounted on a heat sink which has a fan to cool the components. The DC-Link voltage is kept at the constant level of 670VDC by an active rectifier unit.

To evaluate the proposed control scheme, two PMSM were coupled. One machine is controlled by the explained scheme. The other machine is used to load the first machine and is fed by means of a commercial inverter. The parameters of the driving motor, of the load-motor, of the load-inverter and of the LC-Filter-parameters are summarized in the appendices. Fig. 5.2 shows the test bench with the coupled driving-machine and load-machine used for the experiments.

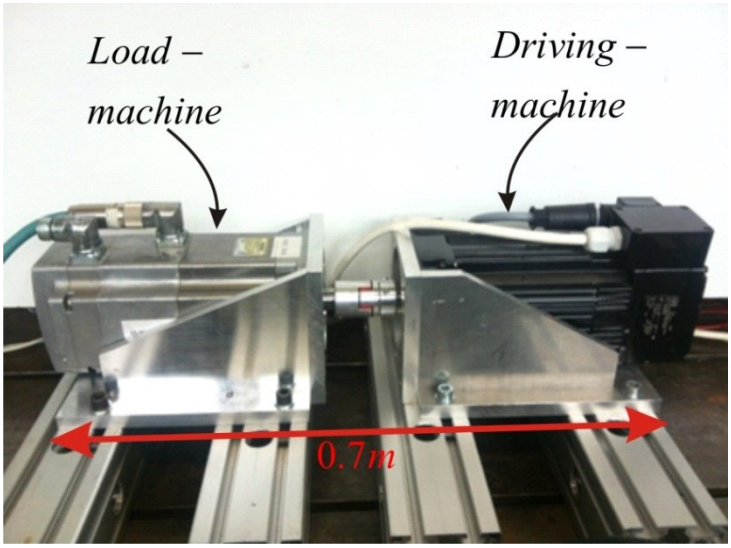

Fig. 5.2. Test bench with the coupled group motor-load used for the experiments. The proposed control was applied to the PMSM -on the right-. The left machine is the load-machine.

5.2. Experimental Results for the Predictive Control of the System PMSM-LC Filter with Observer

5.2.1. Predictive Control

In this section the obtained experimental results are presented for the case where a simple cost function of quadratic form is used in the predictive control of the system LC-Filter-PMSM with an observer.

First, the simple cost function (3.38) is considered. This cost function has a quadratic expression form and takes into account the errors of the stator currents in the *d-q* coordinate system. The current constraints are included as well.

The following experimental results have been carried out with an inverter switching frequency of 4kHz, a resulting sample time Ts=250μs and with 670VDC in the DC-link.

A step change from negative to positive nominal value was applied to the reference of the angular velocity at no load condition and examined. Due to the characteristics of the applied cascade control and due to the high proportional gain of the velocity control, the reference value for the current i_{1q} control is also a step. The reference for the current i_{1d} is constant and equal to zero (see Fig. 5.3). Therefore, the experiments also show the dynamics of torque and flux under different operation conditions.

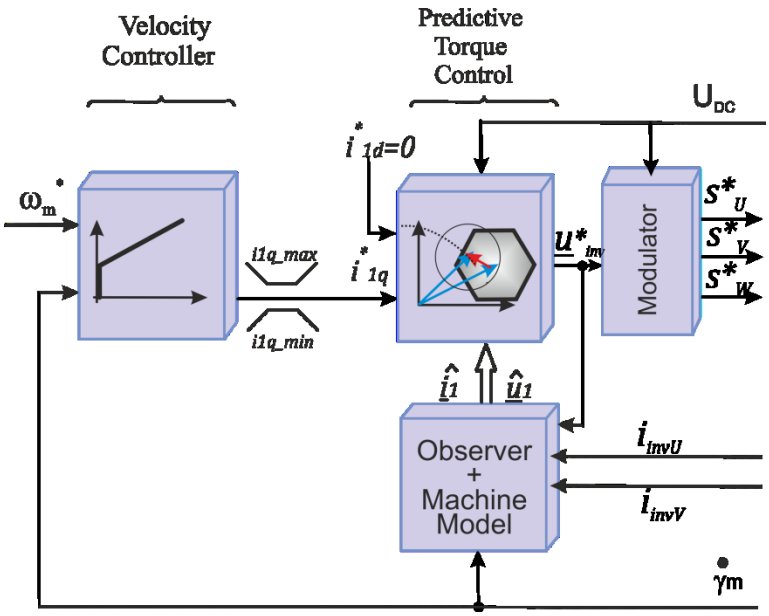

Fig. 5.3: Cascade control scheme

Numerous experiments have been carried in order to examine the behavior of the system depending on the number of levels of the virtual inverter and of the number of the elements of the mesh used for the calculation of the cost function. Sets of 4 and 16 points in the neighborhood of the first voltage reference were used for the mesh; the number of levels of the virtual inverter was changed in the different experiments. In addition the impact of the weight w in the cost function was analyzed.

Fig. 5.4 shows the responses of the mechanic angular velocity, of the components d and q of the stator current space phasor as well as of the stator currents in all three phases. The different traces present a comparison between the results of a simple model based control without any optimization and of a predictive control, which has 4- and 16-points, a weight of w=1.0 and 70 levels in the virtual multilevel inverter. In all cases the response of the currents i_{1d} and i_{1q}.exhibit an excellent dynamic. It is important to mention that no overshoot exists for both the currents i_{1d} and i_{1q}, the settling time is four samples in all cases and the ripple of the currents i_{1q} and i_{1d} are both about +/-2.0% for a mesh of 16-points and about +/-1.0% for a mesh of 4-points.

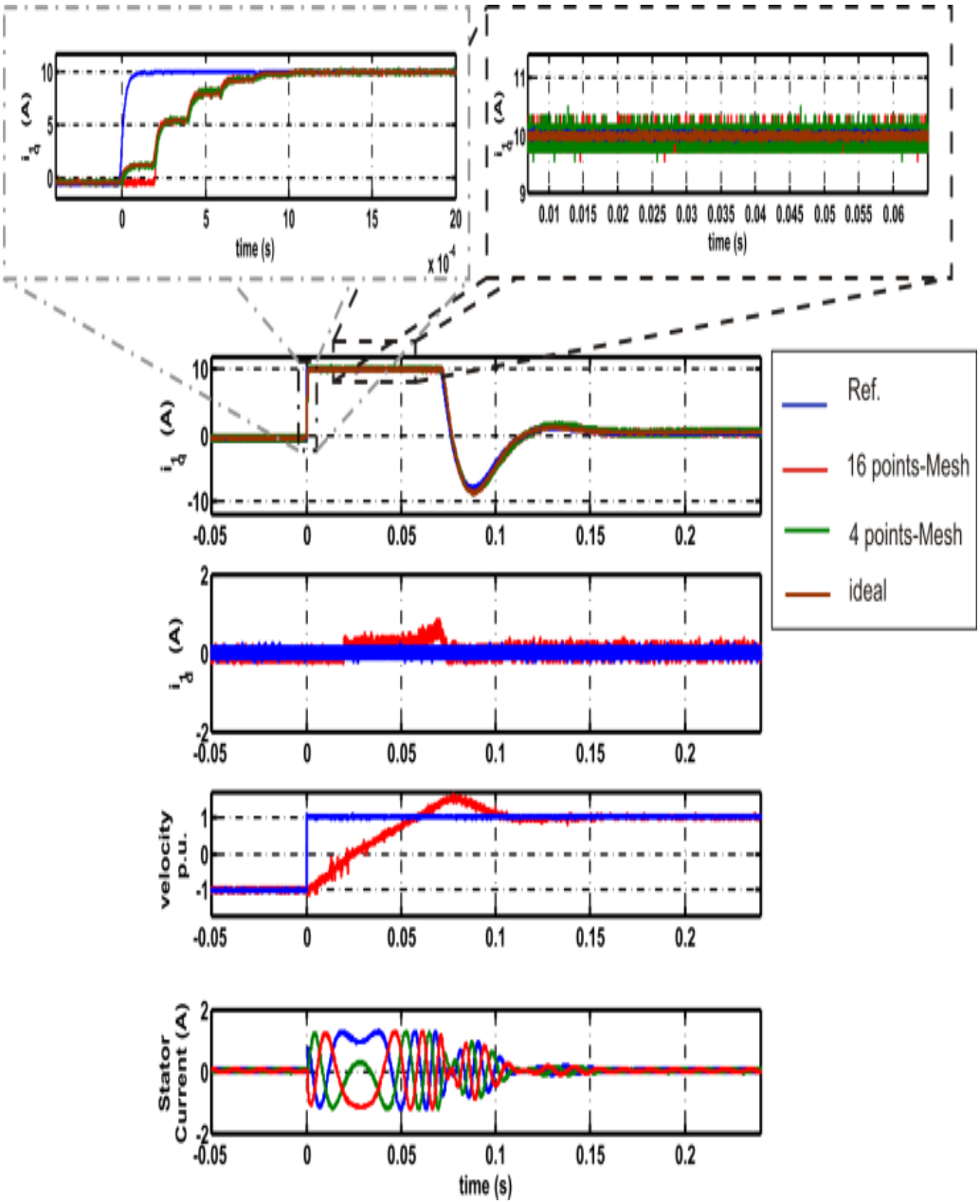

Fig. 5.4. A Zoom of the signal i_1, and the signals i_{1q}, i_{1d}, velocity and current responses to a step change on the velocity reference from $-n_N$ to $+n_N$ for 4- and 16-points voltage space phasor-mesh and 70 levels in the virtual multilevel inverter

The curves of the mechanical velocity and of the phase current show similar characteristics in all cases, they do not hold any additional information and therefore are only depicted for one of the measurements.

From the experimental results it can be conclude that the dynamic behavior of a system, with more than 70 levels in the virtual multilevel inverter and voltages in the linear range of

modulation, is essentially the same with and without an optimization of the voltage. Thus, the proposed controller works fundamentally as a model based or dead-beat controller.

In the following experiments the impact of the number of levels in the virtual inverter is investigated, the size of the voltage mesh is kept constant and only the dynamic response of the torque i.e. of the imaginary component of the stator current phasor is observed. Fig. 5.5 presents the results for a mesh of 4-points working in the linear region of modulation, with a weight w=1.0 and with different number of levels in the virtual multilevel inverter for a step change in the angular velocity reference from negative nominal value to positive nominal value without load.

As already indicated the dynamic response is not sensitive to changes in the number of levels of the virtual inverter but the ripple of the currents in steady state changes depending on the chosen value. The ripple of the current is: +/-15% for 5-levels, +/-13% for 7-levels, +/-10% for 11-levels, +/-8% for 15-levels, +/-7% for 20-levels, +/-1.5% for 30-levels, +/-1% for 70-Levels. It is evident that for small number of levels the ripple increases and in the opposite case for a high number of levels the ripple decreases.

The next experiments analyze the influence of the weight factors used in the cost function. Both the torque error (i.e. i_{1q} error) and the flux error (i.e. i_{1d} error) are important variables, for this reason none of the weight factors can be set to zero. In a comparison, the torque is the more important variable. Consequently, the weight for the i_{1q} error is set to 1 and only the value of w_d is changed, from 0.1 (low importance but still considered in the optimization) to 0.5, until the maximum of 1.0 (high importance). The results of i_{1d} and i_{1q} for different values on the weight w_d are presented in Fig. 5.6 using a mesh of 4 points with 30 levels in the multilevel inverter. In the figure 5.4 only the traces of the current in steady state are zoomed, the transient response is the same regardless of the different weights.

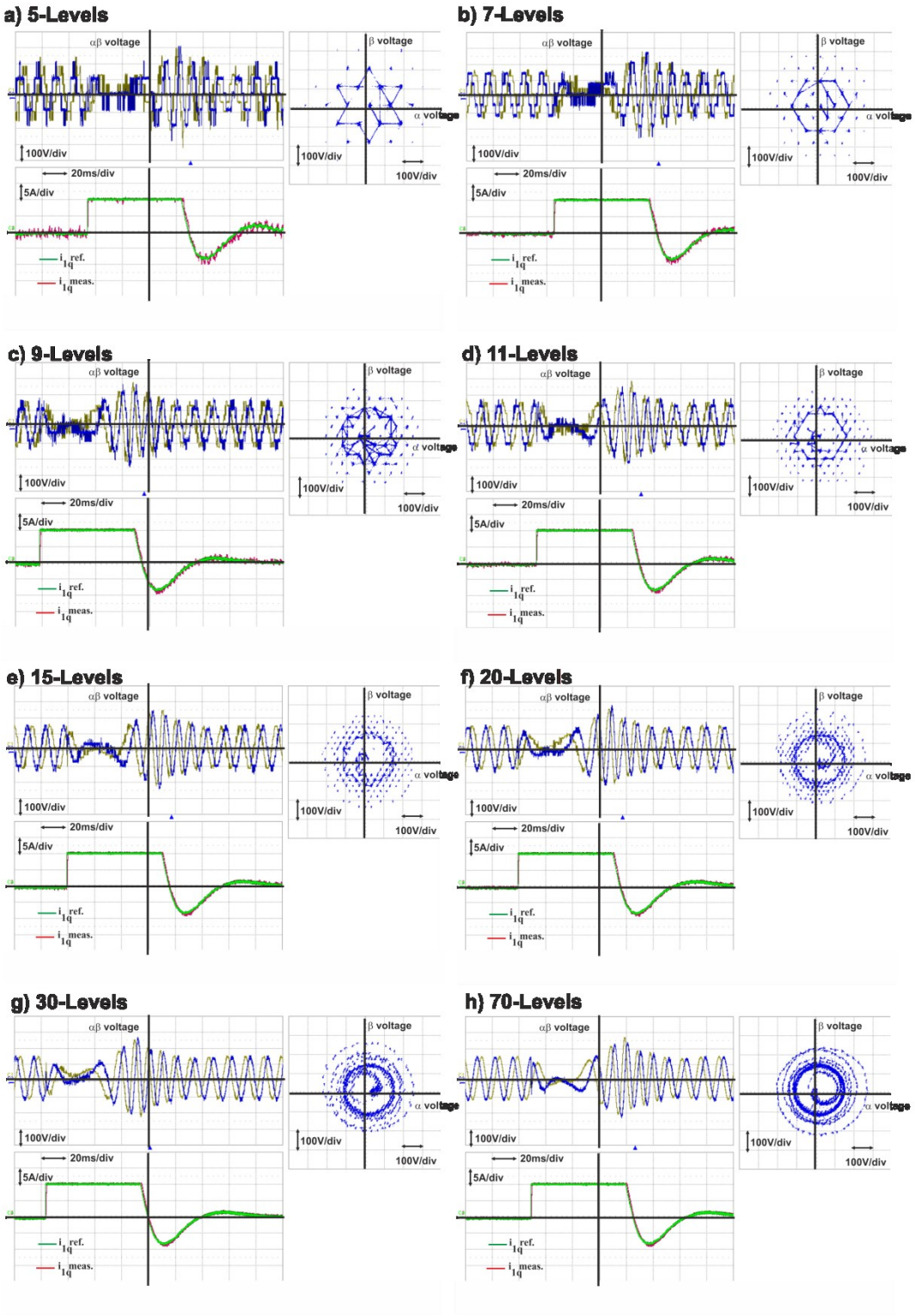

Fig. 5.5**.** Experimental results for different numbers of levels of the virtual inverter. The upper traces show the $\alpha, \beta-$components of the stator voltage as function of the time and the locus of the stator voltage space phasor $u_{1\alpha}$ vs. $u_{1\beta}$; the lower traces depict the response of the current i_{1q}

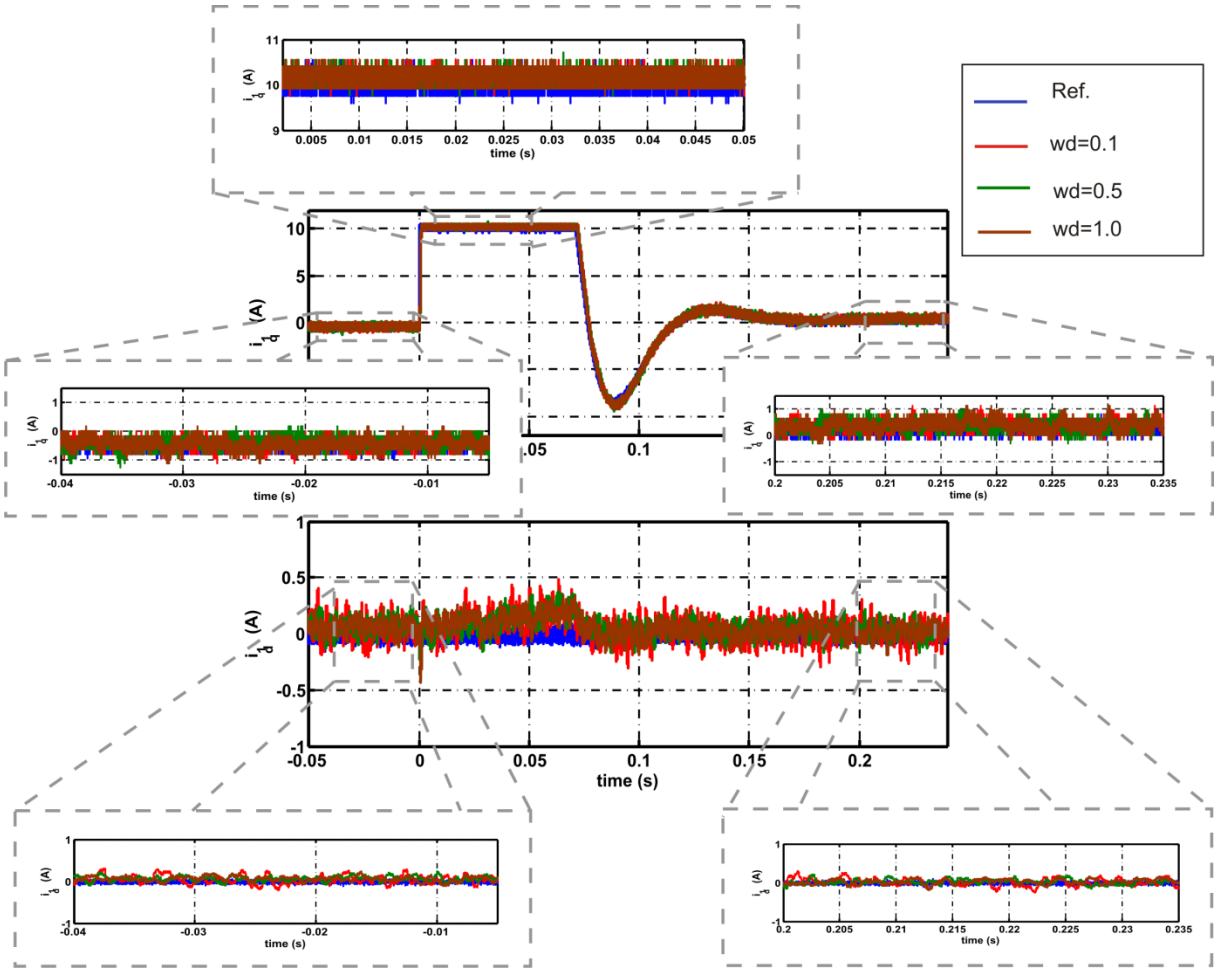

Fig. 5.6. i_{1d} and i_{1q} for different values of the weight w_d

As can be seen in Fig. 5.6, the low value of the weight w_d (0.1) results in a high ripple in the steady state responses for i_{1d} as well as for i_{1q} (+/-7% in the case of i_{1d}, and +/-5% in the case of i_{1q}). For a value of w_d=0.5 the ripples are about +/-3% for i_{1d}, and +/-2% for i_{1q}. For a weight of w_d=1.0 the ripple is approximately +/-2.0% for i_{1d}, and +/-1.5% for i_{1q} . Although good results are obtained with a weight of w_d=0.5, for all following experiments w_d=1.0 is selected because it yield the best results.

This test also verifies the versatility of changing the parameters of the predictive control in real time (in this case the weight values), something conventional controllers struggle with e.g. PI-controllers run the risk of becoming unstable when the control-parameters are changed.

These experimental results have shown that predictive control based on the simple cost function with quadratic terms (3.38) works properly. Other possible cost functions were also

proposed e.g. one with absolute-value of the error such as in (3.7). For the present work, the expression using the absolute-value form can be written as:

$$g = \left| \frac{i_{1_q}^{*}(k+2) - i_{1_q}^{p}(k+2)}{i^{N}} \right| + w \left| \frac{i_{1_d}^{*}(k+2) - i_{1_d}^{p}(k+2)}{i^{N}} \right| + f_{Lim}\left(i_{1_q}^{p}(k+2)\right) + f_{Lim}\left(i_{1_d}^{p}(k+2)\right) + f_{Lim}\left(i^{p}(k+2)\right) \tag{5.1}$$

The operation with this cost function was tested and compared with the cost function with quadratic terms, both with a mesh of 4 points, 30 levels in the virtual multilevel inverter and w=1.0. The results are shown in Fig. 5.7.

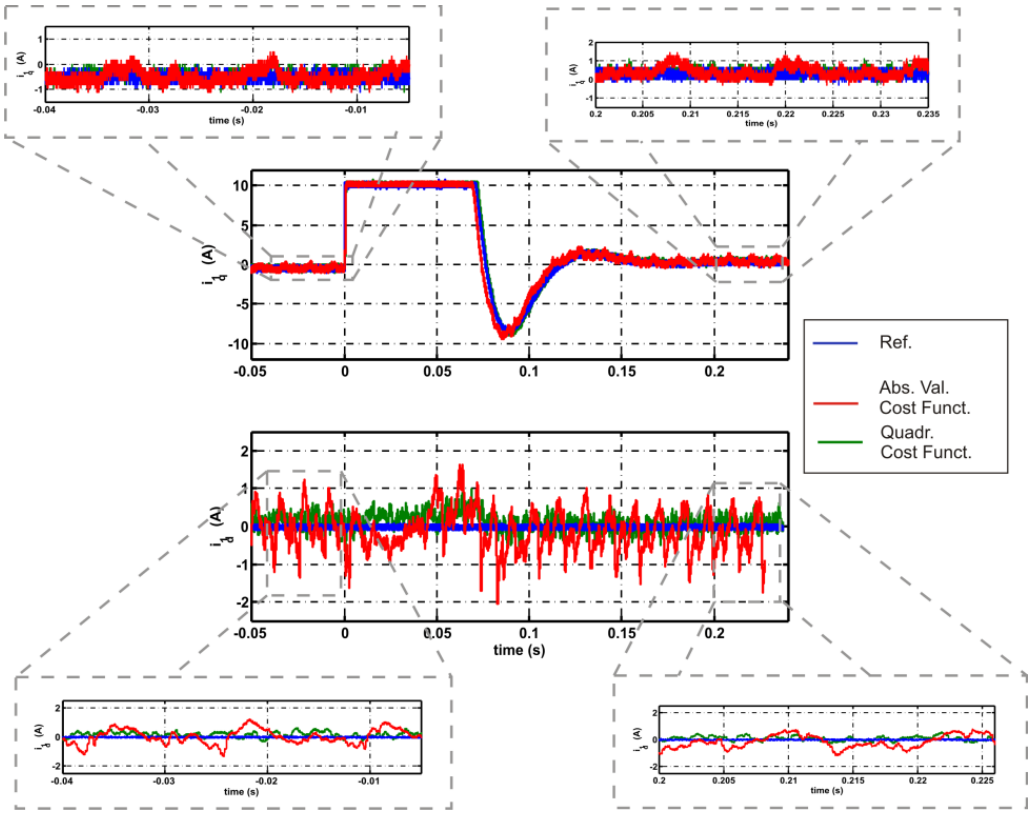

Fig. 5.7. i_{1d} and i_{1q} for two different cost functions: with quadratic terms and with absolute-values terms

Although the cost function according to (5.1) delivers good dynamic results, during the transient results the behavior in steady state exhibits a high ripple. In the case of i_{1d} the ripple is about +/-10% and for i_{1q} is about +/-7.5%. From these experiments it can be concluded that a predictive control with a cost function with quadratic terms yields a lower ripple of the currents in steady state and because of this was preferred within this work.

The proposed control technique was also tested in case of disturbances i.e. for the case that a load toque is suddenly applied. The test was carried out at nominal velocity, and for quadratic-terms in the cost function, with 4 points-mesh, w=1.0 and 30 levels in the virtual multilevel inverter. The experimental results for a change in the load torque from 0% to 90% of the nominal value are presented in Fig. 5.8. The system has a good response to the change. The ripple in i_{1q} and i_{1d} are about +/-0,5%.

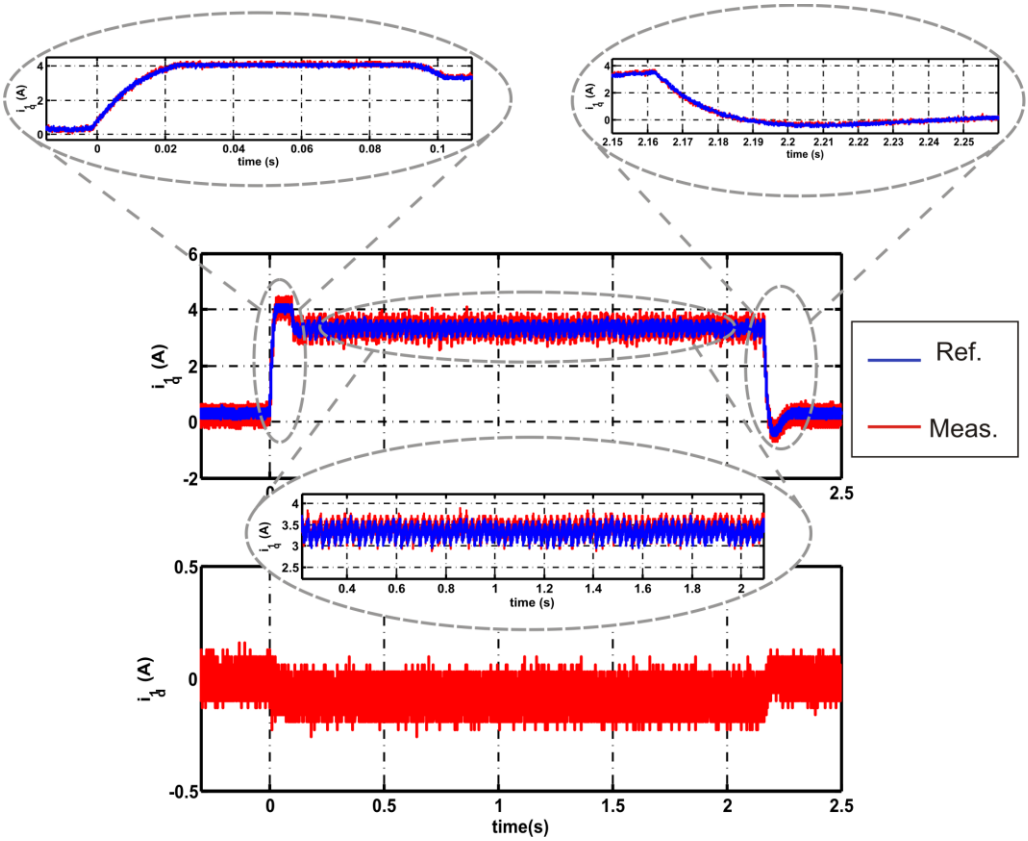

Fig. 5.8. i_{1q} and i_{1d} responses to a change in the load torque working at the nominal velocity

In general, it was confirmed in all cases that the proposed predictive control using a virtual multilevel inverter for the optimization applied to the present systems PMSM-LC-Filter works properly. This also includes disturbances of the load torque. A good dynamic response was verified while keeping i_{1d} =0 and a low ripple on i_{1d} and i_{1q} in steady state.

5.2.2. The Predictive Control at the Voltage Limit of the Inverter

Until now only the operation of the system within the linear range of the modulator was considered, hence the limits of the inverter were not taken into account in the cost function. Yet, if the voltage space phasor demanded by the first estimate in the prediction is located

either in the non-linear-region or outside of the external circle, the procedure proposed in the section 3.4.5 has to be applied.

Further tests were carried out in order to verify the operation of the proposed control scheme in such cases. The tests are similar as above: a step change in the reference of the angular velocity from negative nominal value to nominal positive value and vice versa was applied, both for a mesh of 4 points, a weight w=1.0 and 30 levels in the virtual multilevel inverter. This was done with 15% nominal torque-load (Fig. 5.9 and Fig. 5.10) and with 50% of the nominal torque-load (Fig. 5.11 and Fig. 5.12). In these figures the stator voltage α and β (left-top), the reference as well as the measured value of the current i_{1q} (left-bottom) and the locus of the stator voltage space phasor $u_{1\alpha}$ vs. $u_{1\beta}$ are shown. The point in the left hand graphic marked with the vertical cursor corresponds to the pint in the right part of the graphic marked with a cross. It marks a set of points that exceed the inverter voltage limit, i.e. in the nonlinear region.

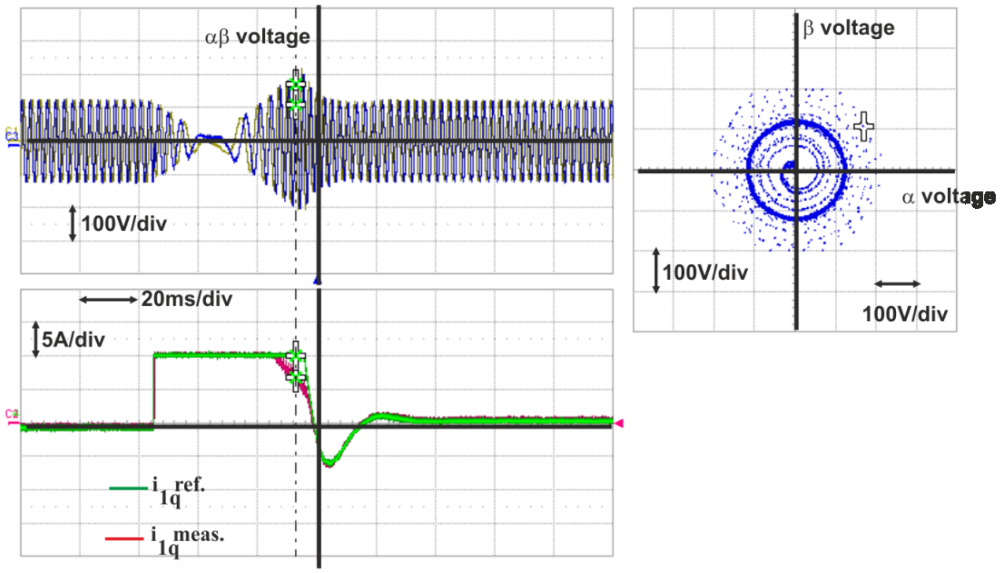

Fig. 5.9, Operation in the nonlinear region for a step change in the angular velocity from negative- to positive -nominal values with 15% nominal torque-load

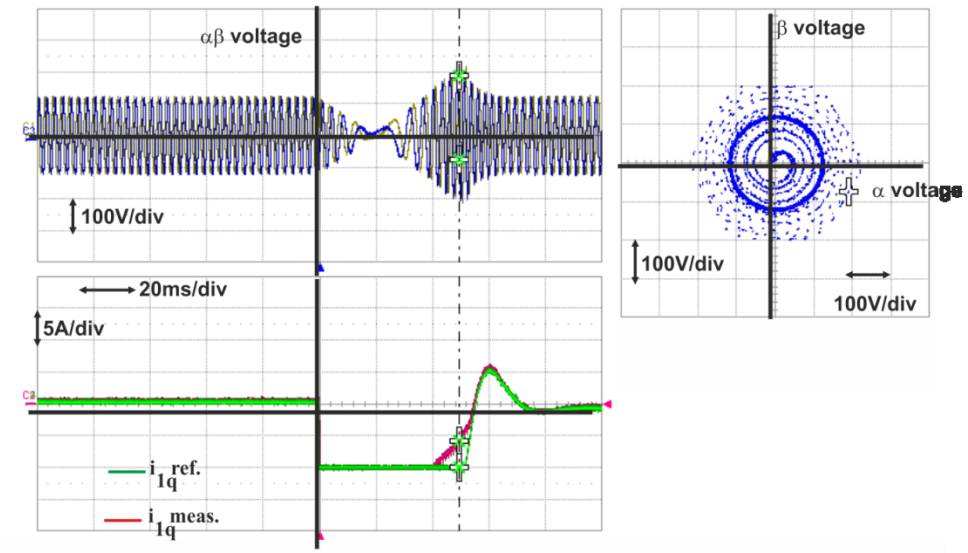

Fig. 5.10. Operation in nonlinear region for a step change in the angular velocity from positive- to negative-nominal values with 15% nominal torque-load

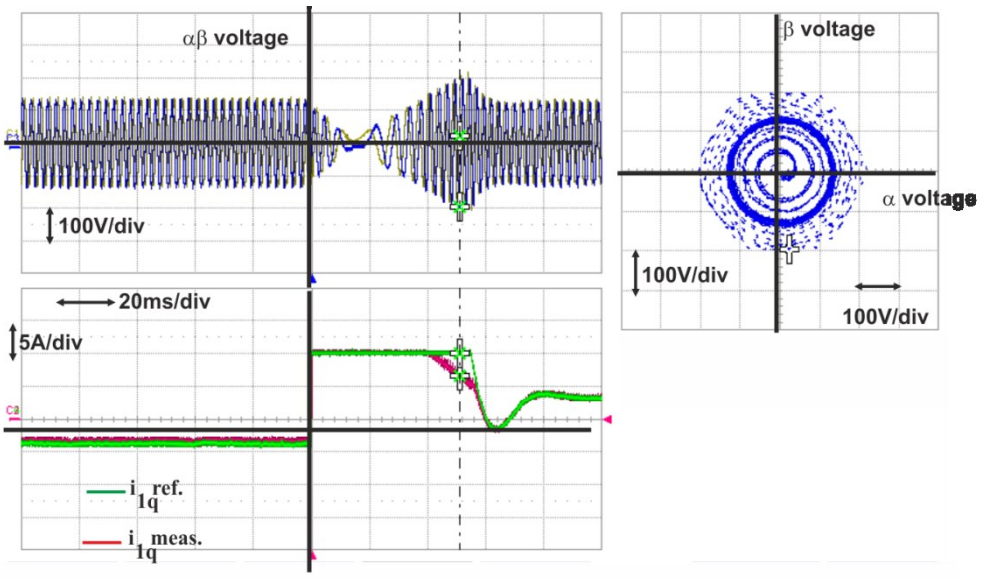

Fig. 5.11. Operation in nonlinear region for a step change in the angular velocity from negative- to positive -nominal values with 50% nominal torque-load

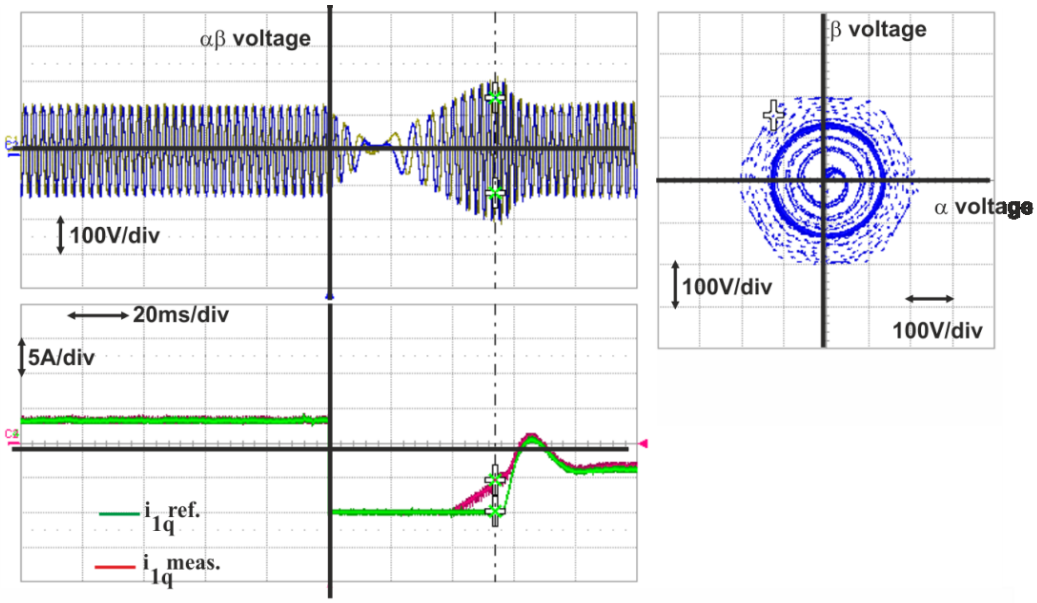

Fig. 5.12. Operation in nonlinear region for a step change in the angular velocity from positive- to negative-nominal values with 50% nominal torque-load

All these measurements show that the proposed control also allows an operation of the drive in the non-linear range of modulation if the constrains of the inverter are included in the cost function and in the optimization.

5.2.3. Predictive Control with Enhanced Cost Functions

Simple cost functions, like the quadratic-form, in the predictive control for the systems PMSM-LC-Filter lead to very good results as presented in the section 5.2.1, nevertheless if the system parameters are incorrect, the results are not satisfactory. Therefore, an improvement of the cost function is necessary to reduce the sensitivity to errors in the parameter of the model.

Thus, other cost functions like the I-control (considering the trajectory) as well as the integral-action forms were proposed, both are explained in the section 3.4.6.

Fig. 5.13 shows the experimental results for the current i_{1q} in the case of the model being calculated with the correct machine parameters (the results and analysis for the current i_{1d} are similar like i_{1q}), the cost function is calculated with quadratic terms, the mesh for the optimization has 4 points, the virtual inverter has 30 levels and w=1.0. The result exhibits a

ripple of about +/-1.5%. Fig. 5.14 shows the same experimental results for the current i_{1q} but with incorrect machine parameters. The stator resistance R_1 is increased to $1.5 \cdot R_{1N}$ and the permanent flux ψ_p is reduced to $0.9 \cdot \psi_{pN}$. These values were selected based on the real variation of the stator resistance and of the permanent flux in a PMSM with an increase of machine temperature of about 100K. For wrong machine parameters a steady state error of 2% appears and the ripple is increased to +/-3% even in the steady state.

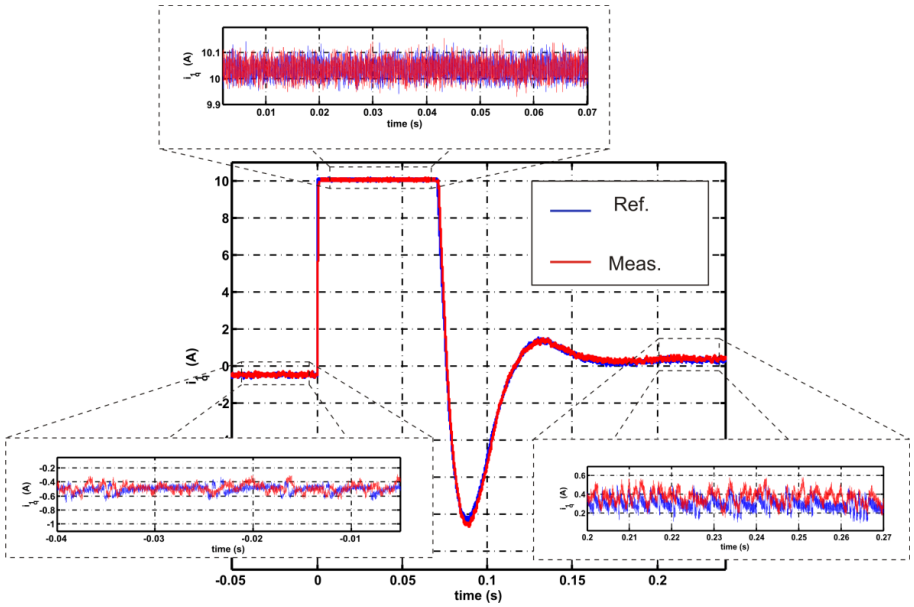

Fig. 5.13. i_{1q} for a cost function with quadratic terms and with correct machine parameters

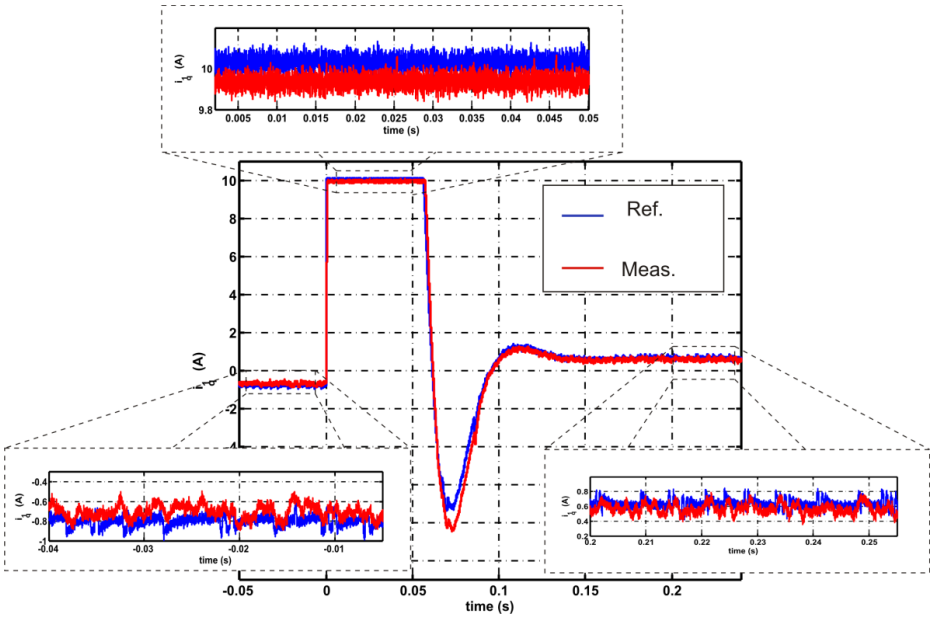

Fig. 5.14. i_{1q} for a cost function with quadratic terms and with wrong machine parameters

The expression for an enhanced trajectory cost function or I-control form is given in (3.48). This cost function is applied to the model with wrong machine parameters and the experiment is repeated. The settings for this simulation were chosen similar to those without the extended cost function e.g. a mesh of 4 points, 30 levels in the virtual multilevel inverter and w=1.0. The results are presented in Fig. 5.15. It can be seen, that the steady state offset-error disappears, but the ripple is increased to +/-3.5%.

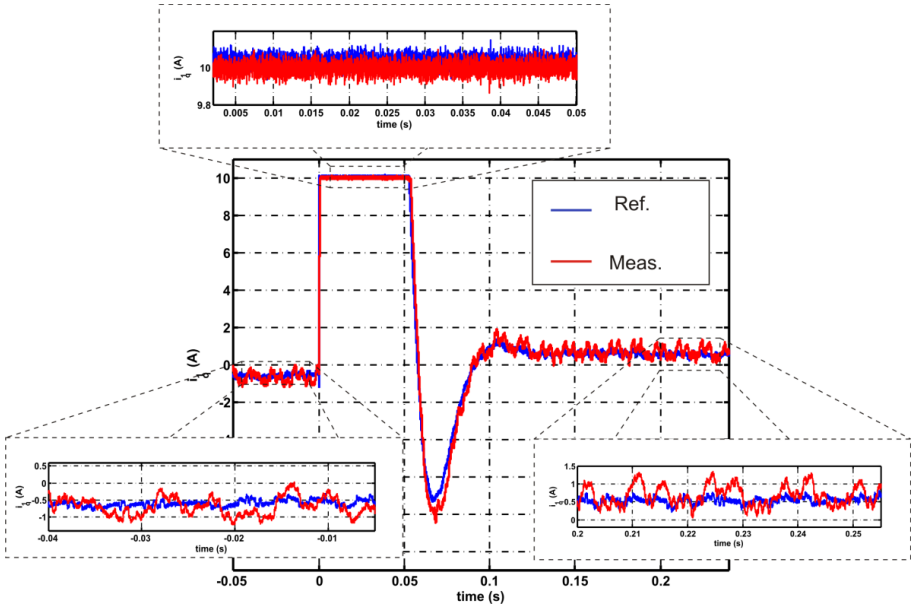

Fig. 5.15. i_{1q} for an enhanced trajectory cost functions (I-control form) and with wrong machine parameters

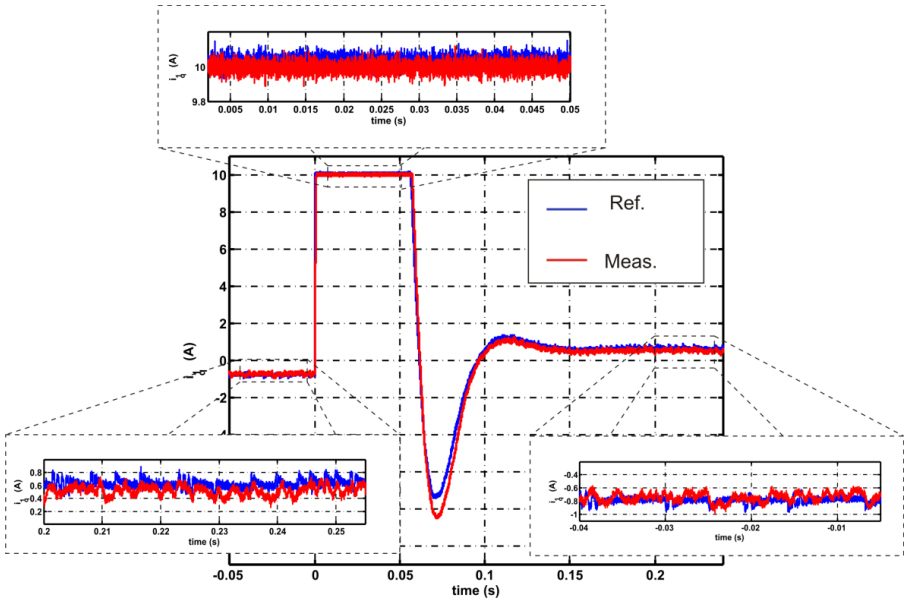

Fig. 5.16. i_{1q} for an enhanced cost functions (integral-action) and with wrong machine parameters

Further experiments were performed with an enhanced cost function extended with the integral-action as described by (3.57). The experiments were performed under the same experimental conditions. The results are shown in Fig. 5.16. A good performance in dynamic behavior as well as in steady state is obtained with this integral-action cost function even with wrong model parameters. The steady state offset-error becomes zero and the ripple is about 2.5%.

By comparing experimental results in both cases i.e. using the cost function trajectory and the integral-actions, the second-one presents a better and robust performance regarding wrong parameters.

5.3. Sensorless Control with On-line Adaptive Parameter Tuning

5.3.1. Sensorless Control

The sensorless predictive control scheme proposed in chapter 4.1 was evaluated for a simple cost functions with quadratic term as well as for the enhanced cost functions. In all cases, the same satisfactory dynamic and the steady states behavior was obtained. Fig. 5.17 shows the comparison of the estimated angular velocity with the measured value, as well as the experimental results for the currents i_{1d} and i_{1q} for a step change in the reference of the angular velocity from negative nominal value to positive nominal with a mesh of 4 points and 30 levels in the virtual multilevel inverter, and w_d=1.0.

As it can be seen, a good performance of the proposed sensorless predictive control is verified with a low error between the real and the estimated velocity values. Thus, the validity of the voltage model method for the estimation of the angular velocity as well as the rotor position, at least at high velocities, can be shown.

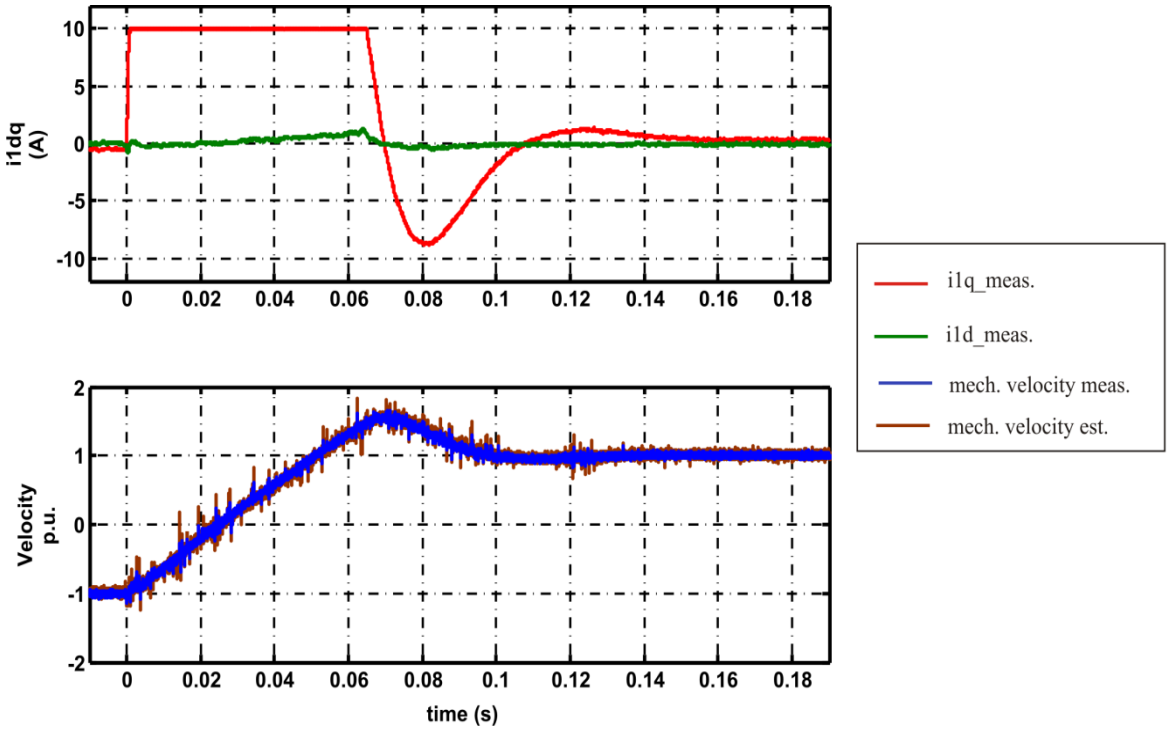

Fig. 5.17. Predictive sensorless operation

5.3.2. *On-line Adaptive Parameter Tuning*

The parameter identification and adaptive parameter tuning based on the voltage model of the machine that was explained in section 4.2 war also experimentally validated. As explained this procedure works only under certain dynamic conditions found in highly dynamic processes. In the laboratory set-up these working cycles are emulated in a test-bench, in which a load torque-profile and a motor velocity-profile is used. The criteria for these profiles were already described and were applied in the experiments that were illustrated in Fig. 5.18.

The real temperature of the housing was monitored though a PT100 and additionally the resistance value was also measured at the beginning and at the end of the test to be compared with the estimated value of the proposed on-line parameter identification method.

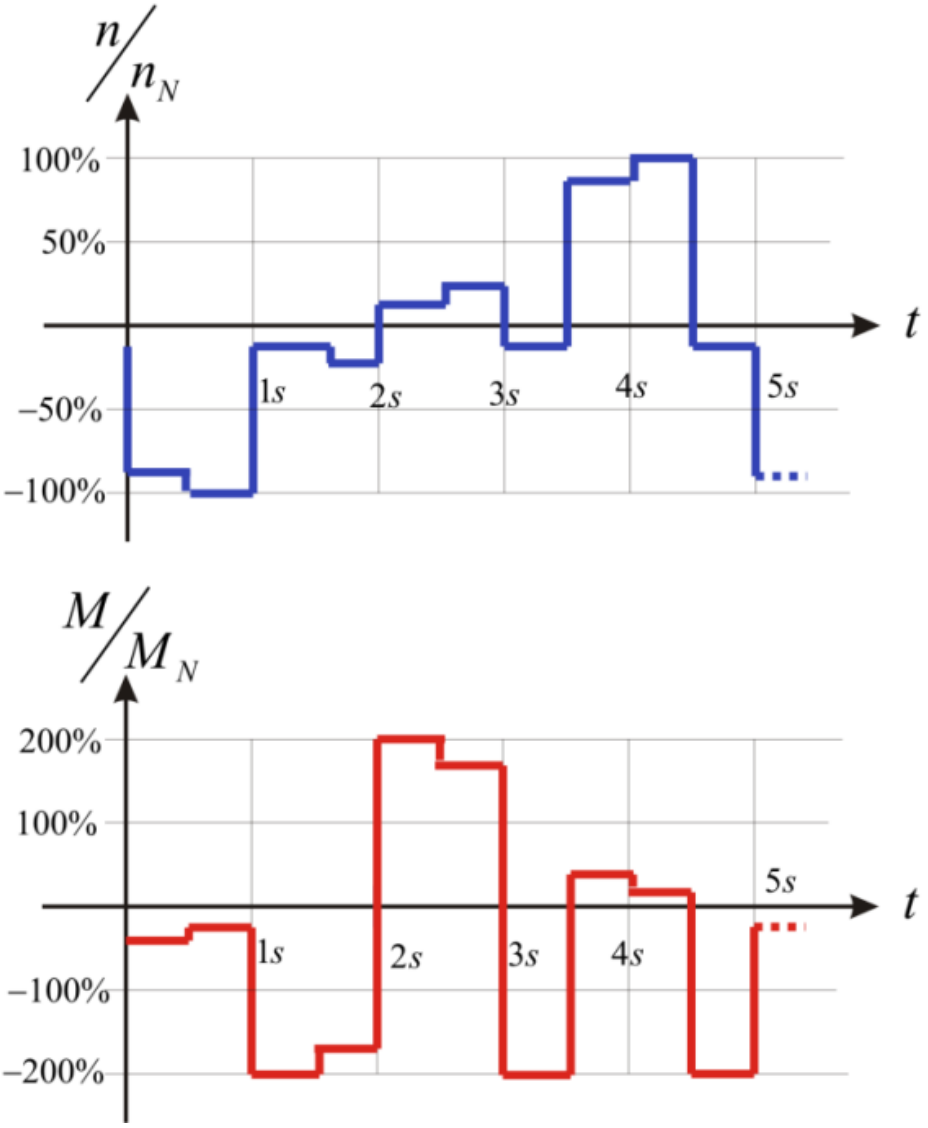

Fig. 5.18. Periodical load torque-profile and motor velocity profile

Fig. 5.19 shows the results of the measurements. The lower trace shows the temperature rise of the housing of the PMSM during the run. The rise of temperature in the machine yields an increase of 50% in the value of the stator resistance R_1 and a decrease of 6% in the value of the permanent flux ψ_p. The adaption procedure is able to follow these changes as shown in the middle and upper traces of Fig. 5.19 showing the identified values of resistance and of the flux respectively. In addition the real measured value of the resistance of the stator winding is highlighted in the diagram.

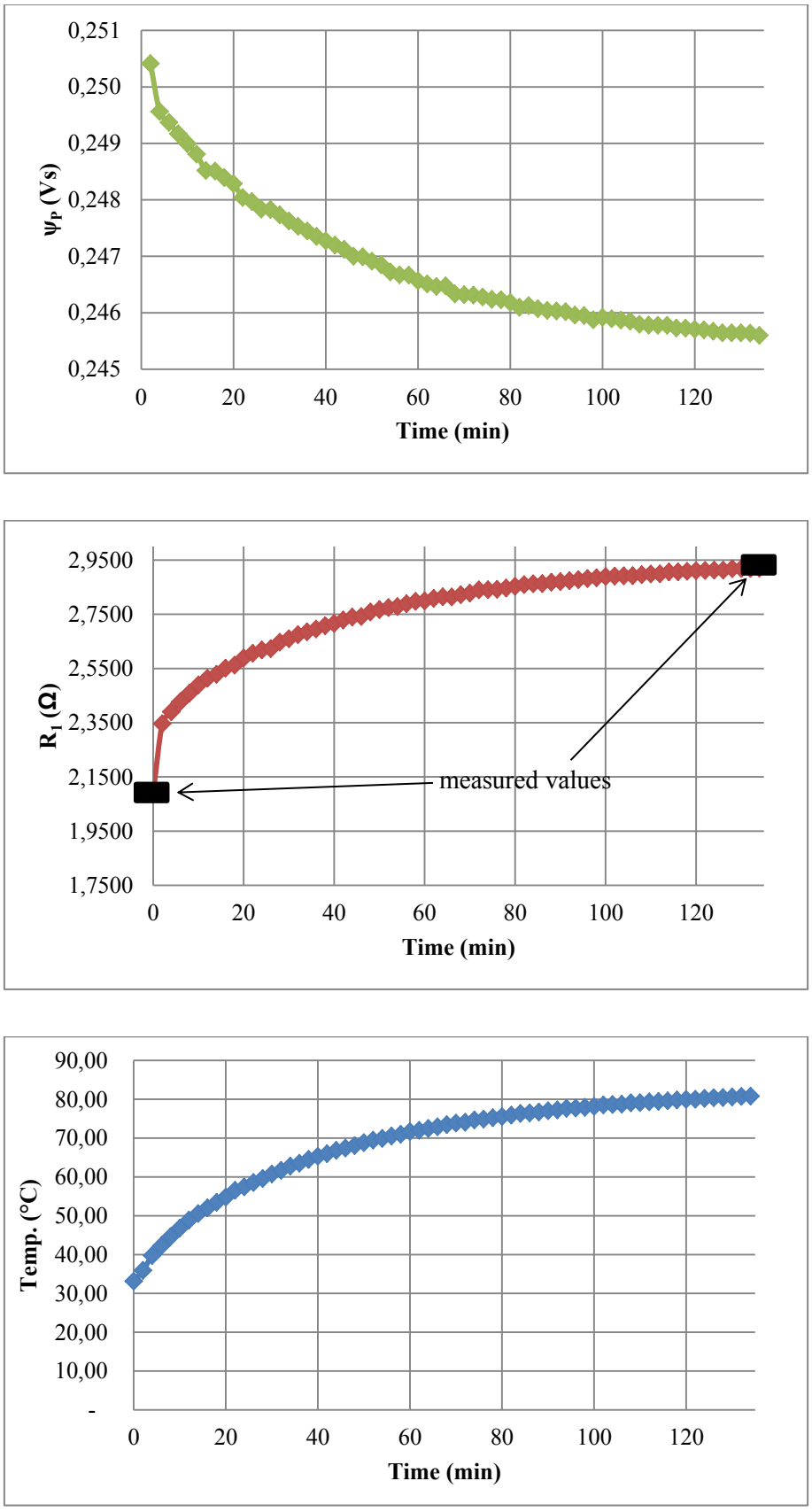

Fig. 5.19. On-line identification of the machine parameters and measured case temperature

5.4. Summary of the Chapter

The theoretic considerations and proposals for the control of a system PMSM- LC-Filter were experimental validated.

First the proposed predictive control was tested by observing the step response of the current components i_{1d} and i_{1q} in different cases. In particular the following aspects were tested:

- Comparison between simple model based control and model based with a cost function
- Number of levels and number of the points of the mesh used for the optimization
- The influence of the weight factors in the cost function
- Behavior under load
- Quadratic and absolute value cost functions
- Enhanced cost functions
- Behavior at the voltage limits of the inverter

Besides experiments for an operation of the system under encoderless predictive control as well as for a corresponding on-line adaptive parameter tuning were carried out.

All experiments validate the theoretical analysis and proposals made in this work.

6. CONCLUSIONS

The main objective of the present work was the examination of a simple approach to the control of a PMSM that combines the advantages of the predictive control theory, the use of a LC-filter, the utilization of a conventional Pulse Width Modulation (PWM) and the application of the Runge-Kutta method for the digital implementation. One new idea is the definition of a virtual multilevel inverter, which discretizes the entire voltage plane to create a finite set of possible solutions that is determined by the number of levels created in the virtual inverter. In this way the process of optimization wins a physical meaning, permits an adjustable resolution and reduces the computational effort.

To complement and to improve the proposed predictive control strategy, a sensorless operation as well as a parameter identification and adaptive parameter tuning procedure was developed and evaluated.

In the first step an operation of a model based control of the PMSM with a sine-wave filter featuring high dynamics could be achieved by using a Luenberger observer to estimate the stator currents and voltages of the PMSM and by measuring the inverter currents and the angular position of the shaft. In a further step, the control was extended to a predictive control with a different cost function. As a new aspect of the control scheme, the voltage plane was divided into a fine mesh of points in order to create a finite set of possible solutions for the optimization. This procedure allows the utilization of a conventional space phasor modulation and of a constant sampling time and reduces the computation required for the optimization procedure. Nevertheless, it became evident that the behavior of predictive control with conventional cost functions in the linear range of modulation is not better than a simple model based control. Yet some consideration and experiments have shown that the proposed predictive control has advantages if the nonlinear region of modulation is taken into account. An experimental validation was obtained that the behavior of the drive at the voltage limits can be managed in a simpler way within the optimization procedure than with conventional PI-Controllers with saturation.

One main drawback of model based control schemes like the one proposed here is its sensitivity to errors in the parameters of the model. Therefore, an online adaptive parameter tuning procedure was proposed and experimentally corroborated. Finally the control scheme was extended to its operation without mechanical encoder obtaining acceptable results at least for higher mechanical velocities of the drive.

7. ABSTRACT

In the frame of this work a predictive control for a permanent magnet synchronous machine with LC-Filter aiming sinusoidal voltage at the machine terminals is presented. The proposed scheme assumes a virtual multilevel inverter for the optimization of the cost function and utilizes a conventional pulse width modulator (PWM) thus being a finite control set predictive control scheme. A first estimation of the voltage space phasor, that has to be synthesized by the inverter, is computed by using the equations of the mathematical model of the system enhanced by a Luenberger observer and based on measured inverter currents and the shaft position. The switching patterns are calculated by assuming that the "virtual" inverter has an arbitrary high number of levels. The cost function in a predictive control scheme is minimized by defining a mesh of voltage space phasors that corresponds to the output states of the “virtual” multilevel inverter. The center of this mesh with a finite number of elements corresponds to the first calculated value of the reference voltage. For the minimization only the points belonging to the mesh are considered and the voltage space phasor chosen in this way is then used for the calculation of the switching signals in a conventional space phasor modulator and sent to the real two-level inverter. The proposed scheme results in an easy implementation and delivers good dynamics in the torque behavior. To ensure the convergence on the digital implementation, the Runge-Kutta method is used in each integration step. The proposed predictive controller is complemented by means of sensorless control as well as on-line identification and adaptive parameter tuning, both based on the voltage model method of the machine and working at the same time. This method identifies and adapts all machine parameters simultaneously (resistance and flux) and it is applicable to high-dynamic drives.

8. ZUSAMMENFASSUNG

Die vorliegende Arbeit befasst sich mit der prädiktiven Regelung einer permanenterregten Synchron Maschine mit Sinusfilter, um die Maschine mit sinusförmigen Größen zu speisen. Das entwickelte Konzept verwendet einen virtuellen mehrstufigen Umrichter, der auf einer konventionellen PWM aufbaut. Zunächst wird eine Schätzung des Spannungsraumzeigers durchgeführt, der mithilfe des Umrichters erzeugt werden soll. Die Berechnung erfolgt auf Grundlage der Gleichungen des mathematischen Models des Systems unter Verwendung eines Luenberger Beobachters und den gemessenen Umrichterströme sowie der Winkelposition. Die Schaltmuster werden berechnet, unter der Annahme, dass der virtuelle mehrstufige Umrichter eine beliebig hohe Anzahl an Stufen hat. Die Kostenfunktion der prädiktiven Regelung wird minimiert, indem ein Netz aus Maschen definiert wird. Dabei entsprechen die Knoten der Maschen den natürlichen Spannungsraumzeigern des virtuellen mehrstufigen Umrichters. Das Zentrum dieses Maschennetzes, das unendlich viele Elemente enthält, korrespondiert mit dem zuvor berechneten Spannungsraumzeiger. Zur Minimierung der Kostenfunktion werden nur diejenigen Werte herangezogen, die dem Maschennetz zugeordnet sind. Nur der Raumzeiger, der bei dieser Optimierung gewählt wird, wird zur Berechnung der Schaltimpulse verwendet. Zur Generierung dieses Raumzeigers kommt eine konventionelle Pulsweitenmodulation (PWM) und einen realer, handelsüblicher Zweipunktwechselrichter zum Einsatz. Das vorgestellte Regelungskonzept ist einfach zu implementieren und liefert eine hohe Dynamik im Drehmoment. Um eine Konvergenz der digitalen Implementierung sicher zu stellen, wird das Runge-Kutta-Verfahren verwendet. Der vorgestellte prädiktive Regler wird komplettiert durch die Verwendung einer sensorlosen Regelung sowie einer Echtzeitidentifikation und -adaption. Das Verfahren erkennt die Maschinenparameter Statorwiderstand und permanent erregter Fluss und passt sie selbstständig an. So ist das Verfahren auch geeignet für hoch dynamische, industrielle Anwendungen.

9. APPENDICES

Parameters of the utilized PMSM

	Value	Unit
Manufacturer	ABB	
Nominal Power	1.54	kW
Nominal Voltage	360	V
Nominal Velocity	3000	min^{-1}
Nominal Current	3.3	A
Nominal Torque	4.9	Nm
Pole pairs	3	
Winding resistance R_{UV}	4.0	Ω
Winding inductance L_{UV}	15.2	mH
Induced voltage	96	$V/1000min^{-1}$
Moment of inertia	8.9	$kg\ cm^2$

Sine-Wave Filter Parameters

	Value	Unit
Inductance	3.3	mH
Capacitance	4.5	µF
DC-Resistance	125.6	mΩ

Load Machine Parameters

	Value	Unit
Manufacturer	Siemens	
Type	Servomotor	
Nominal Power	2.3	kW
Nominal Voltage	400	V
Frequency	50	Hz
Nominal Current	5.6	A
Nominal Torque	7.3	Nm
Nominal Speed	3000	min^{-1}
Pole pairs	4	
Moment of inertia (include brake)	17.3	$kg\ cm^2$
Brake current	0.75	A

Load Driver Parameters

	Value	Unit
Manufacturer	ABB	
Model	ACS850-04-014A-5+E200+J400	
P_n	5.5 / 7.5	kW / HP
U_1	3~380…500	V
I_{1n}	18	A
f_1	48…63	Hz
U_2	3~0…U_1	V
I_{2n}	14	A
f_2	0…500	Hz

10. REFERENCES

1. Leonhard, W.: Control of Electrical Drives. Springer, Berlin; New York (2001)

2. Holtz, J., Qi, X.: Optimal Control of Medium-Voltage Drives—An Overview. IEEE Transactions on Industrial Electronics 60(12), 5472 - 5481 (2012)

3. Pacas, M.: Sensorless Drives in Industrial Applications. IEEE Industrial Electronics Magazine 5(2), 16 - 23 (2011)

4. Morari, M., Lee, J.: Model Predictive Control: Past, Present and Future. Computers and Chemical Engineering, 23, 667-682 (1999)

5. Camacho, E. F., Bordons, C.: Control Predicitivo: Pasado, Presente y Futuro. Revista Iberoamericana de automática e Infromática Industrial (RIAI) 1(3), 5-28 (Oct. 2004)

6. Maciejowski , J. M.: Predictive Control with Constraints. Prentice-Hall (2002)

7. Camacho, E. F., Bordons, C.: Model Predictive Control. Springer (2003)

8. Rodriguez, J., Cortes, P.: Predictive Control of Power Converters and Electrical Drives. John Wiley & Sohns, Ltd, Singapore (2012)

9. Linder, A., Kennel, R., Kanchan, R., Stolze, P.: Model-based Predictive Control of Electric Drives. Cuvillier, Göttingen (2010)

10. Geyer, T.: Model Predictive Direct Current Control. IEEE Industry Application Magazine 18(2), 47 - 59 (March-April 2012)

11. Geyer, T., Papafotiou, G., Morari, M.: Model Predictive Direct Torque Control—Part I: Concept, Algorithm, and Analysis. IEEE Transactions on Industrial Electronics 56(6), 1894 - 1905 (June 2009)

12. Steinke, J. K.: Use of an LC filter to achieve a motor-friendly performance of the PWM voltage source inverter. IEEE Transaction on Energy Conversion 14(3), 649-654 (Sep. 1999)

13. Salomäki, J.: Sensorless control of AC drives equipped with an inverter ouput filter, Ph.D. Thesis, Helsinki University of Technology. Multiprint Oy, Espoo (2007)

14. Szczupak, P., Pacas, M.: Automatic Parametric Model Identification Method for AC-Drives with LC-Filter. In : International Symposium on Diagnostics for Electric Machines, Power Electronics and Drives. SDEMPED, Cracow (2007)

15. Mastellone, S., Papafotiou, G., Liakos, E.: Model Predictive Direct Torque Control for MV Drives with LC Filters. In : 13th European Conference on Power Electronics and Applications, EPE '09 (2009)

16. Mariethotz, S., Morari, M.: Multisampled model predictive control for inverter systems: A solution to obtain high dynamich performance and low distortion. In : Energy Conversion Congress and Exposition (ECCE), Raleigh, NC, pp.1692-1697 (Sep. 2012)

17. Mariethoz, S., Domahidi, A., Morari, M.: High-Bandwidth Explicit Model Predictive Control of Electrical Drives. IEEE Transactions on Industry Applications 48(6), 1980 - 1992 (2012)

18. Kovacs, K. P., Racz, I.: Transiente Vorgänge in Wechselstrommaschinen. Verlag der Ungarischen Akademie der Wissenschaften, Budapest (1959)

19. Stepina, J.: Raumzeiger als Grundlage der Theorie der elektrischen Maschinen. Elektrotechnische Zeitschrift ETZ-A, Bd. 88, 584-588 (1967)

20. Serrrano-lribarnegaray, L.: Ersetzen der mathematischen durch die physikalischen Raumzeiger zur Untersuchung stationärer und dynamischer Vorgänge in rotierenden elektrischen Maschinen. ETZ Archiv Bd.8, 347-352 (1986)

21. Correa, P.: Fault Tolerant Operation of Series Connected H-Bridge Multilevel Inverters. Siegen, Univ., Ph.D. Thesis, Siegen-Germany (2006)

22. Dufoo Ochoa, S.: Diagnostics of Rotor Asymmetries in Inverter Fed Induction Machines. Siegen, Univ., Ph.D. Thesis, Siegen-Germany (2012)

23. Weber, J.: Prädiktive Direkte Drehmomentregelung der Synchronmaschine. Siegen, Univ., Ph.D. Thesis, Siegen-Germany (2004)

24. Kovács, P.: Studies in electrical and electronic engineering 9: Transient phenomena in electrical machines. Elsevier, Amsterdam (1984)

25. Späth, H.: Elektrische Maschinen: Eine Einführung in die Theorie des Betriebsverhaltens. Springer , Berlin (1973)

26. Zhong, L., Rahman, M.: An investigation of Direct an Indirect Torque Controllers for PM Synchornous Motor Drives. Proc. of Second international Conference on Power Electronics and Drives (PEDS´97), Singapore, vol. 2, 519-523 (1997)

27. Blaschke, F.: Das Prinzip der Feldorientierung, Grundlage für die Transvektor-Regelung von Drehfeldmaschinen. Siemens-Zeitschrift 45, 757-760 (1971)

28. Hasse, K.: Zum dynamischen Verhalten der Asynchronmaschine bei Betrieb mit variabler Ständerfrequenz und Ständerspannung. ETZ-A Band 89, Heft 4, 77-81 (1968)

29. Morales-Caporal, R.: Encoderless Predictive Direct Torque Control of the Synchronous Reluctance Machine at Low and Zero Speed, Ph.D. Thesis, University of Siegen. Shaker, Aachen (2007)

30. Quang, N.-P., Dittrich, J.-A.: Vector Control of Three-Phase AC Machines: System Development in the Practice. Springer, Berlin (2008)

31. Meyer, M.: Selbstgeführte Thyristor-Stromrichter. (1974)

32. Gonzalez, S., Verne, S., Valla, M.: Multilevel Converters for Industrial Applications. CRC Press, Boca Raton (2014)

33. Rendusara, D., Cengeli, E., Enjeti, P.: Analisis of Common Mode Voltage-“Neutral Shift” in Medium Voltage PWM Adjustable Speed Drive (MV-ASD) Systems. IEEE-Transactions on Power Electronics 15(6), 1124-1133 (Nov. 2000)

34. Holmes, D. G., Lipo, T. A.: Pulse Width Modulation for Power Converters: Principles and Practice. IEEE Press power engineering series, Hoboken, NJ (2003)

35. Soeterboek, R.: Predictive Control: A Unified Approach. Prentice Hall International, Englewood Cliffs, N.J (1992)

36. Grimble, M. J.: Industrial Control Systems Design. Wiley, Chichester [England]; New York (2001)

37. Cannon, M.: C21 Model Predictive Control-Lecture Notes. (Accessed 2013) Available at: www.eng.ox.ac.uk/~conmrc/mpc/

38. Mikleš, J., Fikar, M.: Process Modelling, Identification, and Control. Springer, Berlin (2077)

39. Laczynski, T., Mertens, A.: Predictive Stator Current Control for Medium Voltage Drives with LC-Filters. IEEE Transactions on Power Electronics 24(11), 2427-2435 (2009)

40. Salomäki, J., Hinkkanen, M., Luomi, J.: Sensorless Control of Induction Motor Drives Equipped With Inverter Output Filter. IEEE Transactions on Industrial Electronics 53(4), 1188 - 1197 (June 2006)

41. Gilat, A., Subramaniam, V.: Numerical Methods: An Introduction with Applications using Matlab. John Wiley & Sons,Inc. (2011)

42. Fukumoto, T., Hamane, H., Hayashi, Y.: Performance Improvement of the IPMSM Position Sensorless Vector Control System by the On-line Motor Parameter Error Compensation and the Practical Dead-time Compensation. In : Power Conversion Conference. PCC '07, Nagoya (2007)

43. Holtz, J.: Developments in Sensorless AC Drive Technology. In : Power Electronics and Drives Systems, PEDS2005. International Conference on (Vol.:1), Kuala Lumpur , pp.9 - 16

44. Kubota, H., Matsue, K., et al.: DSP-based Speed Adaptative Flux Observer of Induction Motor. IEEE Transaction on Industiry Application 29(2), 344-348 (Mar./Apr. 1993)

45. Hinkkanen, M., Luomi, J.: Novel Full-Order Flux Observer Structure for Speed Sensorless Induction Motors. In : Industrial Electronics Society, IECON '01. The 27th Annual Conference of the IEEE, Denver, CO, pp.1333 - 1338 (Nov-Dec 2001)

46. Feuersänger, S., Pacas, M.: Online parameter tracking in PMSM-control schemes with and without encoder. In : PCIM, Nürnberg, Germany (17-19 May 2011)

47. Barinberg, V., Götz, F.: Enhanced Voltage Model for Sensorless Control of a Permanet Magnet Synchonous Motor Drive. SPS IPC Drives, Nürnberg, Germany (2008)

48. Piippo, A., Hinkkanen, M., Luomi, J.: Adaptation of Motor Parameters in Sensorless PMSM Drives. IEEE Transactions on Industry Applications 45(1), 203 - 212 (Jan. 2009)

49. Tetsuya, S., Kubota, K.: Stability analysis of sensor-less induction motor drives with stator resistance adaptation using estimation error index. In : International Conference on Electrical Machines and Systems ICEMS, Seoul, pp.578 - 583 (2007)

50. Vicente, I., Endemaño, A., et al.: Comparative study of stabilising methods for adaptive speed sensorless full-order observers with stator resistance estimation. Control Theory & Applications, IET 4(6), 993 - 1004 (June 2010)

51. Feuersänger, S., Pacas, M.: Sensorless control with online parameter adaption for the PMSM. In : IECON - 37th Annual Conference on IEEE Industrial Electronics Society, Melbourne, VIC, pp.2012 - 2017 (7-10 Nov. 2011)